PAPER-BASED ANALYTICAL DEVICES FOR DETERMINATION OF METAL IONS IN WATER BASED ON USING BARE CELLULOSE AND NEW FLUORESCEIN DERIVATIVE-IMMOBILIZED CELLULOSE MATERIALS

PONGPICHET SRIKRITSADAWONG

A THESIS SUBMITTED IN PARTIAL FULFILLMENT OF THE REQUIREMENT FOR THE DEGREE OF MASTER OF SCIENCE IN APPLIED CHEMISTRY

DEPARTMENT OF CHEMISTRY SCHOOL OF SCIENCE
KING MONGKUT'S INSTITUTE OF TECHNOLOGY LADKRABANG

2023
KMITL-2023-SC-M-012-047

Thesis Title	Paper-based Analytical Devices for Determination of Metal Ions in Water Based on Using Bare Cellulose and New fluorescein Derivative-Immobilized Cellulose Materials
Student name	Pongpichet Srikritsadawong
Student ID	63605038
Degree	Master of Science (Applied Chemistry)
Department	Chemistry
Year	2023
Thesis Advisor	Assistant Professor Dr. Nathawut Choengchan

Abstract

This dissertation presents the development of two cellulose-based analytical devices for quantitative analyses of metal ions in water. The first device is a paper-based analytical device (PAD), which contains microcellulose fibril. It was fabricated using a Whatman™ No.1 filter paper for the measurement of total iron. The device was designed as a double-layered platform. Each platform (25 x 25 mm^2) composed of a single hydrophilic reservoir (Ø 10 mm), located at the center of the PAD. Hydrophobic barrier was patterned by easily painting the waterproof glue around the hydrophilic reservoir. The analytical procedure was started by pipetting bathophenanthroline (Bphen) to the bottom layer. Then adding standard Fe (II) solutions (0.1 - 0.5 mg L^{-1}) to form the detectable red complex. The two layers were mounted together by two-sided tape. Next, the water sample was transferred to the top layer for sample filtration. When the filtrate touched the bottom layer, the Fe (II)-Bphen complex occurred once again. The bottom layer was unpacked and placed to a light studio, and the complex was captured by a smartphone. The color intensity was examined by ImageJ™. The linear standard addition plots were found (r^2 > 0.99). High precision (RSD < 6 %) with good recovery (92.6 – 102 %) were achieved. The PAD was applied to five kinds of water samples. The iron contents were compared to the results by the spectrophotometric method. According to the paired *t*-test, there was not significantly difference at 95 % confidence (t_{stat} = 2.68, t_{cri} = 2.78). The second

device was made of bacterial cellulose nanopaper (BNC). This device was produced by sub-culturing *Azotobacter xylinum* for three days. After harvesting and bleaching, the transparent circular nanopaper sheet (Ø of the fibril cellulose < 100 nm) was obtained with the dimension of Ø 100 mm and 1 mm thickness. The BNC was ready to adapt as a 2D-microcuvette for quantitative analysis. It was immobilized with a new fluorescein derivative (NFD) and subsequent fluorometric determination of Cr (III). To use it as the 2D-microcuvette, it was necessary to exploit it in accompanied with the invented holder. The BNC was put into the *"home-made"* holder, and the remaining fluorescence was monitored by directly inserting the holder to the sample compartment inside the fluorometer. It was observed that the excitation and emission wavelengths of the NFD-immobilized BNC were found to be 485 and 520 nm. These wavelengths were the same as that of the dissolved NFD in methanol. The as-prepared BNC was highly selective to Cr (III) than the other investigated foreign cations. For the determination of Cr (III), the immobilized paper substrate was immersed into the standard Cr (III) solutions (1 to 100 µM) or the spiked Cr (III) water samples. The detection concept is based on quenching of the fluorescence intensity of the immobilized BNC by Cr (III). Good linearity (r^2 > 0.99) was obtained with high precision and accuracy. This guarantees that the NFD-immobilized BNC was successfully developed for using as a 2D-microcuvette for the determination of Cr (III).

Keywords: Bacterial nanocellulose, Determination, Paper-based analytical device, Total iron, Trivalent chromium, Water sample

Acknowledgements

Foremost, I would like to express my sincere gratitude to my advisor Assistant Professor Dr. Nathawut Choengchan for all his support including, his suggestion and motivation throughout my master thesis.

Additionally, I would like to thank my thesis committees namely, Associate Professor Dr. Maliwan Amatatongchai and Associate Professor Dr. Saowapak Teerasong, for their encouragement, insightful comments and hard questions and suggestions.

I would like to thank Associate Professor Dr. Saranya Phunpruch and her students from the Department of Applied Biology, School of Science, KMITL, for their contributions on preliminary preparation of bacterial nanocellulose.

I would like to thank Assistant Professor Dr. Panumart Thongyoo, Department of Chemistry, Faculty of Science and Technology, Thammasat university, for synthesizing and characterizing a new fluorescein derivative, employed for study on determination of Cr (III).

I would like to acknowledge my scholarship, Research Assistant/Teaching Assistant scholarship *(Grant No. RA/TA-2563-M-007)*, School of Science, KMITL in terms of the financial support for my master's degree study.

I would like to acknowledge Applied Analytical Chemistry Research Unit to support the infrastructure, apparatuses, instruments, and chemical reagents for doing my research.

Finally, I would like to thank my beloved family, especially my parents for their eternal loves and cares throughout my life.

Mr. Pongpichet Srikritsadawong

Table of contents

Table of contents (Cont'd)

Table of contents (Cont'd)

Table of contents (Cont'd)

Table of contents (Cont'd)

Table of contents (Cont'd)

List of tables

List of figures

List of figures (Cont'd)

List of figures (Cont'd)

Chapter 1
Introduction

1.1 Research motivation

Recently, the paper-based analytical device or PAD has been widely employed for quantitative analysis, because of its cost-effectiveness and capability for on-site measurement or point-of-care testing. PAD is fabricated by patterning the specific hydrophobic region onto laboratory filter paper. Normally, the PAD was developed for colorimetric determination for the sake of simplicity. To inspect the colored product, a specific detection reagent was immobilized in the hydrophilic zone. Small aliquot of sample was then delivered into specific area of the hydrophilic region, resulting in development of the color. The product was detected by smartphone capturing under controlled illumination condition and analyzing the color intensity with ImageJ^{TM} software [1-3].

As we mentioned above, PAD is applicable for on-site analysis. Therefore, there are much research have developed PAD for quantitative analysis of heavy metal ions in environmental water sample. The one of these metal ions which is necessary for monitoring is iron (Fe)

Fe is a transition metal ion which is toxic at high level. It can be accumulated in the human body via water consumption, leading to risk of cancer and diabetes. Also, Fe can damage the heart and liver [14]. Department of Health, Ministry of Public Health, and Industrial Estate Authority of Thailand limit the level concentration of Fe in drinking water and wastewater must be lower than 0.3 mg L^{-1} [15] and 10 mg L^{-1} [16], respectively. Unfortunately, the general methods for Fe monitoring in water are atomic absorption spectrometry (AAS) [17], inductively coupled plasma spectrometry (ICP) [18], mass spectrometry [19], electrochemistry [20, 21] and fluorometry. [22-25] Although these techniques provide high sensitivity and accuracy, they are tedious, complicated, and not portable for on-site analysis.

In this work, we have thus developed PAD as a portable device for determination of total Fe in water sample, integrated with standard addition method. The PAD is designed as the double layer platform, it is two pieces of rectangular filter paper (25 x 25 mm^2) which is parallel attached by two-sided mounting tape (2 mm

thickness). Each layer is patterned, locating the circle hydrophilic zone (Ø 10 mm) in the middle, whereas the outside area of circle is printed by black-colored ink and then painted with modified glue solution to create hydrophobic area. The double-layered PAD composes of top and bottom layer as use as filtration and detection layer, respectively. The bottom layer was prior immobilized with Bphen and then dropped the working standard of Fe (II), the red product was occurred. To determine the total Fe, the water sample was directly dropped onto the double-layered PAD at the top layer. The suspended particle of sample is filtered, then, the filtrate is penetrated to the bottom layer, Fe (II) in sample is reacted with Bphen and again formed the red product. Note that Bphen is very sensitive and selective for Fe (II) [26, 27]. Therefore, the sample must be pre-treated by hydroxylamine, to reduce Fe (III) to Fe (II), before determination. The red intensity of product on the bottom layer is captured by smartphone and then analyzed by ImageJ™ software for determination of Fe in water sample based on standard addition method.

The colored product on PAD can be not only measure the intensity by ImageJ™ software but also by the fluorometer [4-6] to achieve the higher sensitivity. However, PAD is opaque, it is not suitable for spectrophotometric techniques because of light lost scattering. Thus, the alternative material which is more transparent is therefore selected to develop as the analytical device.

BNC is a natural biofilm which is produced via bottom-up process [7], by sub-culturing a non-pathogenic bacterium, namely *Acetobacter xylinum* in glucose-containing medium. BNC is like a laboratory filter paper, but it is more transparent, because of its cellulose fibers [8]. Moreover, BNC shows some outstanding properties such as hydrophilicity, high mechanical stability, biocompatibility, and biodegradability [9]. BNC is widely used as bio-platform in various applications, for example, food packaging, biomedical material, cosmetic, electronic device [7] including optical material and sensor [8]. From our literacy, there are many publications reported use of BNC for quantitative analysis by spectrophotometer [54-60]. BNC is immobilized with specific reagent, then, the dopped-BNC was reacted with analyte in sample by dropping or incubating. Next, the reacted BNC was placed into sample compartment and detected. Remarkably, light loss scattering is not obtained like the detection on PAD, because BNC is transparent. Therefore, BNC is more interesting than PAD, in terms of optical detection by spectrophotometric techniques. Even there are large numbers

of publications using BNC as the analytical device for quantitative analysis, however, there are few publications, exploring the determination of heavy metal ions, contaminated in water sample.

Trivalent chromium Cr (III) is one of the contaminated heavy metal ions in natural water. Although it provides some positive effects to human health, it also causes harmful effect for living. Cr (III) is the transition metal ion which leads to mutation and cancer. [28,29] Department of pollution control has set the regulation limit of Cr (III) in wastewater from industry, must be lower than 0.25 mg L^{-1} [30]. Therefore, it is necessary to monitor the content of the Cr (III), contaminants in natural water samples. Detection of Cr (III) by instrumental methods, for example, AAS [31], ICP [32], electrochemistry [33], are still employed nowadays, because of its high sensitivity and accuracy, but they are complicated. It is essential to develop an analytical method/device which allows simple procedure with capability of portable. BNC is thus regarding challenging in terms of its benefits. To the best of our knowledge, there is no report using BNC for quantitative analysis of Cr (III) so far.

In this work, we present the simpler determination method, which is fluorometric detection, integrating with BNC. In recent years, there are large number of publications about determination of Cr (III) based on fluorometry using organic dyes as fluorescence sensor [34-40]. However, these publications carried out the detection in solution, the fluorescence quartz cell which is expensive and fragile. In contrast, BNC is more flexible but still transparent. So, we aimed to exploit BNC instead. The developed BNC is immobilized by a new fluorescein derivative (NFD) which is highly sensitive and selectivity fluorescence sensor toward Cr (III). The immobilized BNC was dropped with standard of Cr (III) under the optimal condition. Then, the reacted BNC was placed into sample compartment of fluorometer for detection. In the presence of Cr (III), the fluorescence light of NFD on BNC is quenched [41]. This effect is evaluated by fluorometer without any additional quartz cuvette. This phenomenon is applied to quantitative analysis of Cr (III) in water samples based on external calibration method.

Conclusively, in this work, we have developed two kinds of the cellulose-based analytical devices which are the double-layered PAD and the NFD-immobilized BNC for determination of total Fe and Cr (III) in water sample, respectively. In our study, both the devices show high analytical performances for individual metal ions determination including high sensitivity and selectivity, high accuracy, and precision.

More importantly, they can be applied to quantitative analysis of total Fe and Cr (III) in real water samples (drinking water, tap water, canal water and river water) with satisfied results.

1.2 Objectives of the study

1) To fabricate the double-layered PAD for quantitative analysis of total Fe.
2) To apply and validate the double-layered PAD for the colorimetric determination of total Fe in water samples.
3) To prepare the NFD-immobilized BNC as the 2D microcuvette for measurement of Cr (III).
4) To apply the NFD-immobilized BNC for the fluorometric determination of Cr (III) in natural water samples.

1.3 Scopes of the study

This thesis focuses on the development of the cellulose-based analytical devices for the determination of total Fe and Cr (III) in water samples by:

1) Fabrication of the double-layered PAD for Fe determination in water sample based on colorimetric detection by ImageJ™ software, using Bphen as the chromogenic reagent.
2) Preparation of the NFD-immobilized BNC for Cr (III) determination in natural water sample based on fluorometric detection by fluorometer, using NFD as the fluorescence sensor.

1.4 Benefits of the study

1) The double-layered PAD can be successfully applied to the quantitative analysis of total Fe in water samples with high analytical performances.
2) The NFD-immobilized BNC can be used as both analytical platform and optical sensing device instead of fluorescence quartz cell for the determination of Cr (III) in natural water samples with satisfied results.

Chapter 2
Theory and Literature Review

2.1 Paper-based Analytical Device (PAD) and Detection on PAD [61]

The paper-based analytical device (PAD) has been widely used in the analytical chemistry field because of its remarkable properties such as small device, low-cost, low volume of sample and reagent consumption, fast reaction, portable, biodegradable, and more importantly, the reaction on PAD can be carried out from capillary flow, it is not thus required the powered equipment. Therefore, PAD is thus applied to the various applications including, health diagnosis, environmental monitoring, food quality control, drug analysis, etc.

PAD is made of laboratory filter paper, patterned the hydrophilic and hydrophobic zone for specific detection. The hydrophobic zone was fabricated by the material which is waterproof such as wax, ink or some kind of polymer (polystyrene, polydimethyl siloxane (PDMS)). There are many fabrications techniques which are presented in nowadays as summarized in Table 2.1.

Table 2.1 Fabrication techniques of PAD and its hydrophobic materials.

Fabrication techniques	Hydrophobic material	Advantages	Disadvantages
Photolithography	- photoresist materials	sharp defined features, high resolution	Requires expensive equipment and reagents, complex steps
Screening	- wax - polystyrene	low cost, simple fabrication	low resolution, requires separate screens for different patterns

Table 2.1 Fabrication techniques of PAD and its hydrophobic materials (Cont'd).

Fabrication techniques	Hydrophobic material	Advantages	Disadvantages
Printing	- Wax - UV curable acrylates - customized ink	high throughput, customizable ink material	requires modification to the printer which often reduces the lifespan of the equipment
Stamping	- paraffin - commercial ink - polydimethyl siloxane (PDMS)	low cost, simple fabrication	low resolution, requires a specialized stamp for each pattern, inconsistent process, not suitable for mass production
Dipping	- wax	low cost, simple fabrication	low resolution, required a specialized mold for each pattern, not suitable for mass production
Drawing	- wax, - permanent marker - custom inks	low cost, simple fabrication, heating is not necessary for drawing with marker/custom ink	low resolution, inconsistent process, not suitable for mass production
Spraying	- commercial glue - lacquer	low cost, simple fabrication, better resistance toward organic solvents	low resolution, requires a custom magnetic mask for each pattern

The PAD is fabricated as the above techniques to allow the device for various detections. Generally, the detection on PAD is operated by dropping the specific reagent on the hydrophilic detection zone, then the target analyte is added to react

with the reagent, the product is occurred on PAD, it was further measured the interaction by the appropriate detection method.

There are many methods of detection on PAD, including colorimetry, fluorometry, electrochemistry or Raman scattering. These methods provide different analytical performances. Whatever, the selected method depends on sensitivity and behavior of the reaction on PAD. Nevertheless, the most popular detection method is image capturing. This method based on colorimetry so, it is noted that this method is prefer suitable for the colored-product reaction. In details, when the product is occurred on the PAD, it was then captured the image by camera or smartphone, then the image of product was analyzed the color intensity by software such as ImageJ™. The colored product was measured as red-green-blue (RGB) value which are different in each color shades. So, it is noted that this method is prefer suitable for the colored-product reaction.

2.2 Nanocellulose [62-67]

2.2.1 Cellulose and Nanocellulose

Cellulose is a natural biopolymer which is the most abundant in the world because it is the main component of plants. Dimension of plant cellulose can be classified as shown in Figure 2.1.

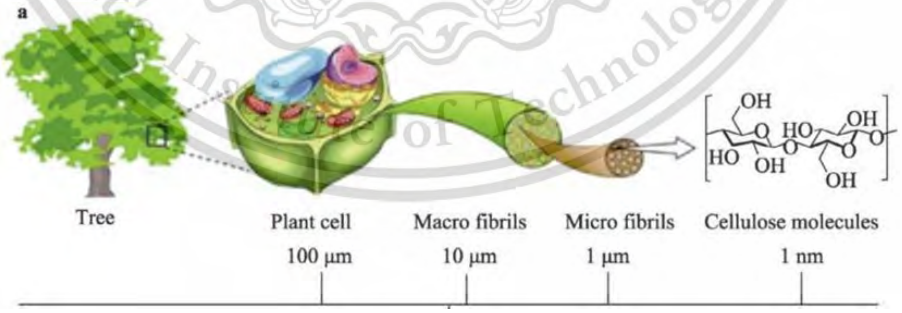

Figure 2.1 Cellulose in plants.

The chemical structure of cellulose is composed of large numbers of molecules of glucose, bounded with ß, 1-4 glycosidic bond, as a long chain. Each chain is bounded

as a larger molecule with hydrogen bond between hydroxyl (-OH) group of glucose as shown in Figure 2.2.

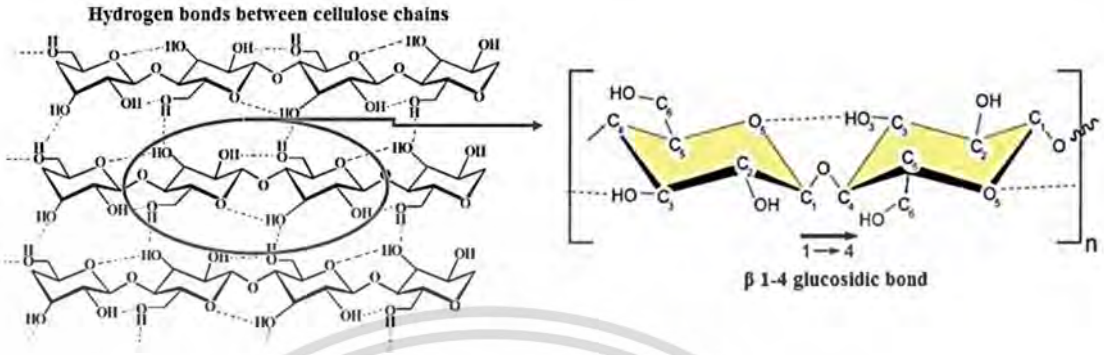

Figure 2.2 The chemical structure of cellulose.

Nanocellulose is cellulose chain whose dimensions are very small in nanometer. It is an interesting alternative material, because it is transparent, high mechanical strength, chemical stable, biocompatible and biodegradable. By these advantages, nanocellulose is thus applied with various fields of research, including medical profession, food industry and optical sensor development, etc.

2.2.1.1 Types of Nanocellulose

Nanocellulose is classified as 2 types, depending on process, and starting material for preparation.

1. Plant Nanocellulose (PNC)

Plant nanocellulose is prepared via 'top-down' process using plant as the starting material. They are classified as 2 types, depending on its morphology of cellulose fiber and preparation method.

1.1) Cellulose Nanocrystal (CNC), its fiber is crystalline region, like a stick. The average diameter of fiber is 5-70 nanometers, and the fiber length is in nanoscale. It is prepared by chemical methods such as acid-hydrolysis.

1.2) Cellulose Nanofiber (CNF), its fiber consists of crystalline and amorphous regions, like a bundle of fiber. The average diameter of fiber is 5-60 nanometers, and the fiber length is microscale. It is prepared by mechanical methods such as microfluidization.

2. Bacterial Nanocellulose (BNC)

Bacterial nanocellulose is prepared via 'bottom-up' process. The non-pathogenic bacteria are sub-cultured into the glucose-containing medium and is treated until nanocellulose fiber is achieved.

CNC, CNF, and BNC are nanocelluloses which are produced from plant or bacteria. Their properties are both similar and different, as summarized in Table 2.1.

Table 2.2 The properties of CNC, CNF, and BNC.

Properties	Types of nanocellulose		
	CNC	CNF	BNC
Crystallinity degree	54–88%	59–64%	65–79%
Degree of polymerization	500–15,000	≥500	800–10,000
Length of fibers	150–300 nm	85–225 nm	70–80 mm
Young's module	50–100 GPa	39–78 GPa	15–30 GPa
Density	1.6 g cm^{-3}	1.566 g cm^{-3}	1.5 g cm^{-3}
Purity	Low	Low	High

2.2.2 Preparation of Nanocellulose

Preparation of nanocellulose, from plant and bacteria, is explained in detail as the following issues:

2.2.2.1 Preparation of Plant Nanocellulose

Normally, the fiber of the plant is composed of cellulose, hemicellulose, and lignin. The purification of cellulose is necessary. Starting with treatment of plant by mechanical process, including milling, pulping, and bleaching, respectively. The

purified cellulose is obtained and is then ready to prepare CNC or CNF by specific individual process. The summary preparation process of plant nanocellulose is shown in Figure 2.3.

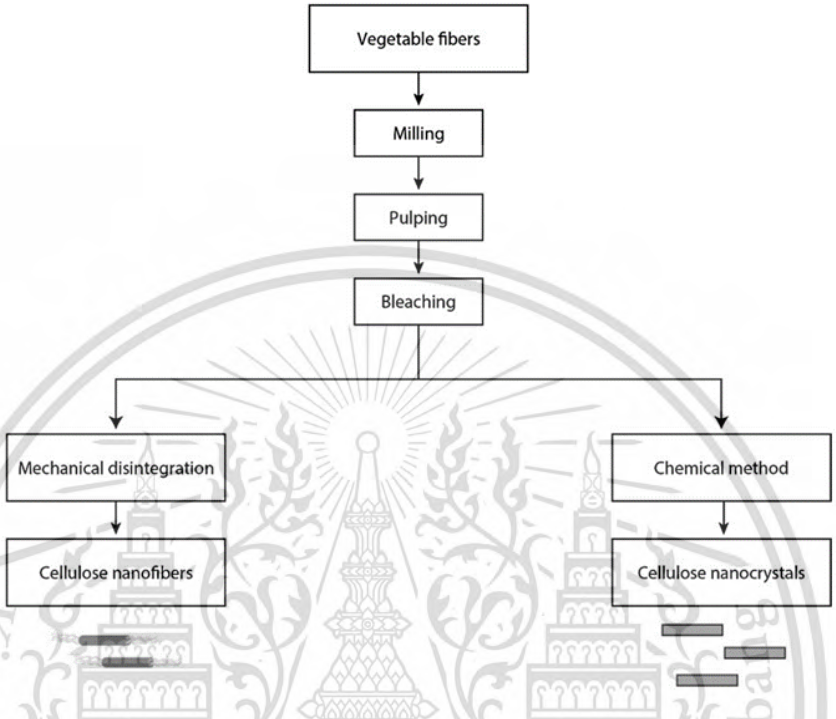

Figure 2.3 Summary of preparation process of plant nanocellulose.

Figure 2.3, demonstrating the preparation process of plant nanocellulose. Normally, the fiber of a plant is composed of cellulose, hemicellulose, and lignin. So, the purification of cellulose is necessary. Starting plant is treated by mechanical process, including milling, pulping, and bleaching, respectively. The purified cellulose is obtained and is then prepared to CNC or CNF by specific process.

2.2.2.2 Preparation of Bacterial Nanocellulose

The non-pathogenic bacteria namely, *Acetobacter xylinum* is sub-cultured into the glucose-containing medium and is treated under optimal time and temperature until the BNC is obtained. In detail, BNC can be occurred by 3 major processes as the following:

1) **Monosaccharide Activation** when the bacteria is treated with the cultured medium. Nucleotide is synthesized, this process activates synthesis of monosaccharide or glucose, within cytoplasm of bacteria.
2) **Polymerization** when the molecule of glucose is increased, they are bounded by ß,1-4 glycosidic bond to form the polymer chain of glucose. Next step, each chain is bounded as a network by hydrogen bonding between hydroxyl (-OH) group of glucose. The larger molecule becomes nanocellulose, eventually.
3) **Excretion** the bacteria excretes the produced nanocellulose out of its cell, into the cultured medium through its cell membrane. The excreted nanocellulose, which is multiplied, is form as the BNC film and then it is harvested to further specific application.

The above information is the preparation process of BNC in cellular scale. This process will be started after sub-culturing the bacteria into the medium. In the next topic, we will describe the method of sub-culturing, which is undergoing in nowadays, to obtain the BNC. There are 5 methods as listed below:

1) **Static Culture** the bacteria were sub-cultured into the medium which the container is static fixed under optimal environment. The bacteria are treated until the nanocellulose was achieved. The obtained nanocellulose is like a thin film, floating above the medium. It was harvested when the needed thickness was obtained. The remaining cultured medium was continued static fixed under optimal environment, the nanocellulose is afresh produced. This process is circular repeated until the bacteria become weaker, or the cultured medium is consumed till not existing. The process of static culture is shown in Figure 2.4.
2) **Static Intermittent Fed Batch Technology** the bacteria were treated until nanocellulose film was obtained, like the process of static culture. However, if the obtained nanocellulose is not harvested, the cultured medium will be added into the same container. When the bacteria are treated with a new batch of medium, the new nanocellulose film is

produced and is interposed with the prior one. The process will be circular until the number of nanocellulose film is enough. Thus, they were together harvested. The process of static intermittent fed batch technology is shown in Figure 2.4.

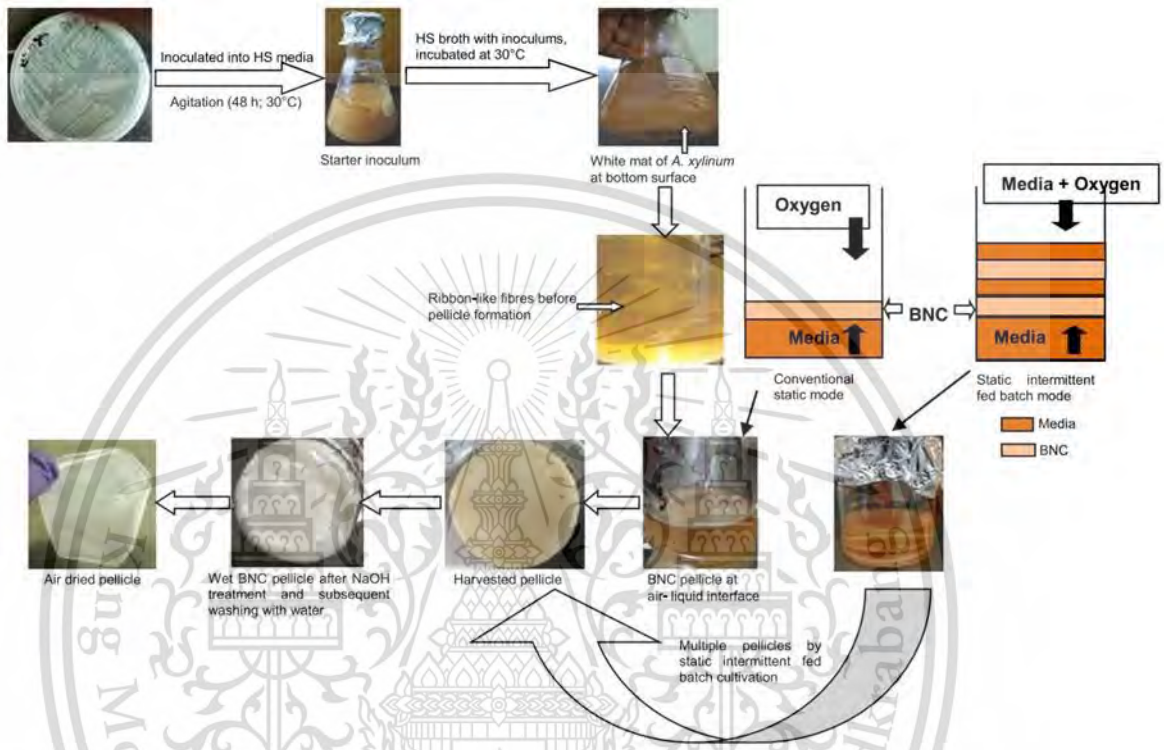

Figure 2.4 The process of static culture and static intermittent fed batch technology.

3) **Cell-free Extract Technology** after the bacteria is sub-cultured into the medium, it was then centrifuged. Bacteria is completely contacted with the medium. Next step, the small plastic beads were put into the sub-cultured medium and then stirred, resulting in the cell membrane of bacteria rupturing. The specific enzyme, which stimulates the production of nanocellulose, was then added together with a new batch of cultured medium. Nanocellulose was rapidly produced because the excretion process is not present in this method. The obtained nanocellulose from this method will be high quality and mass production. The process is summarized in Figure 2.5.

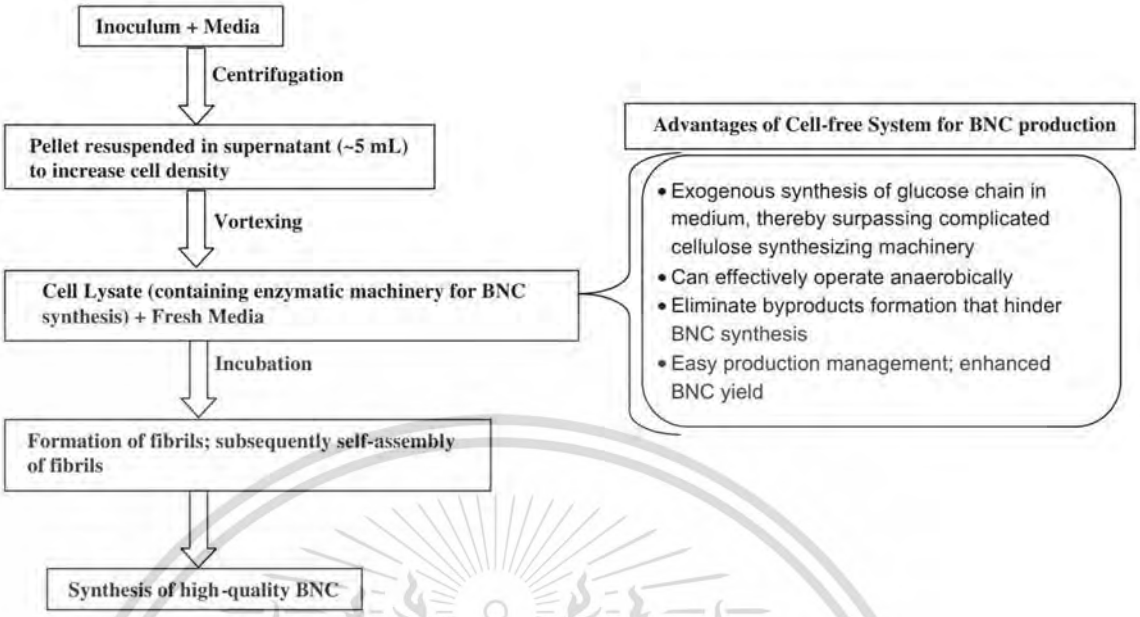

Figure 2.5 The process of cell-free extract technology.

4) **Agitated Culture** This process is like the static culture method. Nevertheless, the sub-cultured container is swirled in horizontal direction to allow bacteria to be completely contacted with the medium. This led to high mass production of nanocellulose.

5) **Bioreactor-based Production** this method is nanocellulose preparation using the bioreactor which there are 3 models as the following:

5.1) Stirred tank reactor the reactor is like the static culture and the agitated culture in larger scale. The preparation process is carried out by sub-culturing the bacteria into the bulky tank and stirring by the blade. The bacteria were treated until nanocellulose was achieved. The reactor is shown in Figure 2.6a.

5.2) Rotating disc reactor the reactor consists of rotating disc, the circle metal attached with membrane, located in the huge mirror box, the half volumes of the box were filled with the medium which has been already sub-cultured the bacteria. When the reactor is turned on, the rotating disc is rolled to contact with medium. The bacteria and medium are

dramatically diffused into the disc through the membrane. The bacteria are sufficiently contacted with the medium and air, leading to nanocellulose forming within the rotating disc. The obtained nanocellulose will be circular piece as big as the disc's size. The reactor is shown in Figure 2.6b.

5.3) Bioreactor with spin filter the reactor is the bulky tank, there is a small sieve in the tank for placing the membrane bag. The membrane bag is filled with the cultured medium. In sub-culturing procedure, the bacteria were treated in the tank filled with the cultured medium. The blade will be turned on for agitation to allow the bacteria to be completely contacted with the medium. When the nanocellulose was achieved, the medium in the tank decreased. This resulted in the medium in the membrane bag is thus diffused to compensate the consumed medium. The bacteria were continuously fed with the medium to produce a fresh nanocellulose. The reactor is shown on Figure 2.6c.

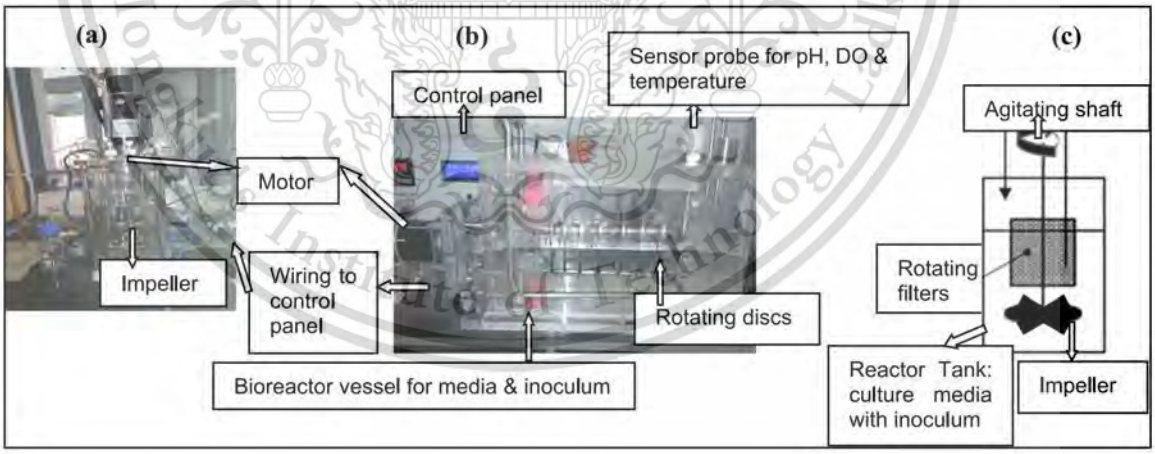

Figure 2.6 The reactor for preparation of bacterial nanocellulose by the bioreactor-based production method.

2.2.3 Application of Nanocellulose

The nanocellulose, produced by plants and bacteria, demonstrate the outstanding properties as mentioned above. Therefore, they were applied in research in various fields as listed below:

2.2.3.1 Medical Profession

Since nanocellulose is biocompatible, flexible, high mechanical strength and chemical stable. Therefore, many publications thus use it as the material for production of artificial organs for human such as bone and ears. Moreover, nanocellulose was produced as the bio scaffold network for adhesion of bone and tissues formation. The interesting application is using nanocellulose as wound dressing because it can well adsorb water, leading to dried wound, also it can gently cover the wound and is not adhere the wound. The examples of these applications are shown in Figure 2.7 and 2.8.

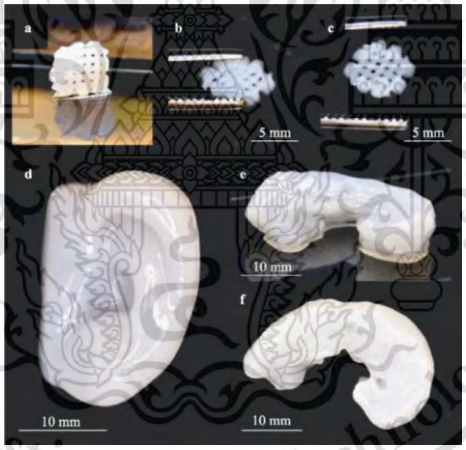

Figure 2.7 Artificial organs, produced by nanocellulose.

Figure 2.8 Wound dressing, produced by nanocellulose.

2.2.3.2 Food Industry

Nanocellulose is flexible, biodegradable, and heating resistant, it can be thus applied as food packaging, instead of plastic packaging, to save the environment. Meanwhile, it still can be developed as smart food packaging. There are some publications, applied nanocellulose as a smart food packaging. Interestingly the package is immobilized with anti-bacteria agent to protect the package from bacteria which can be adhered to during transportation. Another application, the packaging is stuck with the silver nanoparticle-immobilized nanocellulose for using as the spoilage (ammonia) gas sensor. The ammonia gas occurs when the food is spoiled. After the silver nanoparticles are exposed to ammonia, its color is changed from brown to yellow, indicating the food is rancid. This application is shown in Figure 2.9.

Figure 2.9 The silver nanoparticle-immobilized nanocellulose is used as the ammonia gas sensor to indicate the spoiled food.

2.2.3.3 Optical Sensor Development

Transparency is the remarkable property of nanocellulose. Thus, it was therefore developed as the optical sensor by immobilization of specific reagent with target analyte, after the immobilized nanocellulose react with the target one, it was then detected by spectrometric method. The immobilized nanocellulose can be used instead of cuvette accompanied with the spectrometer, well.

2.2.4 Preparation of the Immobilized Bacterial Nanocellulose

In this work, nanocellulose produced by bacteria was used as an analytical device. As we described above, the bacterial nanocellulose must be first immobilized with the specific reagent, it was thus applied as the analytical device for some target

analyte. So, in this topic, we thus explained about preparation of the immobilized BNC to inform the method as presenting in nowadays. There are two methods for preparation as listed below:

2.2.4.1 In-situ Method

The specific reagent was added into the cultured medium containing the bacteria. The bacteria were treated together with the reagent under the optimal condition. Finally, the immobilized BNC is obtained. This process is demonstrated in Figure 2.10.

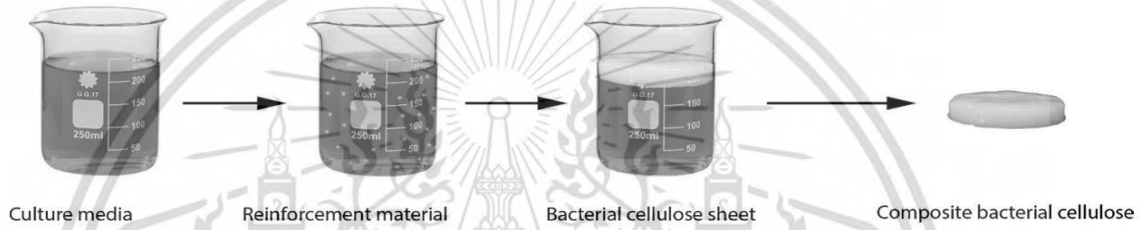

Figure 2.10 In-situ synthesis.

2.2.4.2 Ex-situ Method

This method, the BNC and the specific reagent were individually prepared. When both are ready, the BNC was soaked in the reagent solution under optimal condition. The reagent will be diffused into the BNC until steady. Eventually, the immobilized BNC was achieved. This process is shown in Figure 2.11. It is noted that this method is employed for preparation of the immobilized BNC in this work.

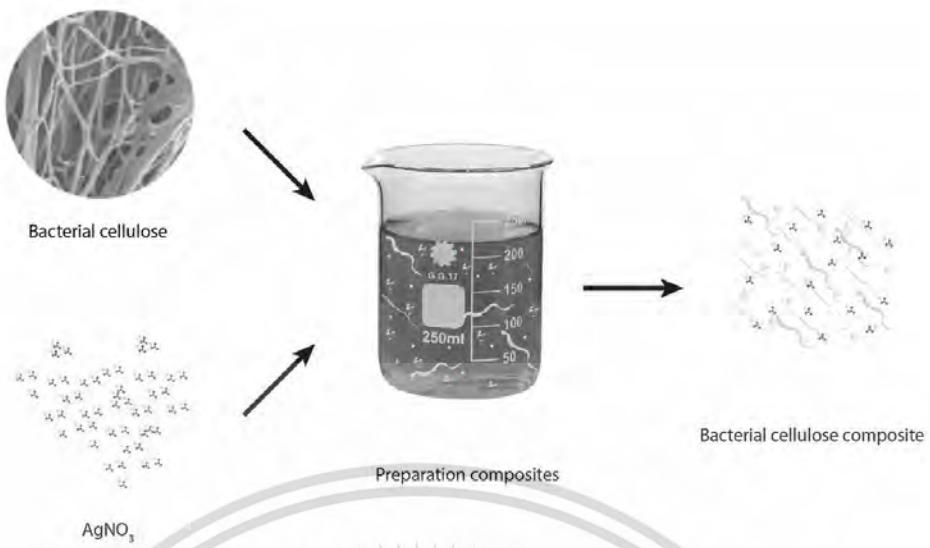

Figure 2.11 Ex-situ synthesis.

2.3 Principle of Fluorescence

Fluorescence is the emission process of the molecule. When the molecule is excited with the photon, it is transferred from ground state to the excited state. However, it is not stable, the molecule then returns to the ground state by emitting the energy which are both radiative and non-radiative process. The emission process can be described in Jablonski's diagram as shown in Figure 2.12.

2.3.1 Jablonski's Diagram [65]

Energy transitions are shown on Jablonski diagrams using either straight or wavy arrows. Radiative transitions (such as absorption and fluorescence) are shown with straight arrows, while non-radiative transitions (such as internal conversion and intersystem crossing) tend to be depicted as wavy arrows.

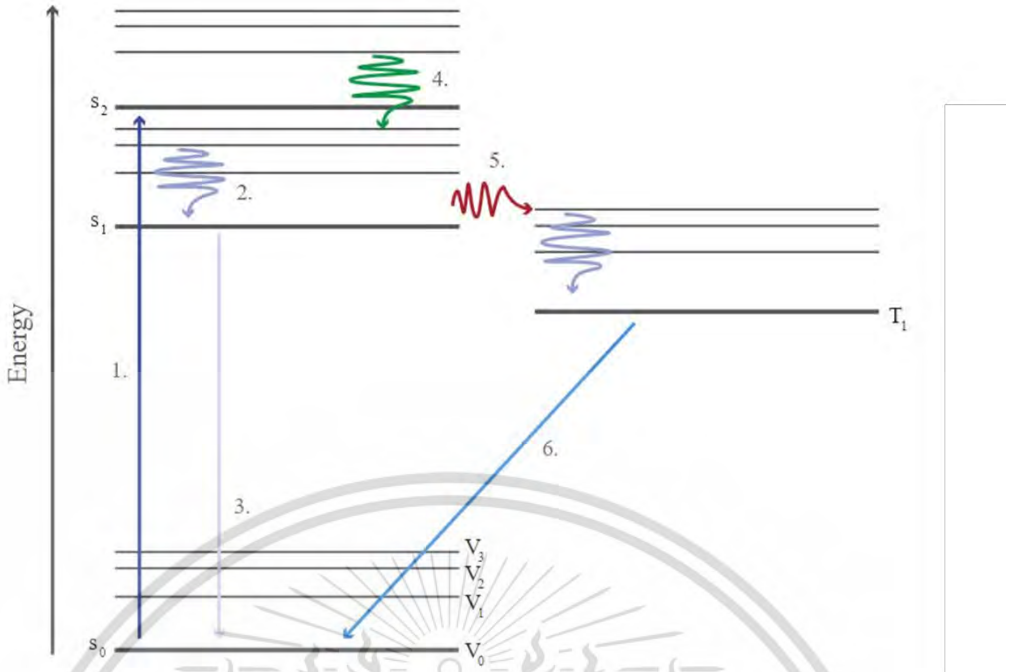

Figure 2.12 Jablonski Diagrams with types of transition: (1) Absorption, (2) vibrational relaxation, (3) fluorescence, (4) internal conversion, (5) intersystem crossing and (6) phosphorescence.

In a Jablonski energy diagram, bold lines represent the base energy of each state (v_0), with additional vibrational energy states in lighter grey lines above this (v_1, v_2, $v_{3, etc}$). The ground state is represented as S_0 as spin angular momentum $S=0$ in the ground state. When an electron enters an excited state, it can have different spin multiplicity, depending on if total spin angular momentum has been conserved. If spin has been conserved, this is a singlet excited state (S_1). However, if angular momentum is not conserved, then the electron enters a triplet energy state (T_1). The excited singlet and triplet states are represented in Jablonski diagrams with different columns, as shown in the diagram above.

In the Jablonski diagram above, six different types of transitions are described as the following list:

2.3.1.1 Absorbance

This represents the absorbance of a photon by an electron. The energy of the photon is high enough that the electron can be excited into a higher energy state.

Absorption between energy levels can be explored with optical spectroscopy if this transition energy is between 1.1 - 3.8 eV.

2.3.1.2 Vibrational Relaxation

This is a non-radiative loss of energy between vibrational energy levels. This excess vibrational energy is lost as kinetic energy to other vibrational modes, either of the same molecule or of a different molecule. This energy is loss happens very rapidly (10^{-14} - 10^{-12} seconds) and is often measured using Raman spectroscopy or IR spectroscopy.

2.3.1.3 Fluorescence

Fluorescence is a type of photoluminescence in which the spin state of the electron relaxes back into the ground state, and a photon is emitted. It is represented on a Jablonski diagram by a straight line. The spin state of the electron stays the same from the excited state to the ground state, so this is a singlet-singlet transition ($S_1 \longrightarrow S_0$). This is an allowed transition, so fluorescence often occurs a very short time after the electron is excited. Fluorescence can be measured with optical spectroscopy if this transition energy is between 1.1 - 3.8 eV.

2.3.1.4 Internal Conversion

Internal conversion is a type of non-radiative emission, where an electron moves from a higher energy excited state to a lower energy excited state. This occurs when the vibrational modes of different electronic levels overlap. No photon is emitted, and the electrons spin state remains the same throughout the transition.

2.3.1.5 Intersystem Crossing

Intersystem crossing is another form of non-radiative emission. Unlike internal conversion, the spin state of the excited electron changes. The Jablonski diagram above shows an electron moving from the excited singlet state (S_1) into the excited triplet state (T_1). Often intersystem crossing results in phosphorescence emission.

2.3.1.6 Phosphorescence

Phosphorescence is a type of fluorescence in which an electron relaxes into the ground state via emission of a photon. However, unlike in fluorescence, the electron must change spin states for this to occur. This is a forbidden transition, so happens over a much longer time scale. Phosphorescence can be measured with optical spectroscopy if the transition is between 1.1 - 3.8 eV.

2.3.2 Instrumentation of Fluorometer [66]

The radiative process as fluorescence is measured by fluorometer, the instrumentation consists of 4 sections as describe:

2.3.2.1 Light Source

The popular light source is Xenon lamp and Mercury arc lamp because of its high intensity, leading to high sensitivity.

2.3.2.2 Monochromator

The diffraction grating is used as monochromator to select the specific wavelength. There are two monochromators in fluorometer, namely excitation monochromator and detection monochromator, they are used for selection of the excitation and emission detection wavelength, respectively.

2.3.2.3 Cuvette

The plastic cuvette cannot be accompanied by the fluorometer, only quartz cuvette is required for fluorometric detection, because the excitation wavelength is almost used in UV range. Therefore, plastic which can absorb the UV light, is not thus employed.

2.3.2.4 Detector

The photomultiplier tube (PMT) is widely used as detector in fluorometric detection because the signal must be amplified to obtain the high sensitivity.

Typically, the light source of fluorometer is in right angle (90°) with the detector as Figure 2.13.

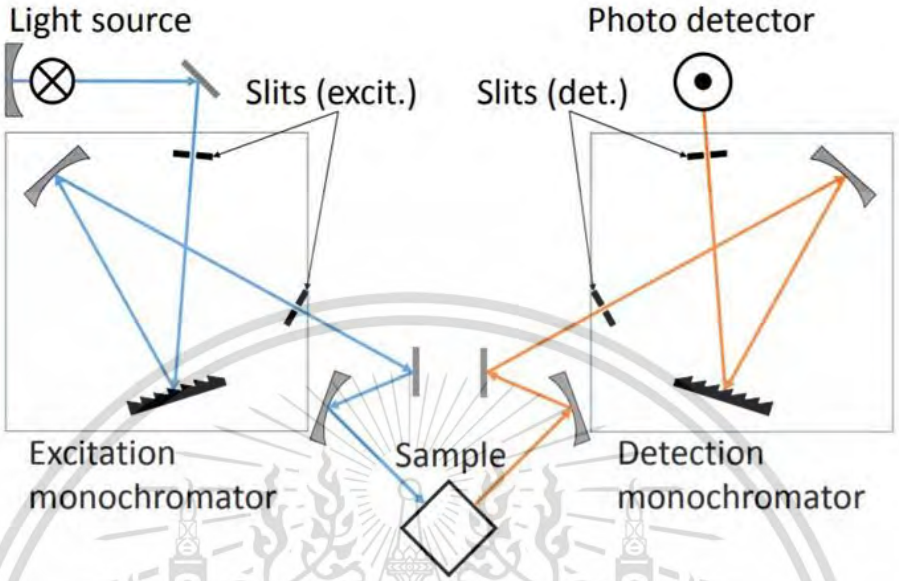

Figure 2.13 Instrumentation of fluorometer.

2.3.3 Fluorescence Sensor [46]

Fluorescence sensor is a substance molecule, which is used for detection of specific analyte such as metal ions, non-metal ions, gas, biomolecules, etc. The fluorophore in the sensor can emit the fluorescence light and can be changed after interacted with the target analytes. The fluorescence sensor is classified as 3 types, depending on interaction with the analyte, as the following list:

2.3.3.1 No Association Fluorophore

The fluorophore sensor collided with the target analyte, leading to loss of energy of fluorophore. The original high fluorescence intensity of fluorophore is thus reduced. The mechanism is shown in Figure 2.14.

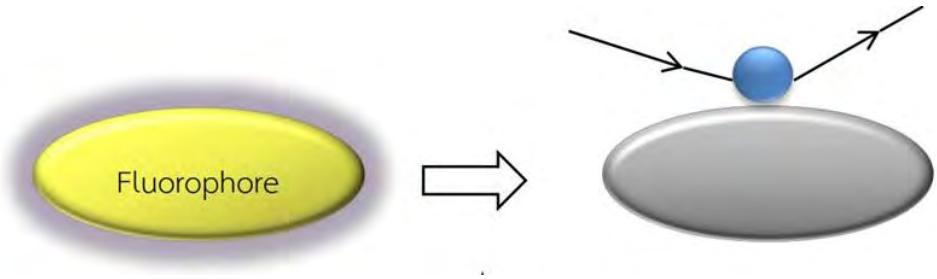

Figure 2.14 The molecule of fluorescence sensor in type of no association fluorophore.

2.3.3.2 Complexing Fluorophore

The fluorophore is formed by the chelating complex with the target analyte. This reaction can be reversed. When the complex occurs, the fluorescence intensity is changed, it may be decreased or increased. These phenomena are indicated as chelating enhancement of quenching (CEQ) and chelating enhancement of fluorescence (CEF), respectively. The phenomenon is illustrated as Figure 2.15.

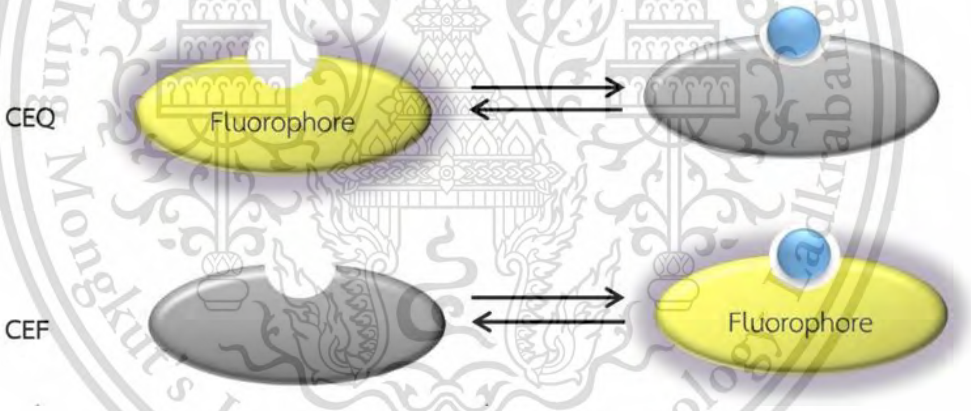

Figure 2.15 The molecule of fluorescence sensor in type of complexing fluorophore.

2.3.3.3 Fluorophore Linked to a Receptor

This type, the sensor is designed as the fluorophore linked with the receptor. Some design, the fluorophore may be linked with the receptor via spacer. When the receptor is bound with the target analyte, the fluorescence intensity of fluorophore in changed through the chemical process, such as electron transfer, charge transfer, energy transfer, exciplex formation, etc. The changing of fluorescence can be like CEQ or CEF process. The mechanism of interaction is shown in Figure 2.16.

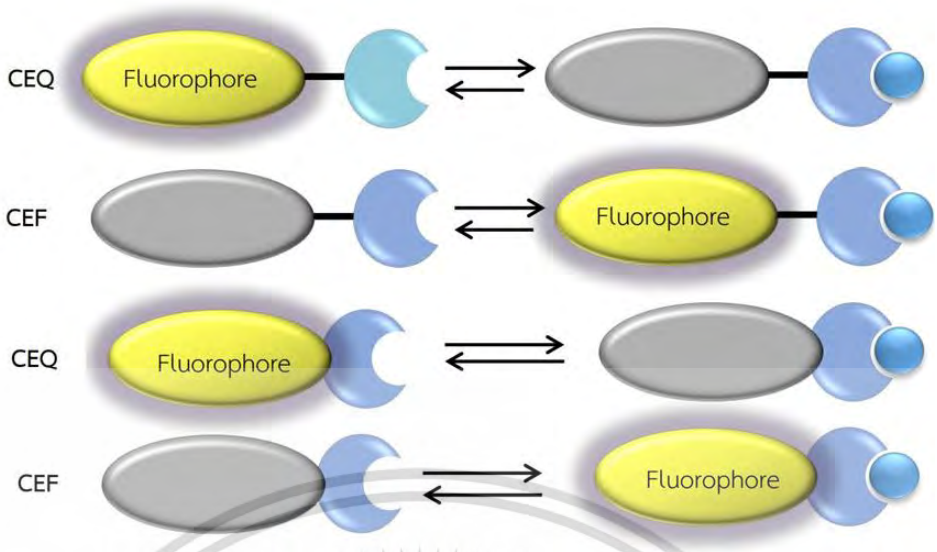

Figure 2.16 The molecule of fluorescence sensor in type of fluorophore linked to a receptor.

2.3.4 Fluorescence Quenching [67]

2.3.4.1 Static quenching

Static quenching occurs from complex formation between fluorophore (F) and the target analyte which is quencher (Q) in the ground state. This complex cannot emit fluorescent light. This causes the number of free fluorophores which will be excited to the excited state to decrease, leading to less fluorescence light. The static quenching process in shown in Figure 2.17.

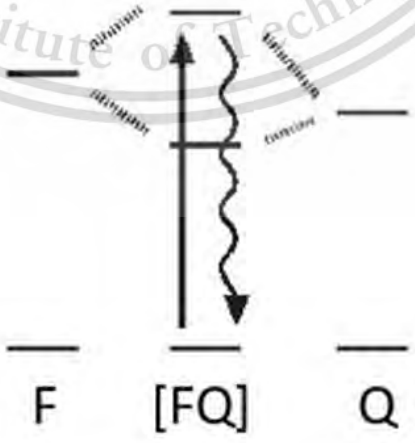

Figure 2.17 Static quenching process.

2.3.4.2 Dynamic Quenching [68]

Dynamic quenching occurs from interaction between fluorophore and quencher, such as halogen atom, metal ions, biomolecules, etc. in the excited state. This led to the number of free fluorophores which will be deactivated to the ground state, decreasing, leading to less fluorescence light. The dynamic quenching is described as minor mechanism:

1) Intersystem Crossing or Heavy Atom Effect

Quenching by heavy atoms halogens and oxygen is thought to occur by intersystem crossing. An encounter with a heavy atom or a triplet oxygen molecule is thought to cause the excited singlet state to become an excited triplet (Figure 2.18). Since the triplet states are usually long lived and quenched by oxygen, they are likely to be quenched to the ground state by the same quencher or return to the ground state by non-radiative decay. It is not always clear which mechanism is dominant. Various reports have suggested oxygen quenching occurs by mixed mechanisms that include intersystem crossing, charge transfer, and electron exchange. Depending upon the structure of the fluorophore, quenching by halogens has also been attributed to charge transfer, intersystem crossing, and/or electron exchange. In general, it seems that halocarbons quench by intersystem crossing and halides quench by charge transfer. Additionally, many fluorophores undergo photo destruction in the presence of halocarbons.

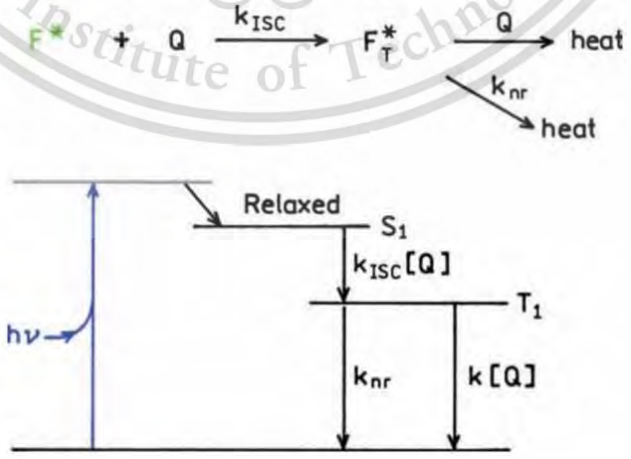

Figure 2.18 Quenching by intersystem crossing.

2) Electro Exchange or Dexter Interaction

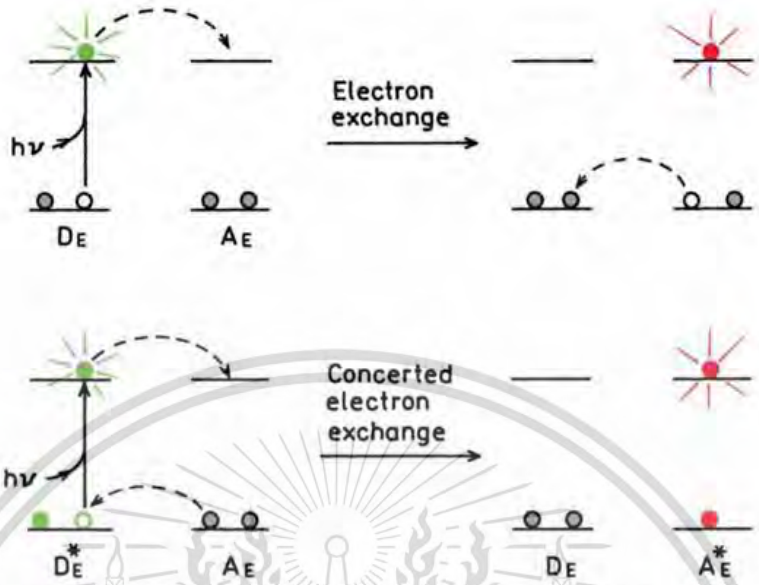

Figure 2.19 Schematic for stepwise (top) or concerted (bottom) electron exchange.

Figure 2.19 shows a schematic for the electron exchange or Dexter interaction. This interaction occurs between a donor D_E and an acceptor A_E, where E indicates electron exchange. The excited donor has an electron in the LU orbital. This electron is transferred to the acceptor. The acceptor then transfers an electron back to the donor. This electron comes from the HO orbital of the acceptor, so the acceptor is left in an excited state, leading to the fluorescence light is not occurred. Note that the mechanism process can occur as both stepwise electron exchange and concerted electron exchange.

3) Photoinduced Electron Transfer or PET

The third mechanism for quenching is photoinduced electron transfer (PET). In PET a complex is formed between the electron donor D_P and the electron acceptor A_P, yielding $D_P{}^+A_P{}^-$ (Figure 2.20). The subscript P is used to identify the quenching as due to a PET mechanism. This charge transfer complex can return to the ground state without emission of a photon, but in some cases exciplex emission observed. Finally, the extra electron on the acceptor is returned to the electron donor. The terminology for PET can be confusing because the excited fluorophore can be either the electron

donor or acceptor. The direction of electron transfer in the excited state is determined by the oxidation and reduction potential of the ground and excited states. When discussing PET, the term donor refers to the species that donates an electron to an acceptor.

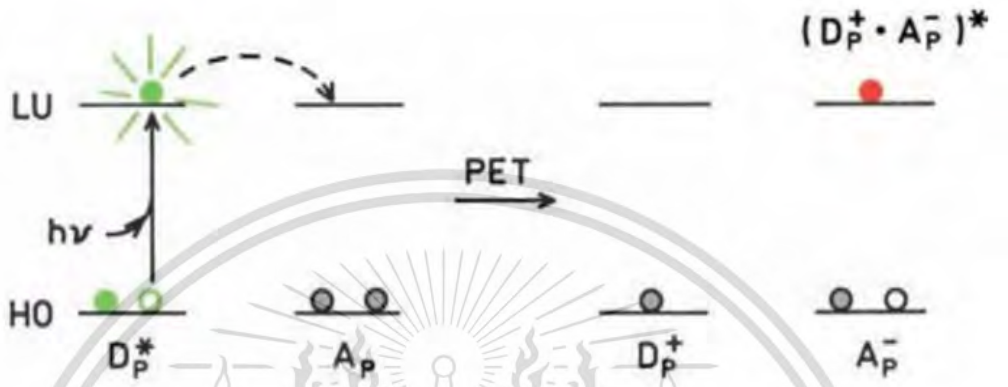

Figure 2.20 Molecular orbital schematic for photoinduced electron transfer.

2.3.4.3 Stern-Volmer's Equation [69]

Stern-Volmer's equation can be described about fluorescence quenching effect, which is resulted from concentration of fluorophore, quencher. The quenching effect can be described from this relationship of the following equation:

Assign to $[M]$ is the concentration of fluorophore in the ground state.

$[M^*]$ is the concentration of fluorophore in the excited state.

$[Q]$ is the concentration of quencher in the ground state.

when $[M]$ is excited by photon, can occur the possible photo-interaction as:

Photo excitation	$M \rightarrow M^*$	$k_{abs}[M]$
Fluorescence	$M^* \rightarrow M$	$k_f[M^*]$
Non-fluorescent relaxation	$M^* \rightarrow M$	$k_{nf}[M^*]$
Quenching	$M^* + Q \rightarrow M + Q$	$k_q[M^*][Q]$

When k is rate constant of each photo-interaction

Normally, the concentration of fluorophore in one experiment is constant.

$[M]$ Constant and $I_{abs} = k_{abs}[M]$, leading to the equation 1.

$$\frac{\partial[M^*]}{\partial t} = I_{abs} - (k_f + k_{nf} + k_q[Q])[M^*] \quad (1)$$

In the absence of quencher $[Q] = 0$ is

$$\frac{\partial[M^*]}{\partial t} = I_{abs} - (k_f + k_{nf})[M^*] \quad (2)$$

When the concentration of fluorophore is constant, resulting in the concentration of fluorophore which is excited by photon, is similarly constant. So, $[M^*]$ constant, leading to $\frac{\partial[M^*]}{\partial t} = 0$, when the equation 3 is considered, which describe about fluorescence quantum yield.

$$\Phi = \frac{Number\ of\ emitted\ photons}{Number\ of\ absorbed\ photon} = \frac{Rate\ of\ emission}{Rate\ of\ absorpsion} \quad (3)$$

As we well recognize that, rate of absorption is $I_{abs} = k_{abs}[M]$ Meanwhile, rate of emission is $k_f[M^*]$ when they replace into the equation 1 and 2. The equation 4 and 5 is observed, which explain about quantum efficiency in the presence and absence of quencher, respectively

$$\Phi_Q = \frac{k_f}{k_f + k_{nf} + k_q[Q]} \quad (4)$$

$$\Phi_0 = \frac{k_f}{k_f + k_{nf}} \quad (5)$$

The ratio of the quantum yields is equal to the ratio of the observed emission intensities without and with the quencher molecules:

$$\frac{I_0}{I_Q} = \frac{\Phi_0}{\Phi_Q} = \frac{k_f + k_{nf} + k_q[Q]}{k_f + k_{nf}} = 1 + \frac{1}{k_f + k_{nf}} k_q[Q] \quad (6)$$

Inserting the fluorescence decay relationship in the absence of the quencher molecules ($k_f + k_{nf} = \frac{1}{\tau}$). we thus obtain the result as the equation 7 (also known as Stern-Volmer's equation):

$$\frac{I_0}{I_Q} = 1 + \tau k_q[Q] \qquad (7)$$

2.4 Detection Principle in This Work

For the detection of Fe (II), Bphen was employed as the specific reagent. Bphen can be selectively formed the stable red complex product with Fe (II) by the mole ratio of Fe (II) to Bphen as 1:3. This reaction can be detected by colorimetry and naked eyes. The mechanism is shown in Figure 2.21

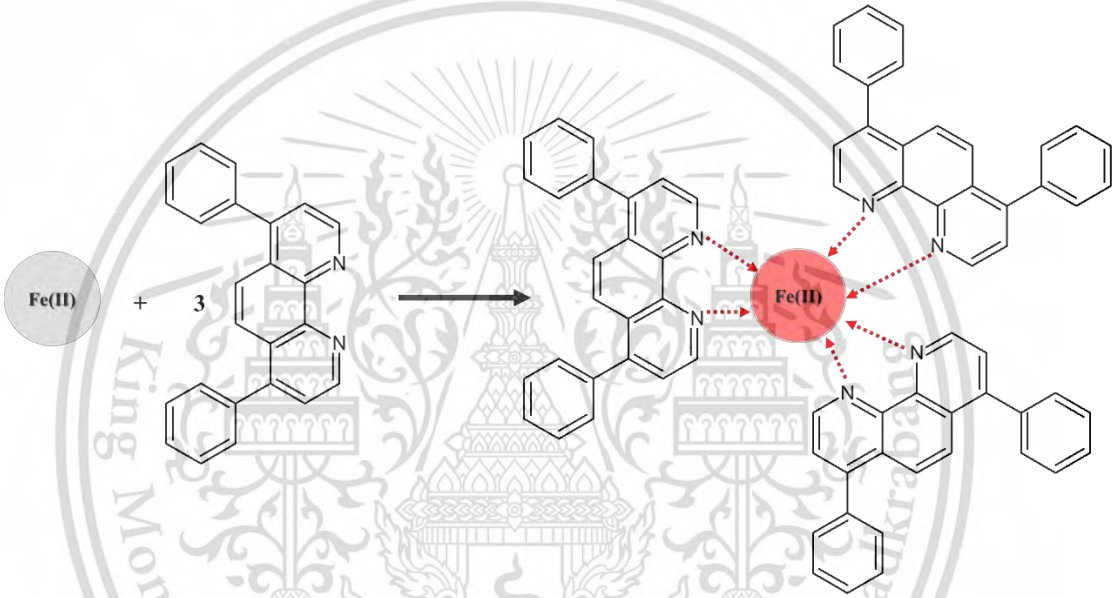

Figure 2.21 The mechanism of complex formation between Fe (II) and Bphen.

For the detection of Cr (III), a new fluorescein derivative (NFD) was used as the specific reagent. NFD can be selectively quenched the fluorescence intensity by Cr (III) via static quenching mechanism. The mole ratio of interaction between Cr (III) to NFD as 1:2. This interaction can be measured by fluorometry. The mechanism is shown in Figure 2.22.

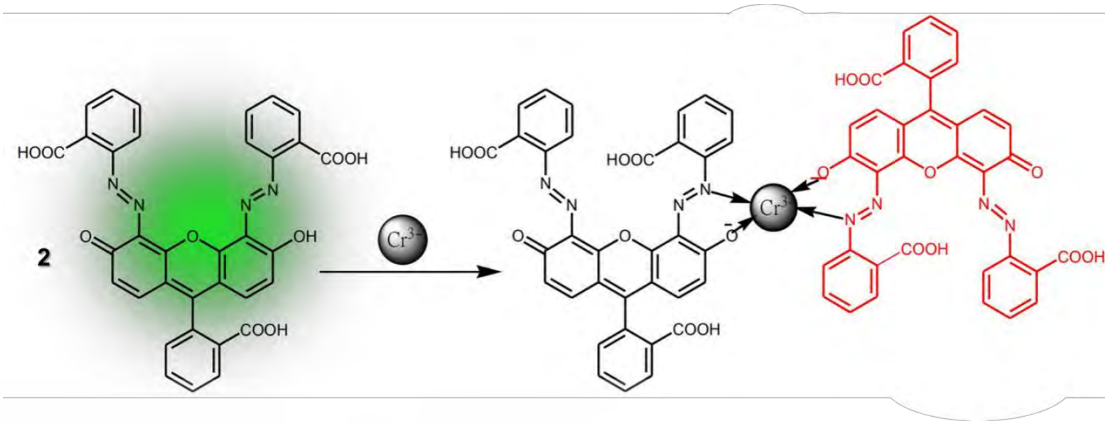

Figure 2.22 The mechanism of complex formation between Cr (III) and NFD.

2.5 Literature Reviews

2.5.1 Determination of Fe

2.5.1.1 Instrumental Method

Yaman, M. et al. [17] have developed a method for speciation and separation of Fe (II) and Fe (III) using solvent extraction technique. The extracted Fe (II) and Fe (III) was determined by flame atomic absorption spectrometry. PAN was employed as complexing agent for Fe (II) and chloroform was used as organic solvent. The Fe (II)–PAN complex was extracted into chloroform phase, leading to the remaining Fe (III) in water phase. The developed method was applied to the determination of Fe (II) and Fe (III) in tea infusion, fruit juice, cola and pekmez. The method is sensitive, simple and need the shorter time in comparison with other similar studies.

Proch, J. et al. [18] report high performance liquid chromatography (HPLC), coupled to either microwave induced plasma optical emission spectrometry (MIP OES) or inductively coupled plasma optical emission spectrometry (ICP OES). A cation–exchange column and a mobile phase based on pyridine–2,6–dicarboxylic acid (PDCA) were employed to separate Fe (II) and Fe (III) within 300 s. The applicability was presented with different sample matrix types: post–glacial sediments, archaeological pottery, soils located in the proximity of industry wastes disposal site, river sediments and yerba mate *(Ilex paraguariensis)*. Obtained results were compared in terms of the excitation source (microwave induced or inductively coupled) and supplied gas (nitrogen or argon). The research introduces HPLC–MIP OES for iron speciation analysis and its applicability were critically evaluated with HPLC–ICP OES.

Okabe, S. et al. [19] present characterization and determination of Fe (II) co-existing with Fe (III) using a simple method of electrospray ionization mass spectrometry (ESI-MS). 1,10-Phenanthroline forms stable tetrahedral complexes with Fe (II) in the gas phase of ESI-MS which is observed in a high-*m/z* region and are well separated. The method is extended for determining Fe (II) concentration in natural river water samples by measuring the peak intensity of $[Fe(phen)_2]^{2+}$ (*m/z* 208) and obtaining a calibration curve (R^2 = 0.9992) of the peak intensity. The Fe (II) concentrations in Tama River samples were obtained by the standard addition method (Fe (II) 0.23 μmol/L, R^2 = 0.9998), and total concentration of iron in Tama River sample was 0.59 μmol/L (ICP-MS), thus about 40% of iron is present as Fe (II).

Ugo, P. et al. [20] examined the possibility to combine potentiometric and voltametric measurements, in order to determine the concentration and information on the redox state of electroactive ions even when they are present at trace (submicromolar) concentration levels. As a model case, the speciation of iron (II) and iron (III) is studied both for the cations Fe (II) and Fe (III) and for the anions $Fe(CN)_6^{4-}$ and $Fe(CN)_6^{3-}$. For the first situation, electrodes coated with Nafion are employed while for the latter electrodes coated with the anion exchanger Tosflex are examined. The ratios between oxidised and reduced species are measured at trace levels. Relevant equations ruling the potentiometric responses at the coated electrodes have been derived by proper adjustment of the Nernst equation. Ion-exchange voltammetry at the coated electrodes allowed the measurement of parameters, such as ion-exchange distribution coefficients, which are relevant for the experimental testing of the suitability of these equations. Voltammetry at the coated electrodes also allowed the sensitive determination of the total concentration of both ions of the same redox couple. The applicability of the method for practical purposes has been checked determining redox potential and concentration profiles for iron and reduced sulphur species in the pore-waters of sediments.

Dieker, J. W. et al. [21] describes the flow injection analysis for the simultaneous measurement of Fe (II) and Fe (III) by amperometric detection. The flow-through cell contains a glassy carbon electrode. Selection of the appropriate voltammetric technique, choice of the indication potentials, sample size, composition of the carrier stream, etc., are discussed. The limit of determination is about 10^{-6} M; the calibration curves are linear in the concentration ranges 10^{-3}–10^{-5} M for Fe (III) and

5×10^{-4}–10^{-5} M for Fe (II). To illustrate the potentialities of the proposed method, standard rocks have been analyzed.

2.5.1.2 Fluorometry and Colorimetry

Gong, X. et al. [22] synthesized an oxadiazole-based chemosensor (sensor 1) for Fe (III)/Fe (II) detection. Sensor 1 displayed fluorescence quenching response towards Fe (III) and Fe (II) with high selectivity and sensitivity over all other metal ions. Job's plot, mass spectra, DFT calculation and fluorescence titration disclosed that fluorescence quenching was caused by forming 1:1 complex between sensor 1 and iron ions. Sensor 1 presented highly sensitive fluorescence response. Its fluorescence intensity showed linear relationship with the concentration of iron ion. The lower detection limit is observed as 7.78 μM for Fe (II) ion and 6.95 μM for Fe (III) ion, respectively. Sensor 1 can be used as test strips to detect iron ions in water samples. Fluorescence cell imaging also demonstrated sensor 1 can recognize iron ions in living cells.

Iqbal, A. et al. [23] explained a new kind of convenient, low-cost, environmentally friendly, and simple one step synthetic route for the preparation of C-dots-based CDs (CA + Phen) fluorescent turn-off selective probe for Fe (II) and Fe (III). Under optimal condition, Fe (II) and Fe (III) achieve the detection limit as low as 20 nM and 35 nM, respectively. The CDs (CA + Phen) exhibited a low cytotoxicity and could label the HK-2 cells. Additionally, this CDs (CA + Phen) has been successfully applied for the determination of Fe in milk. Endowed with relatively high sensitivity and selectivity, the sensor holds the potential to be applied for the detection of Fe (II) and Fe (III) in aqueous media.

Lv, P. et al. [24] prepared the novel carbon dots (CDs) doped lanthanide coordination polymers (LnCPs) for fluorescence ratio-metric measurements of Fe (II) and Fe (III). Herein, blue-light emitting CDs, as the Fe (III)-sensitive probe, were incorporated into the Fe (II)-sensitive LnCPs through the self-adaptive ability. The obtained composite probe can be efficiently excited at a single wavelength and shows good separate emission peaks. Under the reduction capability of ascorbic acid (AA), which can reduce Fe (III) to Fe (II), this composite probe enabled ratio-metric determination of AA. The rational design strategy for multi-analyte assay, and the facile

preparation and operation make the method possible for simultaneous monitoring two or more relevant analytes.

Senanayake, D. A. K. et al. [25] reported the application of bathophenanthroline (BPhen) as the fluorescence sensor for selective detection of Fe (II). Under optimal condition, the quenching effect of Bphen in the presence of Fe (II) is obtained with the good analytical performances, the LOD of 19 nM and the linear range of 63 nM – 224 nM with r^2 = 0.9919 are achieved. This revealed that this method is highly sensitive, and it can be applied for quantitative analysis of Fe (II).

Perry, R. D. et al. [26] demonstrated use of Bphen to form a red complex with Fe (II) and apply to the colorimetric determination of total iron at low molarities in aqueous solutions. The reduction of Fe (III) ions is necessary for these determinations using L-ascorbic acid. Under optimal condition, the satisfied result of the determination is obtained.

2.5.1.3 Paper-based Analytical Device

Ferreira, F. T. S. M. et al. [27] presented a PAD for the qualitative analysis of iron in urine samples. The colorimetric reaction between Fe (II) and Bphen is employed as the detection principle. The iron in sample must be reduced as the Fe (II) form with hydroxylamine. The developed μPAD shows the iron determination in the range 0.07–1.2 mg/L, with a limit of detection of 20 μg/L and a limit of quantification of 65 μg/L, Moreover, the accuracy of the developed device was investigated by analyzing urine samples with the PAD and validating with the AAS method; the relative deviation between the results of two method was lower than 9.5%.

Mentele, M. M. et al. [47] fabricated PAD by wax printing to detect the metal-containing aerosols. This method employs rapid digestion of metals by adding acid to a punch, leading to air sampling filter. Punches were put on a PAD; the digested metals were moved to detection reservoirs using the water as carrier. These reservoirs were immobilized the reagents for colorimetric detection of Fe, Cu, and Ni. The detection of metals was carried out by image capturing and then analyzing the color intensity using a image processing software. The results show calibration curves were generated for each metal, with detection limits in range of 1.0 to 1.5 μg. This method can provide rapid determination of metal at the level below the regulatory limits.

Ogawa, K. et al. [48] presented a PAD for detection of the Fe (III) in form of Fe (II). The PAD was fabricated using a wax printer. The hydroxylamine was used as reducing agent to reduce Fe (III) to Fe (II) for complex formation with specific reagent as 1,10-phenanthroline. The color intensity was proportional to the concentration of Fe (III) in the range of 40-350 ppm. When the PAD was applied to the determination of Fe (III) in a natural hot spring water sample, the accuracy is excellent, the results by the proposed method were agreed with the spectrophotometry which is validation method. The PAD provides rapid and small-scale operations.

2.5.2 Determination of Cr (III)

2.5.2.1 Instrumental Method

Kiran, K. et al. [31] synthesized bis-[2-Hydroxy-1-naphthaldehyde] thiourea as a complexing agent toward Cr (III) accompanied with the preconcentration cloud point extraction technique. After complexation, the analyte was extracted to the surfactant-rich phase in the Triton X-100. Then, it was detected by AAS. This method shows the relative standard deviation was 2.13% and the limits of detection as 0.18 μg L^{-1}.

Geraldo D.M. et al. [32] proposed the method, a cloud point extraction system for determination of species of chromium in the natural water samples which are Cr (III) and Cr (VI). The complex formation of Cr (III) with 1-(2-pyridilazo)-2-naphtol (PAN) in a surfactant solution (Triton X-114) was employed to separate the analyte from the matrix The Cr (VI) assay is carried out by reducing to form of Cr (III) by ascorbic acid, then it form the complex with PAN. Then, the amount of chromium was measured by AAS method Under the optimized conditions, linear range of 2.5–80 μg L^{-1}, limit of detection and quantification of 0.7 and 2.5 μg L^{-1}, respectively, and the relative standard deviation (n = 10) are lower than 5.5%. The proposed procedure was applied to river water samples. The recoveries of 84–115% and a relative standard deviation lower than 4.2% are achieved.

Mari Pantsar, K. et al. [33] proposed a method that utilizes inductively coupled plasma mass spectrometry as a detector for coupling with column ion chromatographic determination of chromium species. The coupled column system consists of a cation guard column and an anion column. In the detection the smallest

concentration which can be detected is 0.3 µg/l and 0.5 µg/l for Cr (III) and Cr (VI), respectively.

Bo-Hao, C. et al. [34] determined Cr (VI) in rice using ion chromatography (IC) and inductively coupled plasma mass spectrometry (ICP-MS). Cr(VI) is separated within 4.5 min using NH_4NO_3 solution at pH 8.8 as mobile phase. The detection limit of (LOD) Cr (VI) is 0.06 ng mL^{-1}. This methodology is used for the determination of Cr (VI) in different rice samples to evaluate the toxicity of rice. This method shows recoveries of Cr (VI) are 98–102% and high precision (RSD < 6.3%).

2.5.2.2 Fluorometry Using Organic Dyes

Yan W. et al. [35] introduced a new rhodamine-based fluorescent chemosensor or FD8 for using as the selective fluorescence probe toward Cr (III) ions. In the presence of Cr (III), FD8 show the enhancement of fluorescence. By this phenomenon, the detection limit of Cr (III) is achieved as 1 µM.

Yanmei Z. et al. [36] presented a rhodamine-based chemosensors (RF) using for the selective sensing of Cr (III). With the optimum condition, the response was linear in the range 0–10 µM. The detection limit is obtained as 0.023 µM. The proposed phenomenon was also applied to intracellular Cr (III) imaging in living cells and determination Cr (III) in tap and river water sample.

Vinod K. et al. [37] synthesized two novel fluorescent rhodamine derivatives L1 and L2. They were designed as the extremely selective and sensitive “turn-on” fluorescent probes toward Cr (III). In the presence of Cr (III), the spirolactam ring of probes was opened, leading to the enhancement of fluorescence intensity. The interaction is occurred through 1:1 metal–ligand complex formation. The L1 and L2 show a good binding constant and low detection limit toward Cr (III). Also, they were successfully examined the reversibility of complexation, so, the probes can be reused for determination of Cr (III) in next further study.

Jie M. et al. [38] designed the "off-on" rhodamine-based fluorescence probe for the selective signaling of Cr (III) by exploiting the guest-induced structure transform mechanism. This system shows a sharp Cr (III)-selective fluorescence enhancement response against the background of environmentally and biologically relevant metal ions including Cr(VI), Al(III), Fe (III), Cd(II), Co(II), Cu(II), Ni(II), Zn(II), Mg(II), Ba(II), Pb(II), Na(I), and K(I). Under optimum conditions, the fluorescence intensity enhancement of this

system is linearly proportional to Cr (III) concentration from 5.0 x 10^{-8} to 7.0 x 10^{-6} mol L^{-1} with a detection limit of 1.6 x 10^{-8} mol L^{-1}.

Dongping W. et al. [39] synthesized a new boradiazaindacene (BODIPY) derivative (1a) for selective detection of Cr (III) based on fluorometry. The 1a molecule behaves as strong red fluorescence in the presence of Cr (III). This phenomenon is not occurred by other metal ions. So, this confirmed that the 1a sensor is highly selective with Cr (III).

Zhanxian L. et al. [40] designed a fluorescent probe for the selective and sensitive of Cr (III). It was synthesized for detection of Cr (III) based on the photoinduced-electron transfer mechanism. The interaction of Cr (III) is reacted between naphthyridine and 7,10-diphenylfluoranthene. In the presence of Cr (III), the probe shows the enhancement of fluorescence, selectively. The proposed method is not only carried out in solution, but also in living cell. The results in both show the good fluorescence response.

Subarna G. et al. [41] prepared a thiophene-coumarin hybrid molecule, (6E)-6-((thiophen-2-yl)methyleneamino)-2H-chromen-2-one (TMC) for selective detection of Cr (III). TMC and its Cr (III) complex are well characterized by spectroscopic techniques such as ^{1}H NMR, FTIR and elemental analysis. In the presence of Cr (III), TMC show the fluorescence enhancement. The detection limit of this method is 1 × 10^{-6} M. Binding constant is investigated by the Benesi-Hildebrand plot (B-H plot) and which is obtained as 8 × 10^{4}, L mol^{-1}, indicating a strong interaction between TMC and Cr (III). Moreover, TMC is capable to detect intracellular Cr (III) in living cells.

Jiangang Z. et al. [42] synthesized a novel carbazole derivative, *N,N'*-bis(9-ethyl-9*H*-carbazol-3-yl)-(ethane-1,2-diamine) and applied as the fluorescence sensor of Cr (III). The fluorescence emission at 438 nm of the sensor is selectively quenched by Cr (III) with the stoichiometry as 1 : 1, this phenomenon cannot be occurred with other ions. The complex is formed between the carbazole derivative, and Cr (III) and their association constant is 1.4 × 10^{4} L mol^{-1}. The results indicate that the sensor can provide a rapid, selective and sensitive response to Cr (III) in a linearity range of 1.0–20 μmol L^{-1}. The limit of detection is obtained as 0.10 μmol L^{-1}. The carbazole derivative is a good probe and appropriate to Cr (III) determination.

Yin S.W. et al. [43] synthesized a pyrene compound (1) for using as ratiometric fluorescent chemosensor toward Cr (III). This is the first ratiometric

chemosensor based on pyrene that is developed for Cr (III). In the presence of Cr (III), the fluorescence signal at two wavelength of the sensor is changed. In the detection, the analytical performance show a linear range from 2.0×10^{-7} to 1.0×10^{-5} M with the detection limit is 4×10^{-8} M. Remarkably the probe is highly specific for Cr (III), the foreign metal ions cannot interacted. In addition, the sensor is applied for determination of Cr (III) in real sample such as river and pond water with satisfactory results.

Aiyun Z. et al. [44] designed a new fluorescent probe 4PBI-Cz based on novel dibenzimidazole group for determination of Cr (III). In the presence of Cr (III) the fluorescence of 4PBI-Cz become turn-off. This phenomenon shows the detection limit is 3.5 nM, which can be indicated the high sensitivity of the probe. This work present that the new proposed dibenzimidazole group is an interesting sensor for the determination of Cr (III).

Shanthi S. et al. [45] designed and synthesized a new 5-(furan-2-yl)-7, 8, 13, 14-tetrahydrodibenzo[a,i]phenanthridine (4a) for the highly selective determination of Cr (III). The sensor 4a displays colorimetric and fluorometric recognition of Cr (III) ion due to the coordination via the electron rich furan oxygen atom and pyridine nitrogen atom of 4a. In the presence of Cr (III), the blue emission of 4a become enhanced. The phenomenon show fast response time within 30 s and the detection limit is observed as 142 nM toward Cr (III). The binding mechanism of 4a with Cr (III) was established by FTIR analysis, ^{1}H NMR titration experiment, HRMS and Job's plot analysis. The 4a has been successfully applied for detection of Cr (III) in environmental water samples and fluorescence bio-imaging in *E-coli* bacteria with satisfactory results.

2.5.2.3 Paper-based Analytical Device

Elavarasi M. et al. [49] presented a PAD for sensing of Cr (III) based on colorimetry. The gold nanoparticles (AuNPs) were used as the immobilizing reagent into the PAD. In the presence of Cr (III), leading to aggregation of AuNPs, the coloe of AuNPs is chaged from red to blue. The color intensity was then monitored, calibrated with the color intensity obtained from series of standard Cr (III). Under the optimized conditions, a linear relationship (correlation coefficient r = 0.99) was obtained between the measured color intensity and the concentration of Cr (III) in the range of 10^{-3} to 10^{-6} M. The limit of detection is 1.53×10^{-7} M. This method also provides high

selectivity towards Cr (III), and it can be successfully tested in the presence of interfering metal ions.

Jaruwan M. et al. [50] presented PAD which is fabricated by screen-printed technique for determination of Cr (III) and chloride based on colorimetry and distance-based detection, respectively. The silver nanoparticles were used as the reagent for two analyte. The detection shows a limit of detection of 15.0 μg L^{-1} and a linear range of 50.0–1000.0 μg L^{-1} for Cr (III) detection. For Chloride determination, the method provides LOD and a linear range of 10.0 mg L^{-1} and 10.0–500.0 mg L^{-1}, respectively. The PAD was applied in instant noodle seasonings and the results significantly agreed with the result from traditional titration validation method at 95 % confidence.

Hitoshi A. et al. [51] described a PAD for the determination of hexavalent chromium Cr (VI) in water samples. The PAD was fabricated by photolithography and immobilized with reagents (1,5-diphenylcarbazide) for a colorimetric detection. Cr (VI) and 1,5-diphenylcarbazide form a violet-colored complex on PAD. It was then captured with a digital camera and the color intensity wereanalyzed using images processing software. The green intensity analysis was the best sensitive and show a linear working range (40 - 400 ppm; r^2 = 0.981). The detection limit of 30 ppm is obtained. The recoveries were between 94 and 109% in applicable testing for water samples, and good results were obtained.

Abdellah M. et al. [52] proposed PAD for the determination of total chromium (Cr) in water, soil, and lettuce irrigated with wastewater in Ethiopia. The PAD, which were printed by wax printing, were added the specific reagents to the pretreatment and detection zones. Soil and lettuce samples were determined by the PADs and a UV-Vis spectrophotometry. The results from two method are compared approaching a paired t-test. The significant test showed that the results are not significantly different between at the 5% level. This implies that the PAD has good accuracy and reliability and can be applied to monitoring of Cr in environmental samples.

Abdellah M. et al. [53] presented PAD for colorimetric determination of hexavalent chromium (Cr (VI)) and trivalent chromium (Cr (III)) via online oxidation. The PAD was designed, there are left and right channels. The colorimetric reaction of Cr (VI) with 1,5-diphenylcarbazide (DPC) is carried out in the left channels whereas total Cr was determined in the right channels. The online oxidation is occurred by using a

cerium (IV) (Ce (IV)) immobilized in the pretreatment zone of the PAD to oxidize Cr (III) to Cr(VI) and then reacted with DPC. The Cr (III) amount was observed as different values of total Cr and Cr (VI) amount. This work show limits of detection and quantification were 0.008 and 0.02 mg L^{-1} for Cr (VI) and 0.07 and 0.1 mg L^{-1} for Cr (III), respectively. The linear ranges is obtained as 0.02–100 mg L^{-1} and 0.1–60 mg L^{-1} for Cr (VI) and Cr (III), respectively. The RSDs were less than 7.5%. Moreover, the results from this method were agree well with the result obtained by ICP-OES. The recoveries are achieved in the range of 92–108% for Cr (III) and 108–110% for Cr (VI) using PAD, and 106–110% for total Cr. Thus, the PAD can br applied for the determination of both Cr (III) and Cr (VI) in real sample to monitor the environmental pollution.

2.5.2.4 Nanocellulose-based Analytical Device for Quantitative Analysis

Nahid P. et al. [54] introduced a silver nanoparticles (AgNPs)-immobilized transparent bacterial cellulose nanopapers (BCN) as a sensing platform for determination of cyanide ion (CN^-) and 2-mercaptobenzothiazole (MBT) in water samples. The platform is prepared by in-situ method, then it was characterized by field emission scanning electron microscopy (FE-SEM), UV–visible spectroscopy (UV–vis), Fourier-transform infrared spectroscopy (FT-IR), thermogravimetric analysis (TGA) and energy-dispersive X-ray spectroscopy (EDX). For the detection principle, the surface plasmon resonance of AgNPs was measured the changing of signal in the presence of the target analyte by spectrometry. The results show the linearity in the range of 0.2–2.5 μg mL^{-1} and 2–110 μg mL^{-1} with a detection limit of 0.012 μg mL^{-1} and 1.37 μg mL^{-1} for CN^- and MBT, respectively.

Erhan Z. et al. [55] developed a nanopaper which is a sheet made of cellulose nanofibers, immobilized with a carbon quantum dots-embedded for selective sensing of iodide in sea water based on quenching effect. The obtained nanopaper was cut into small rectangular pieces and reacted with the iodide. Then it was place into the sample compartment of fluorometer, accompanied with the home-made holder for using as the microcuvette. Next, the fluorescence light of the nanopaper was measured. The results show limit of detection (LOD) and limit of quantification (LOQ) as 48 and 144 μM, respectively.

Shadab F. et al. [56] proposed a “nanopaper-based analytical device (NAD)”, which is curcumin-embedded bacterial cellulose (BC) nanopaper. This is prepared for

using as a colorimetric assay kit for determination of iron and iron-chelating drug (deferoxamine ,DFO) in biological fluids such as serum blood, urine and saliva. The iron sensing based on the decrease of the absorbance or color intensity of curcumin in the presence of Fe (III). However, adding of DFO drug, Fe (III) was chelating formed with the drug, the absorption or color intensity of curcumin is thus recovered This phenomenon is utilized for selective colorimetric monitoring of this drug. In the detection, the absorption or color changing can be monitored by spectrometer and smartphone camera, respectively. The results of the proposed method are agreed well with the results from a clinical reference method. Therefore, it is confirmed that the developed NAD is applicable for determination of Fe (III) and DFO in real samples.

Tina N. et al. [57] introduced a nanopaper-based analytical device (NAD) or for sensing of human serum albumin (HSA) in blood serums. The curcumin-embedded BC nanopaper was utilized as the paper substrate. The hydrophilic zones were created on the paper substrate through creating the hydrophobic walls by laser printing technology. The color changes effect of curcumin by HSA can be monitored with naked eye accompanied with smartphone camera or spectrometry. The results of two method are linear in the range of 10-300 μM and 25-400 μM, respectively. The developed NAD can be successfully applied to the determination of HSA in human blood serum samples with satisfactory results.

Shadab F. et al. [58] described a nanopaper-based analytical device (NAD) is for a colorimetric detection of zoledronic acid (ZA) based on metal-complexing indicator-displacement assay. The Bacterial cellulose nanopaper (BCN) was doped with curcumin and then the hydrophilic and hydrophobic area were patterned via laser printing onto the BCN. The color intensity of the test zones is decreased in the presence of Fe (III) However, addition of ZA, the color of the zone is changed from light yellow to dark yellow. The changing is monitored by using a digital camera, or by a spectrophotometer. Under optimal conditions, the results are linear in the 0.01–100 μM, the detection limits are achieved as 8.8 and 8.0 nM for smartphone and spectrophotometric methods, respectively. The method is applied to the determination of ZA in urine, serum, saliva, and in pharmaceutical samples.

Aurachat L. et al. [59] presented a gold nanoparticle (AuNPs)-immobilized bacterial cellulose (BC) nanopaper for the determination of hydrogen peroxide (H_2O_2) based on redox reaction. The absorption of AuNPs is located at 525 nm, however the

absorbance is decreased in the presence of H_2O_2. This resulted from redox reaction which the AuNPs in BC is oxidized to form of Au (III) by H_2O_2, leading to decreasing of the mentioned absorbance. This phenomenon can be detected by naked-eyes or spectrometer. The result from spectrometric method shows the detection limit as 0.79 % (v/v). When the method was applied to determination of H_2O_2 in wound cleaner and hair dye samples, the good analytical recovery is obtained in the range of 88.8 to 97.2 %. Moreover, the H_2O_2 contents in all samples are not different with the label values this guarantee the high accuracy and high precision (RSD is lower than 3.3 %). These results confirmed that the as-prepared nanopaper is successfully applied for determination of H_2O_2 in real samples.

Elham S. et al. [60] designed a curcumin-embedded bacterial cellulose nanofiber as a sensing platform for the determination of lead (Pb (II)) ion in rice sample. The as-prepared platform was characterized by FT-IR and FE-SEM analyses. In the detection, a color of curcumin is changed from orange to red in the presence of Pb (II). The selectivity of the sensing platform was tested by the various bivalent of heavy metal ions, such as Ba, Ca, Cd, Mg, Ni and Zn ions. The results proved that the developed sensor was highly selective toward Pb (II). The sensing method provides the detection limits of 0.9 μM when image processing software is employed for detection. The designed sensing platform is successfully applied for monitoring of Pb (II) ion.

Chapter 3

Research methodology

3.1 Paper-based Analytical Device for Determination of Total Iron

3.1.1 Chemical Reagents

Chemical name	Chemical formular	Brand, Country
Ammonium ferrous sulfate hexahydrate	$Fe(NH_4)_2(SO_4)_2 \cdot 6H_2O$	Sigma-Aldrich, USA
Bathophenanthroline	$C_{24}H_{16}N_2$	Sigma-Aldrich, USA
Absolute ethanol	EtOH	Thermo Fisher Scientific, Thailand
Concentrated sulfuric acid	conc. H_2SO_4	RCI Lab Scan, India
Hydroxylamine	$NH_2OH{\cdot}HCl$	Sigma-Aldrich, USA
Orthophenanthroline	$C_{12}H_8N_2$	Sigma-Aldrich, USA
Trisodium citrate dihydrate	$Na_3C_6H_5O_7 \cdot 2H_2O$	Sigma-Aldrich, USA

3.1.2 Apparatus and Instrument

1) Laboratory filter paper no.1 (Whatman™, United Kingdom)

2) Controlled lighting studio box, size 400 mm x 400 mm x 400 mm (Audio box™, Thailand)

3) Two-sided mounting tape (3M Nanmee™ , Thailand)

4) Glue additive (Galen™, Thailand)

5) Paintbrush no. 4 and no. 6 (Horse™, Thailand)

6) Scissors (Scotch™, Thailand)

6) Micropipettes and tip

7) Volumetric flasks

8) Beakers

9) Inkjet printer 1100P (HP, Thailand)

10) UV-visible spectrophotometer J360 (JASCO, Japan)

3.1.3 Preparation of Chemical Reagents

All chemical reagents are analytical reagent (AR) grade. Deionized-distilled water, purified by ZENEER UP 900, Human corporation (Korea) were used throughout the work.

3.1.3.1 1 g L^{-1} of Bathophenanthroline 10.0 mL

0.0050 g of bathophenanthroline was dissolved in 10.00 mL-volumetric flask with absolute ethanol. This chromogenic reagent was kept in dark before use.

3.1.3.2 100 mg L^{-1} Stock Standard Solution of Fe (II) 100 mL

0.0702 g of ammonium ferrous sulfate hexahydrate was dissolved in 50.0 mL water. Then, 100 µL of concentrated sulfuric acid was added. It was diluted to 100.0 mL with water.

3.1.3.3 Working Standard Solution of 0.1, 0.2, 0.3, 0.4, 0.5 Fe (II) 25.0 mL

A series of the stock standard solution of Fe (II) (100 mg L^{-1}) was pipetted into volumetric flask (25.00 mL) with the specific volume as shown in Table 3.1. Then, it was adjusted to the mark with water. Finally, the working standard solutions of Fe (II) were obtained.

Table 3.1 The specific volumes of 100 mg L^{-1} stock standard solution to prepare the series of Fe (II) standard working solution.

Final concentration of Fe (II) (mg L^{-1})	Specific volume to pipette (µL)
0.0	0
0.1	25
0.2	50
0.3	75
0.4	100
0.5	125

3.1.4 Preparation of Water Sample

Many kinds of water sample, including drinking, tap, canal water and river water, were collected for determination of iron without any on-site pretreatment. The methos for the preparation of the samples were different accordingly to the detection methods as concluded in the following sections.

3.1.4.1 For Determination of Total Fe by the Developed PAD

300 µL of water sample (without any prior filtration) was mixed with 200 µL of 10% (w/v) hydroxylamine. Then, the mixed solution was diluted in 10.00 mL-volumetric flask.

3.1.4.2 For Validation Method

The water sample was vacuum filtered by 0.45 µm filter membrane. Then, the filtrate was prepared, following the validation procedure as described in Section 3.1.8.2.

3.1.5 Fabrication of Paper-based Analytical Device

The PAD was patterned by Microsoft Powerpoint™ and was printed onto an A4-sized laboratory filter paper. The hydrophobic zone was produced by painting a waterproof glue solution onto both front and back side of the paper. The glue was prepared by dissolving 5 g of Galen™ glue additive in 5.0 mL of absolute ethanol. The solution was mechanically stirred and kept overnight before use. After painting, the PAD was dried at ambient temperature for removal of the glue solvent. It was divided into small pieces. A single PAD consists of the hydrophilic area (Ø 10 mm) located in the paper sheet rectangular-shaped (25 x 25 mm^2). Two pieces of the PAD were attached with two-sided mounting tape before the determination of iron. Summary of the process for the fabrication of the PAD is presented in Figure 3.1.

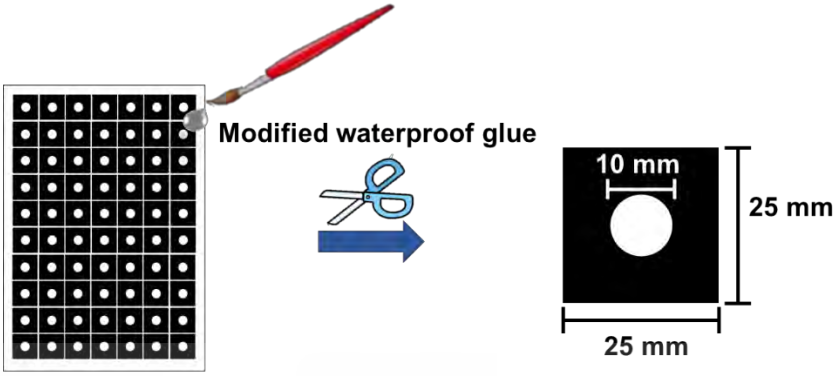

Figure 3.1. Summary of the process for the fabrication of the PAD.

3.1.6 Optimization

Factors affecting the sensitivity and the other performances of the developed method were studied. The optimization study was carried out using the designed PAD (the single layer platform) as presented in Figure 3.1. Effect of each parameter was examined as describe in detail in the following procedure.

3.1.6.1 Effect of Bphen Volume

Effect of the volume of Bphen was varied as 7, 10, 12 and 15 µL. The appropriate volume is evaluated as the minimum volume which can be fully spread in the hydrophilic zone.

3.1.6.2 Effect of Sample Volume

Effect of the sample volume was varied as 100, 110, 120, 130 and 140 µL. Each volume was dropped into the top layer of double-layered PAD (See Figure 3.2) and count time for 5 min. The volume that can penetrate through the top layer to be exposed onto the bottom layer within 5 min, is selected.

3.1.7 Analytical performances study

To study the analytical performances of the method, the PAD was initially immobilized with the chromogenic reagent by dropping of 10 µL of 1.0 g L^{-1} Bphen and was dried at ambient temperature for 3 min before use.

3.1.7.1 Working Range

100 µL of the working standard solutions of Fe (II) in the concentration range of 0.0-0.5 mg L^{-1} was individually dropped onto PAD. The reaction was left for 15 min, then, the colored product was captured with smartphone and analyzed the red intensity by ImageJ™ software.

3.1.7.2 Selectivity

The standard solution of Fe (II) (4.0 mmol L^{-1}) and the foreign ion solutions (4.0 mmol L^{-1}) of Fe^{3+}, Bi^{3+}, Zn^{2+}, Mn^{2+}, Cd^{2+}, Hg^{2+}, Ba^{2+}, Ag^{+}, Na^{+} and K^{+} were studied. The reaction was left for 15 min. Then, each PAD was captured with smartphone.

3.1.7.3 Precision

100 µL of 0.1 mg L^{-1} standard Fe (II) was spiked to PAD. The reaction was left for 15 min before the colored product was captured with smartphone and analyzed the red intensity by ImageJ™ software (n = 10), The results are evaluated RSD.

3.1.7.4 Minimum Detectable Level (MDL)

The standard Fe (II) solution was prepared in the concentrations of 0.015, 0.03, 0.06, and 0.09 mg L^{-1}. The minimum concentration which can develop the red-colored product on the PAD and can be visually detected by naked-eyes is considered MDL.

3.1.8 Application for Total Fe Determination in Water Sample and Validation

The developed PAD was applied for the determination of iron in many kinds of water samples, including drinking water, tap water, canal water and river water. The samples were spiked with the Fe (II) standard to obtain the final concentration of 10 mg L^{-1}. They were further diluted into the range of calibration for detection method.

3.1.8.1 Determination of Total Fe by the PAD

Figure 3.2 represent the procedure for the quantitative measurement of the iron content in water by the PAD, approaching standard addition is shown in Figure 3.2. 10 µL of 1 g L^{-1} Bphen and 100 µL of standard Fe (II) solutions (0.0 to 0.5 mg L^{-1}) were

individually dropped onto the hydrophilic zone of the bottom layer (Figure 3.2A). The top and the bottom layers were then assembled (Figure 3.2B) using a two-sided mounting tape (2 mm thickness). Later, 120 µL of the water sample was transferred onto the top layer (Figure 3.2C). After 15 min, the bottom layer was then removed and was brought to the controlled lighting box. The photographic image of the product was recorded by iPhone14™ Pro Max (Figure 3.2D). The red intensity was examined by ImageJ™. The standard addition curve of the color intensities and the concentrations of the spiked Fe (II) standards were made. The obtained concentrations were statistically compared to the results by the spectrophotometric method.

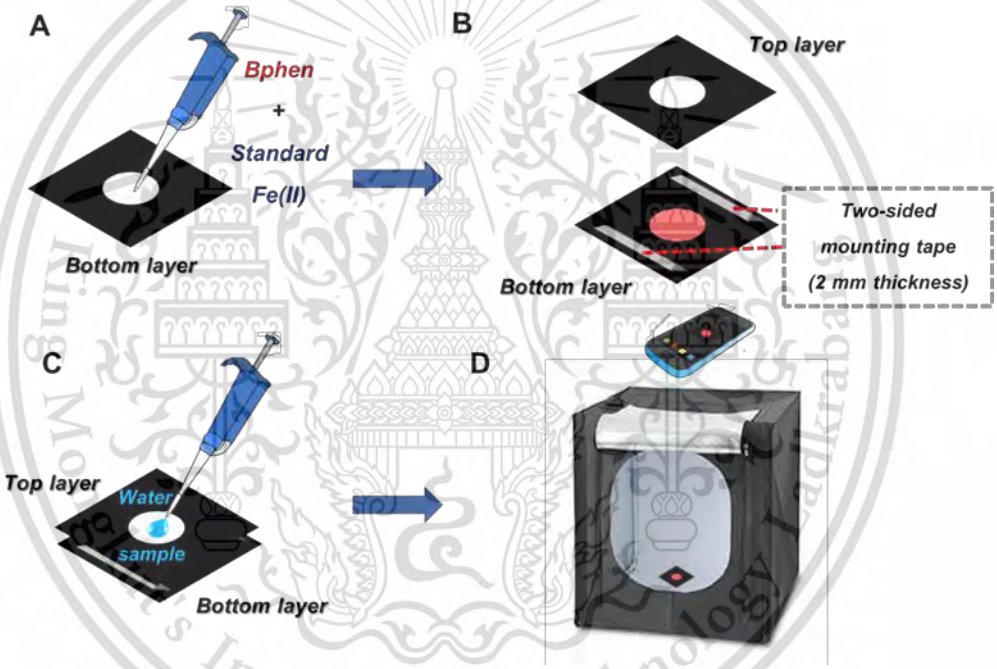

Figure 3.2 The analytical procedure for the determination of the iron in water by the PAD, approaching standard addition.

3.1.8.2 Validation

The spectrophotometric method was employed as the validation technique. The iron concentration was determined by the external calibration plot. The standard curve was made by plotting the absorbance (510 nm) against the standard Fe (II) concentration (0 to 5 mg L^{-1}). In this method, water sample was filtered to eliminate the suspended particles before the measurement. Aliquot of 5.0 mL of the filtrate was

pipetted into 25.00 ml-volumetric flask. Then, add 0.25 ml of 10 % (w/v) hydroxylamine and 0.5 ml of 0.5 % (w/v) orthophenanthroline monohydrate. Followed by adding 2 drops of 25 % (w/v) sodium citrate. The final volume was adjusted to the mark with DI water. The solution was measured at 510 nm using an UV-visible spectrophotometer.

3.2 Bacterial Nanocellulose-based Analytical Device for Determination of Trivalent Chromium

3.2.1 Chemical Reagents

Chemical name	Chemical formular	Brand, Country
Chromium (III) nitrate nonahydrate	$Cr(NO_3)_3 \cdot 9H_2O$	Sigma-Aldrich, USA
Nee fluorescein derivative	$C_{34}H_{20}N_4O_9$	Synthesized in this work
99.9 % Methanol	99.9% CH_3OH	Thermo Fisher Scientific, Thailand
Potassium hydrogen phthalate	KHP	Sigma-Aldrich, USA
Sodium tetraborate	$Na_2B_4O_7$	
Sodium hydroxide pellets	NaOH	SDFCl, India
D-Glucose	$C_6H_{12}O_6$	Sigma-Aldrich, USA
Disodium hydrogen phosphate	Na_2HPO_4	CARLO ERBA, Italy
Citric acid	$C_6H_8O_7 \cdot 7H_2O$	Ajax Finechem Pty Ltd, Australia
Trisodium citrate	$Na_3C_6H_5O_7$	Sigma-Aldrich, USA
Peptone	$C_{13}H_{24}O_4$	SRL, India
Yeast extract	-	JT group, Japan

3.2.2 Apparatus and Instrument

1) Micropipettes and tips

2) Volumetric flasks

3) Beakers

4) Cylinder

5) Dropper

8) Petri dish

9) Erlenmeyer flask

10) Thermometer

11) Vortex (INC, USA)

12) pH meter (Mettler Toledo, Thailand)

13) Hot plate (DKSH, Thailand)

14) Field emission scanning electron microscope (JSM-6610LV, JEOL Ltd., Japan)

15) UV-Visible Spectrophotometer (Jasco V-630, Japan)

16) Spectrofluorometer (Jasco FP-6200, Japan)

3.2.3 Preparation of Chemical Reagents

All chemical reagents are analytical reagent (AR) grade. Deionized-distilled water, purified by ZENEER UP 900, Human corporation (Korea) were used throughout the work.

3.2.3.1 10 μM of New Fluorescein Derivative, 100 mL

0.0007 g of new fluorescein derivative was dissolved in 100.0 mL-volumetric flask with 99.9 % (v/v) methanol. This was kept in dark before use.

3.2.3.2 1000 μM Stock Standard Solution of Cr(II) 50 mL

0.02 g of chromium (III) nitrate nonahydrate was dissolved in 10 mL of water. Then, it was diluted in 50.0 mL-volumetric flask.

3.2.3.3 Working Standard Solution of Cr (III) 10 mL

A series of the stock standard solution of Cr (III) (1000 µM) was pipetted into volumetric flask (10.00 mL) with the specific volume as shown in Table 3.2. Then, it was diluted with water to the mark. Finally, the working standard solutions of Cr (III) were attained.

Table 3.2 The specific volumes of 1000 µM stock standard solution of Cr (III) to prepare the series of Cr (III) standard working solution.

Final concentration of Cr (III) (µM)	Specific volume to pipette (µL)
0	0
1	10
10	100
30	300
50	500
80	800
100	1000

3.2.3.4 100 µM KHP Buffer pH 7.0, 100 mL

0.0020 g of KHP was dissolved in 100 mL of water. The solution was adjusted to obtain the pH value of 7.00 by 0.1 M HCl or 0.1 M NaOH.

3.2.4 Preparation of Water Sample

Many kinds of water samples, namely canal water and river water, samples. The canal water samples were collected from Prawet Canal in Bangkok while the river water samples were collected from Cho Pra Ya River in Nonthaburi Province and Kok River in Chiang Rai Province. They were vacuum filtered through a 0.45-µm nylon

membrane filter. Then, the filtrate was further used for quantitative analysis of Cr (III), for both determination by the developed and validation method.

3.2.5 Preparation of Bacterial Nanocellulose and Characterization

Bacterial nanocellulose (BNC) was produced by static sub-culturing the bacteria namely, *Acetobacter xylinum* in the Hestrin-Schramm (H.S.) medium. The H.S. medium was prepared by mixing glucose (10 g), yeast extract (2.5 g), peptone (2.5 g) disodium hydrogen phosphate (1.35 g) and citric (0.6 g) in 500 mL water. Then, the solution was mixed homogeneously using mechanical stirring and was adjusted to obtain a pH value of 5.25 by 1 M HCl or 1 M NaOH. The bacteria were treated in the as-prepared medium for 3-5 days and then was harvested when 1 mm thickness of nanocellulose film was obtained. The nanocellulose was then bleached in alkaline solution under the following two steps i.e., step 1: soaking in 5 % (w/v) NaOH for 1 hr. and step 2: immersing in 100 mL of bleaching solution (1 % (w/v) NaOH in 0.2 % (v/v) H_2O_2) for 1 hr. with heating (80 °C). After bleaching, it was rinsed with water for several times until the pH value of the nanocellulose at 7.00 of was achieved. Eventually, the bleached BNC was ready-to-use and further applied to analytical device for determination of Cr (III). The bleached BNC was characterized by FE-SEM, to investigate the morphology of the cellulose fiber. It is noted that the BNC must be dried before scanning through FE-SEM. To dehydrate the BNC, it was placed in air-flow location for 1-2 days, the dried BNC was obtained.

3.2.6 Synthesis of New Fluorescein Derivative and Characterization

Figure 3.3, illustrating pathway of synthesis of the new fluorescein derivative (NFD). In detail, the procedure of synthesis is described as the following: Firstly, anthranilic acid (1.3830 g) was dissolved in 10.0 mL of pure methanol in beaker. Then, 3.0 mL of concentrated HCl was gradually added. The mixed solution was left on ice bath until the temperature was cooled down to 0-5 °C. After that, it was transferred into another beaker, containing cooled (0-5 °C) sodium nitrite solution (0.7077 g in 3.0

mL of DI water). Then, fluorescein solution (0.9018 g in 5.0 mL of 20 % NaOH) was added, resulting in the dark orange solution being obtained. When the reaction was finished, the solvent was evaporated by rotary evaporator. The obtained crude was then purified twice through column chromatography. Stationary and mobile phases of the first column were Florisil™ and 100 % ethyl acetate, respectively. For the second column, we exploited Sephadex LH-20™ as the stationary phase and 50:50 % methanol: dichloromethane as the mobile phase. A fraction of the required eluate was re-evaporated. Finally, the fine dark, orange-colored crystal of the new fluorescein derivative was achieved. Reaction for synthesis of the dye is represented in Scheme 1. This fluorescein derivative was used for preparation of the stock dye solution (10 μM) by dissolving 0.0006 g in pure methanol and adjusted to 100.0 mL in volumetric flask. This solution was further used as the fluorescence sensor for determination.

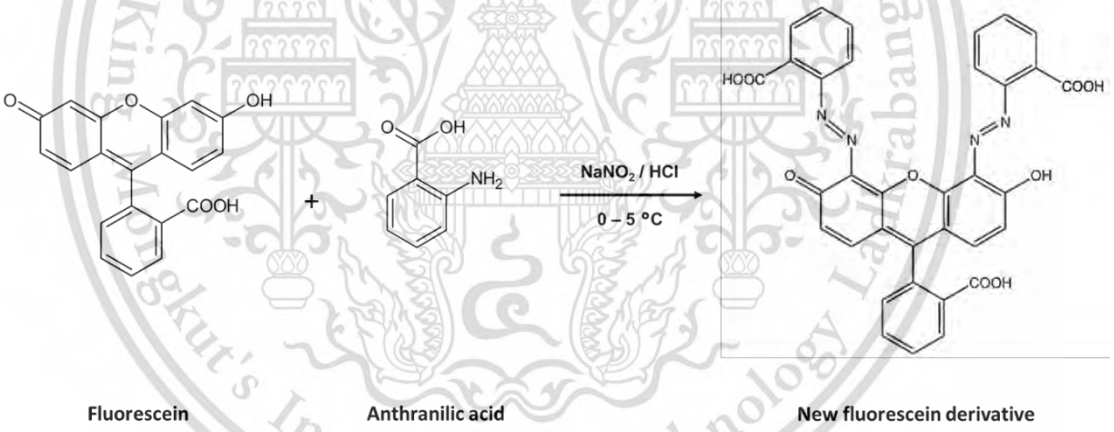

Figure 3.3 Synthesis pathway of the new fluorescein derivative.

3.2.7 Study on Characteristics of NFD

The characteristics of the as-prepared NFD were studied in terms of excitation and emission wavelength, effect of pH, selectivity, fluorescence response toward Cr (III), stoichiometry, linearity range, and applicability for the determination of Cr (III) in water sample.

3.2.7.1 Excitation and Emission Wavelength

Excitation of NFD was carried out by monitoring the absorption spectrum of 10 μM NFD solution by UV-Visible spectrophotometer in the range 200-800 nm. The maximum absorption was considered as the excitation wavelength and was employed for investigating the appropriate emission wavelength.

3.2.7.2 Selectivity Study

Selectivity study was performed by individually spiking of the investigated foreign ions, including Fe (III), Fe (II), Mn (II), Cd (II), Zn (II), Cu (II), Hg (II), Ag (I), Ba (II), Mg (II), Na (I) and K (I) into the NFD solution. Each metal ion solution was prepared in water to obtain the final concentration of 100 μM. Aliquot of 1 mL of each ion solution was homogeneously mixed with 4 mL of 10 μM NFD in a 10 mL-dark bottle for 1 min. The emission spectra were measured by spectrofluorometer at 2 min after mixing.

3.2.7.3 Effect of pH

Effect of pH was examined on both fluorescence of the NFD and the formation reaction between Cr (III) and NFD. The studied pH values were ranged from 3.00 to 12.00. Potassium hydrogen phthalate and sodium tetraborate solution were exploited for preparation of the buffer solutions in the acidic (pH = 3.00 - 7.00) and alkaline (pH = 8.00 - 12.00) regions, respectively. To study the effect on the fluorescence of the dye, the experiment was undergone by mixing 3 mL of pH buffer (100 μM) with 1 mL of water and 2 mL of NFD solution in a 10 mL-dark bottle. The solution was mixed by vortex stirrer for 1 min and was then measured the emission spectra by spectrofluorometer at 2 min. To study the effect of pH on the complex formation between Cr (III) and the NFD, the experiment was carried out by mixing 3 mL of pH buffer (100 μM) with 1 mL of 100 μM Cr (III) and 2 mL of NFD solution in a 10 mL-dark bottle. Then, the emission spectra of the mixed solution were monitored similarly as the above-mentioned procedure.

3.2.7.4 Stoichiometry

We employed Job's method to investigate the stoichiometry in terms of mole fraction between the NFD ligand and Cr (III) ion. The experiment was carried out by adding 1 mL of 100 μM of KHP buffer (pH 7.0) in a 10 ml-dark bottle, followed by 10 μM of standard Cr (III) and 10 μM of NFD according to the specific volumes as presented in Table 3.3. The solution was vortexed for 1 min and measured the fluorescence intensity at 2 min after mixing (λ_{ex} = 485 nm, λ_{em} = 520 nm). The Job's plot between the mole fraction and the fluorescence intensity was plotted to identify the stoichiometry.

Table 3.3 Summary of the specific volumes of 10 μM of standard Cr (III) and 10 μM of NFD to be prepared for the stoichiometry study.

Bottle no.	Mole fraction of Cr (III)	Mole fraction of NFD	Specific volumes of standard Cr (III) to prepared (mL)	Specific volumes of NFD to prepared (mL)
1.	1.0	0.0	4.00	0.00
2.	0.9	0.1	3.60	0.40
3.	0.8	0.2	3.20	0.80
4.	0.7	0.3	2.80	1.20
5.	0.6	0.4	2.40	1.60
6.	0.5	0.5	2.00	2.00
7.	0.4	0.6	1.60	2.40
8.	0.3	0.7	1.20	2.80
9.	0.2	0.8	0.80	3.20
10.	0.1	0.9	0.40	3.60
11.	0.0	1.0	0.00	4.00

3.2.7.5 Fluorescence Response of NFD toward Cr (III)

The standard solution of Cr (III) for the study on the fluorescence response of NFD toward Cr (III) was prepared in the concentration range from 0 to 100 µM. The analytical procedures are described as these following steps: pipetting aliquots of 1 mL of KHP buffer (pH 7.00), 1 mL of water, 1 mL of standard Cr (III) and 2 mL of NFD. The solution was mixed in a 10 mL-dark bottle by vortex for 1 min. Then, the fluorescence intensity of the solution was recorded at 2 min (λ_{ex} = 485 nm, λ_{em} = 520 nm). The corresponding emission intensity were plotted versus the concentration of Cr (III) to investigate the linear relationship between the intensity and the Cr (III) concentration.

3.2.7.6 Applicability for Determination of Cr (III) in Water Sample

The applicability of using the NFD for the quantitative analysis of Cr (III) in natural water samples was evaluated. The investigated samples were natural water collecting from river water, canal water, and hot spring water. The method for the quantification is based on the standard addition method throughout the work for elimination of the effect of the sample matrices.

All water samples were vacuum filtered as mentioned in Section 3.2.2 before the analysis. The procedure of the determination is summarized as the following lists: pipetting aliquots of 1 mL of KHP buffer (pH 7.00), 1 mL of natural water sample, 1 mL of standard Cr (III) solutions (as working range of 1, 10, 30, 50, 80 and 100 µM) and 2 mL of NFD in a 10 mL-dark bottle and were mixed for 1 min. Then, the fluorescence intensity was recorded at 2 min (λ_{ex} = 485 nm, λ_{em} = 520 nm). The intensity was plotted versus the concentration of the standard Cr (III) solution to construct the standard addition calibration for the quantitative analysis of Cr (III).

3.2.8 Preparation of NFD-immobilized BNC

BNC was developed as the analytical device for determination of Cr (III), using the NFD, fluorescence sensor which is highly selective toward Cr (III). The device is prepared by immobilizing the NFD into the BNC by ex-situ method. Briefly, the ready-to-use BNC is cut into rectangular piece (1.5 x 3 cm), then, it is soaked in 5 mL of 10 μM NFD under dark for 9 hr. The immobilized BNC is obtained and ready to use as analytical device.

3.2.9 Design of Paper Holder

In this work, we have developed the NFD-immobilized BNC for using as the analytical device, accompanied with fluorometer. So, the paper holder is thus made, being a platform to place the immobilized BNC in detection method.

The paper holder is designed by Microsoft powerpoint™ and printed into black-colored paper, cut into the designed pattern. In the detection method, the immobilized BNC was placed in the middle part of paper holder. Then, the left and right parts were consecutively folded into the middle part. The folded holder was put into the sample compartment of fluorometer. Design of the paper holder is presented in Figure 3.4.

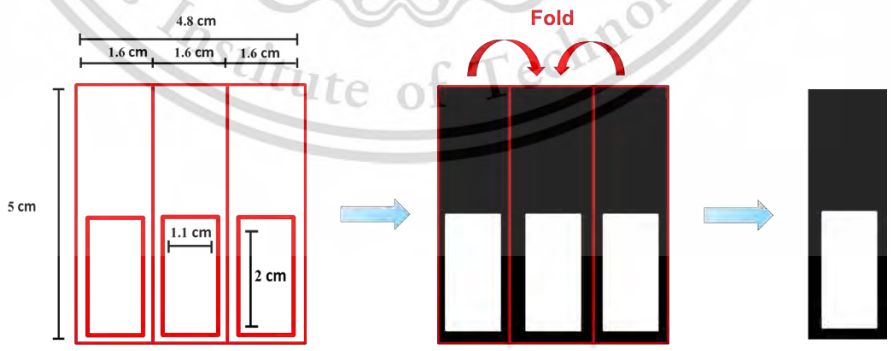

Figure 3.4 Design of the paper holder for the NFD-immobilized BNC.

3.2.10. Immobilization Conditions

The major conditions which affect the sensitivity of the detection of Cr (III) by the immobilized BNC which are concentration of NFD, and soaking time are studied. The NFD solution was prepared as the following concentrations: 1, 5, 10 and 20 μM. The cut BNCs (15 x 30 mm^2) were individually soaked in each NFD solution. After 1 hr., fluorescence intensity of each BNC was monitored by the fluorometer (BNC was situated in the paper holder). The other soaking times, 3, 6, 9, 12 and 24 hrs. were also examined.

3.2.11. Application to the Cr (III) Determination in Water Samples and Validation

The immobilized BNC was applied for the determination of Cr (III) in canal water and river water. The samples were spiked with the Cr (III) standard to obtain the final concentration of 10 μM. They were further diluted into the range of the linear working range for the detection method.

3.2.11.1 Determination of Cr (III) by the immobilized BNC

Determination of Cr (III) in water sample, starting with constructing the calibration and then the water sample was detected using the linear calibration for quantitative analysis. Firstly, 1 mL of 100 μM KHP buffer (pH 7.0) was dropped into the immobilized BNC. Next, 1 mL of standard Cr (III) was dropped, and then left for 20 min. The immobilized BNC was placed into the paper holder and put into the fluorometer. The fluorescence intensity at 520 nm (excitation wavelength at 485 nm) was recorded. The series of standard Cr (III) (1, 10, 30, 50, 80 and 100 uM) were detected as the mentioned procedures. The water sample determination was performed under the same procedures. The obtained fluorescence intensity was calculated by equation of calibration to evaluate the Cr (III) content.

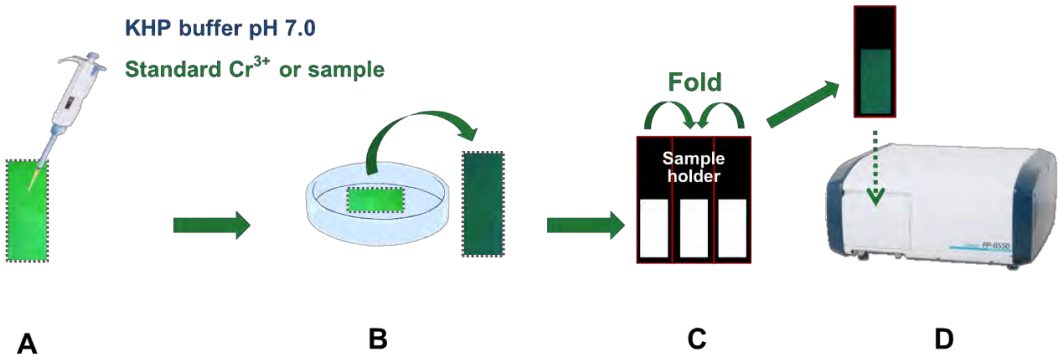

Figure 3.5 The analytical procedure for the determination of the Cr (III) in water by the immobilized BNC.

3.2.11.2 Validation

The inductively-coupled plasma-optical emission spectrometry (ICP-OES) was employed as the validation technique. The Cr (III) concentration was determined by the external calibration plot. The standard curve was made by plotting the emission intensity versus the standard Cr (III) concentration (0.0 to 3.0 μM). Then, the water sample was analyzed, the obtained intensity was calculated into the concentration of Cr (III) in sample by the standard equation of calibration.

Chapter 4

Main Results and Discussion

4.1 Paper-based Analytical Device for Determination of Total Iron

4.1.1 Optimization

The optimization study, including effect of Bphen and sample volumes, were undergone using the designed PAD (the single layer platform) as presented in Figure 3.1. The result of each effect is discussed as the following:

4.1.1.1 Effect of Bphen Volume

The volume of Bphen was varied as 7, 10, 12 and 15 µL. The result is shown in Fig 4.1.

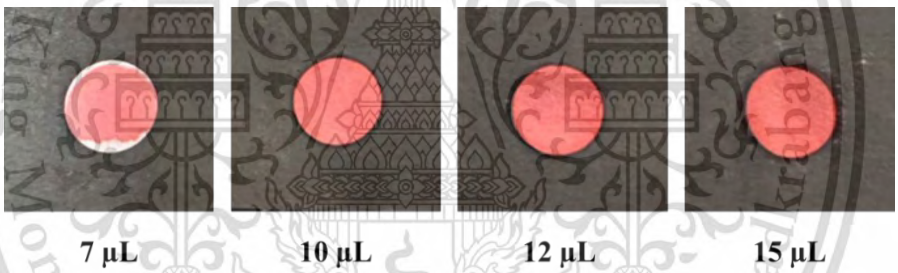

Figure 4.1 Effect of Bphen volume.

Figure 4.1 demonstrates that the minimum volume which can be fully spread in the hydrophilic zone is 10 µL. Higher volumes caused much consumption of the reagent. So, 10 µL of Bphen is thus selected as appropriate volume.

4.1.1.2 Effect of Sample Volume

The volume of sample was varied as 100, 110, 120, 130 and 140 µL. The result is illustrated in Figure 4.2.

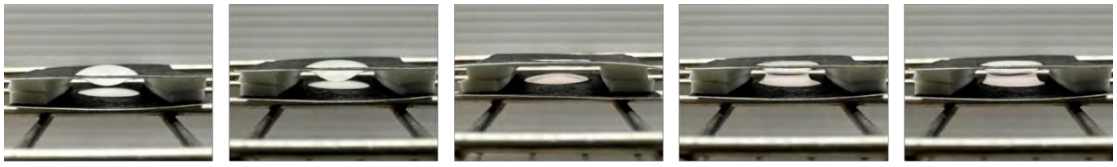

Figure 4.2 Effect of sample volume.

Figure 4.2 demonstrates that the volume that can penetrate through the top layer to be exposed onto the bottom layer is 120 µL. At lower volumes, the droplet of sample was not penetrated to the bottom layer within 5 min. Meanwhile, the higher volumes flow to the bottom layer rapidly. Nevertheless, it was observed that the droplet is trapped in between the space of the two layers. This is because of liquid overloading. Therefore, 10 µL of Bphen is selected as appropriate volume.

4.1.2 Analytical Performances Study

The studied analytical performances are working range and sensitivity, selectivity precision and minimum detectable level (MDL). The results of these performances are presented in the below sections.

4.1.2.1 Working Range

The standard addition curve was constructed to evaluate the working range and sensitivity. The y-axis is the red intensity of the colored product, which is subtracted with a blank PAD. The x-axis is the Fe (II) concentration in the concentration range from 0.0 to 0.5 mg L^{-1}. The results are shown in Figure 4.3.

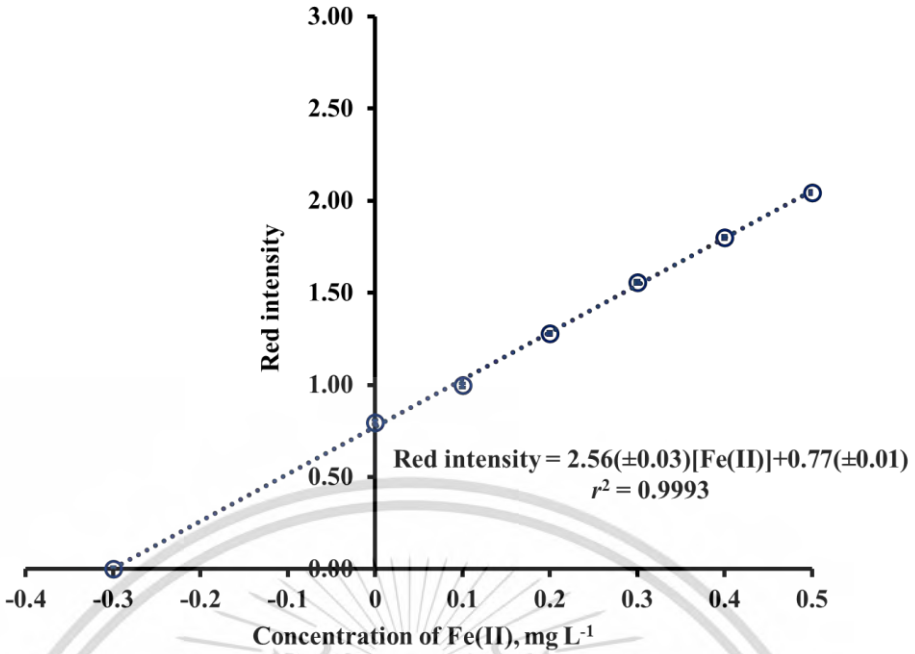

Figure 4.3 An example of the standard addition curve between red intensity and the concentration of Fe (II).

It is observed from Fig. 4.3 that good linear relationship (r^2 = 0.9993) and high sensitivity (in terms of the slope of the standard addition plot is 2.56 $\pm$ 0.03) are obtained. This relationship can be also detected by naked eyes as shown in Figure 4.4.

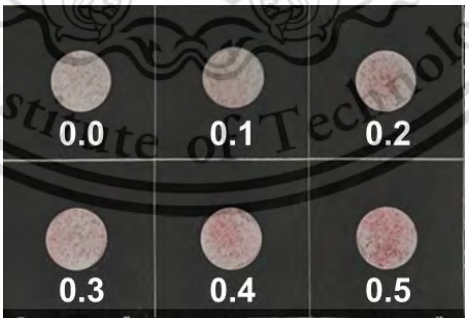

Figure 4.4 The optical images of the colored product, corresponding with the standard addition curve.

4.1.2.2 Selectivity

The standard solution of Fe (II) (4.0 mmol L^{-1}) and the foreign ion solutions (4.0 mmol L^{-1}) of Fe^{3+}, Bi^{3+}, Zn^{2+}, Mn^{2+}, Cd^{2+}, Hg^{2+}, Ba^{2+}, Ag^{+}, Na^{+} and K^{+} were investigated. The result is demonstrated in Figure 4.5

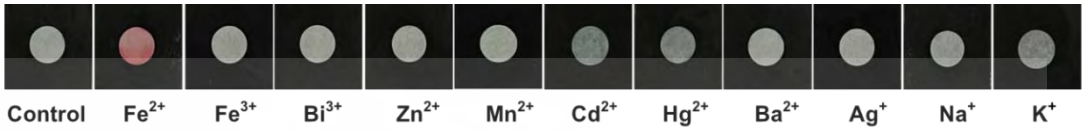

Figure 4.5 The optical images of the single PADs attained when the metal ions are spiked onto the PAD.

Figure 4.5 clearly demonstrates that only Fe^{2+} causes the red-colored product. This phenomenal is not occurred with the other ions although at high concentration. It can be summarized that the immobilized Bphen on the PAD is highly selective to Fe (II). Therefore, the interferences effect is negligible.

4.1.2.3 Precision

Precision was evaluated in terms of relative standard deviation (RSD, %) via replicate measurements of ten pieces of PAD. Dropping of the standard 0.1 mg L^{-1} Fe (II) solution onto the Bphen-immobilized PADs was carried out. The red intensity of the product was examined. Result in Table 4.1 indicate that the developed PAD provides good precision (RSD = 5.81 %).

Table 4.1 The optical images of red-colored product and its red intensity values.

242.185	245.731	236.723	245.986	245.417
				
210.926	227.184	213.684	234.225	220.129
				
Mean of red intensity = 232.22				
SD of red intensity = 13.49				
RSD of red intensity = 5.81 %				

4.1.2.4 Minimum Detectable Level (MDL)

Minimum detectable level (MDL) is defined as the lowest/minimum concentration in which the red-colored product on the PAD can be visually detected. The low concentrations of standard Fe (II) solution from 0.01 to 0.09 mg L^{-1} were investigated. The results are shown in Figure 4.6.

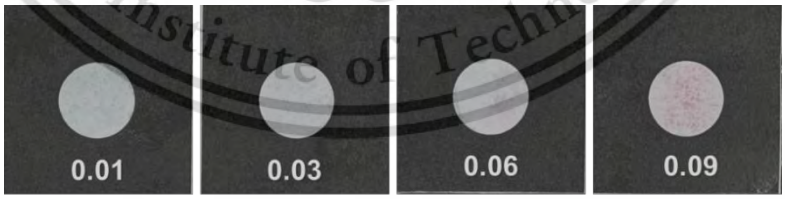

Figure 4.6 The optical image of colored product at Fe (II) concentration below 0.1 mg L^{-1}

Figure 4.6 illustrates that the minimum concentration of Fe (II) which can be developed the red-colored product with Bphen on PAD is 0.09 mg L^{-1}. This can be also

detected with naked eyes. Thus, the minimum detectable level or MDL of the developed PAD is considered as 0.09 mg L^{-1}.

4.1.3 Application to the Total Iron Determination in Water Sample and Validation

In this research, we present the developed PAD for the determination of the total iron ions in water sample. The PAD is assigned as a double-layer analytical platform. The top layer is exploited for the sample filtration while the bottom layer is used as for the colorimetric detection. By this design, any filtration devise is negligible. This cause the developed PAD is easy-to-use and portable for the on-site analysis. We also apply the concept of the standard addition for the quantification method by preliminarily dropping the standard and the reagent onto the bottom layer before assembling the top and the bottom layers each other.

Conceptualization of the work can be explained in detail as the following main idea. After the as-collected water sample is reduced by hydroxylamine to convert the iron (III) ions to the iron (II) ions, it is directly dropped onto the top layer. The original color of sample is decolorized. In addition, the suspended particles, existing in the sample, are trapped by the top layer (See Figure 4.7A). The filtrate is then penetrated through the top layer and is contacted to the bottom layer where the standard and the reagent have been previously transferred. The iron (II) ions in sample are selectively formed the stable complex with the Bphen ligand. This results in the red product (See Figure 4.7B).

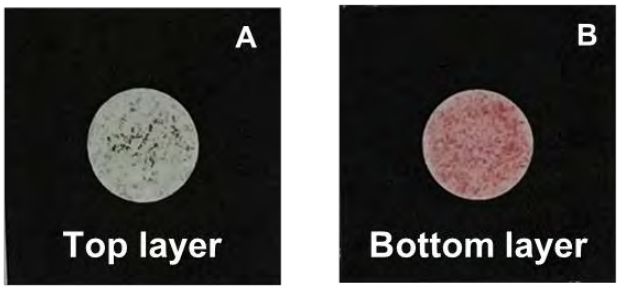

Figure 4.7 The optical images of: (A) the top, and (B) the bottom layers of the developed PAD after applying for the determination of the total iron ions in water sample.

4.1.3.1 Determination of iron by the PAD

The water samples are drinking, tap canal and river water. They were fortified with the standard solution of Fe (II) to attain the final concentration of 10 mg L^{-1}. Firstly, the analytical recovery of the method was investigated. The results are concluded in Table 4.2

Table 4.2 Summary of the results of study on the analytical recovery of the developed PAD for the determination of the iron content in water samples.

Water sample	Iron concentration (as mg L^{-1}, Mean ± SD*)		Recovery (%)
	Fortified	Observed	
Drinking	10.00	10.04 ± 0.20	100.40
Tap	10.00	10.15 ± 0.59	101.53
Canal 1	10.00	9.65 ± 0.18	96.50
Canal 2	10.00	9.26 ± 0.22	92.60
River	10.00	10.24 ± 0.40	102.40

Note: * The experiments were carried out in three replicate measurements.

Table 4.2 indicates that the developed PAD is applicable for the determination of Fe (II) in various kinds of water samples, both simple and complicated matrices. This method provides the good analytical recoveries (92.6-102 %). The matrix effect is negligible because the determination is carried out by standard addition method. Therefore, we can conclude that the developed PAD has high accuracy for the quantitative analysis of real sample.

4.1.3.2 Validation

To verify the developed PAD, the total iron concentrations in water samples, determined by the proposed PAD and by the spectrophotometric method were compared. The results are shown in Table 4.3.

Table 4.3 The comparison of the total iron concentrations in water samples, obtained by the proposed PAD and by the spectrophotometric method (the UV-vis. method).

Water sample*	Iron concentration (as mg L^{-1}, Mean $\pm$ SD**)	
	PAD	Spectrophotometric method
Drinking	10.04 ± 0.20	10.38 ± 0.03
Tap	10.15 ± 0.59	10.46 ± 0.03
Canal 1	9.65 ± 0.18	9.82 ± 0.01
Canal 2	9.26 ± 0.22	9.61 ± 0.07
River	10.24 ± 0.40	10.16 ± 0.00

Note: * Canal 1 and Canal 2 were collected from Prawet and Sansaeb Canals while River was obtained from Chao Pra Ya River.

** The experiments were carried out in three replicate measurements.

The results in Table 4.3 are statistically compared by Paired *t*-test. The results are not significantly difference at the confidence level of 95 % (t_{stat} = 2.68, t_{cri} = 2.78). Therefore, the developed offers the accurate results.

4.2 Bacterial Nanocellulose-based Analytical Device for Determination of Trivalent Chromium

4.2.1 Characterization of Bacterial Nanocellulose

After harvesting, it is observed from Figure 4.8A that the color of the original BNC is pale yellowish-brown. After bleaching with hydrogen peroxide and alkaline solution, its color turns milky-white. Additionally, it becomes more transparent as depicted in Figure 4.8B. This guarantees that the as-prepared BNC biofilm is capable of being used as the 2D-microcuvette.

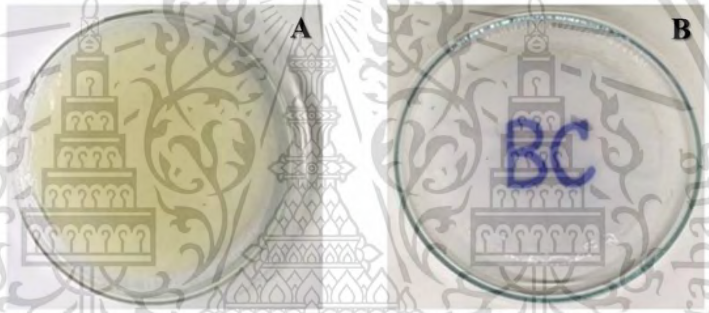

Figure 4.8 The optical images of BNC: (A) before and (B) after the bleaching processes.

Later, morphology of the dried BNC was studied by SEM, and the result is depicted in Figure 4.9. It is found that the dimension of the cellulose fibril is smaller than 100 nanometers. This causes the as-prepared BNC offers high transparency as the incident light can be transmitted through the nanofibril.

.

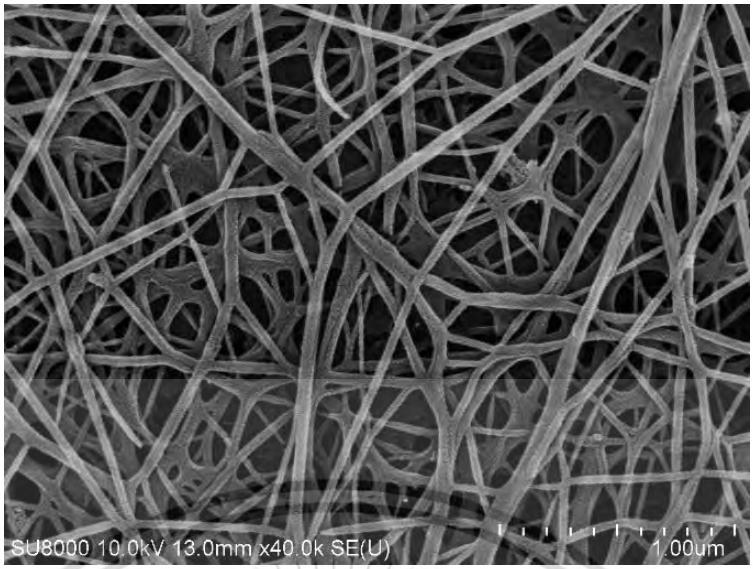

Figure 4.9 An example of the optical SEM image of the as-prepared BNC.

4.2.2 Synthesis of new fluorescein derivative and characterization

The new fluorescein derivative (NFD) was characterized by FTIR, ESI-MS, ^{1}H- and ^{13}C-NMR for the structure elucidation. The raw data result from spectroscopy techniques are show in Appendix A. Briefly, we observed the information as the following summary. FTIR (KBr, cm^{-1}): 3043, 1582, 1474, 1385, 1345, 1208, 925 and 758.04. ESI-MS *m/z*: 662 $[M + CH_3OH + H]^+$. ^{1}H-NMR (400 MHz, CD_3OD): δ (ppm) 7.97 (d, 1H), 7.71-7.55 (m, 8H), 7.52-7.24 (m, 4H), 7.09 (d, 1H), 6.88 (d, 1H) and 6.39 (d, 1H). ^{13}C-NMR (100 MHz, CD_3OD): δ (ppm) 180.87, 176.39, 175.52, 171.33, 157.95, 157.12, 154.60, 150.03, 139.79, 139.14, 133.64, 133.62, 132.62, 132.28, 130.15, 129.66, 128.38, 128.37, 128.19, 128.01, 127.47, 127.41, 127.40, 126.66, 126.18, 125.81, 125.29, 125.05, 121.61, 111.29, 108.75, 103.63 and 102.08. From all these characteristic signals, it can be interpreted the structure of the NFD as depicted in Figure 4.10. It can be concluded that the as-synthesized NFD is composed of the native fluorescein molecule in conjugation with anthranilic acid. Fluorescein acts as the fluorophore while the acid plays a role as the ionophore.

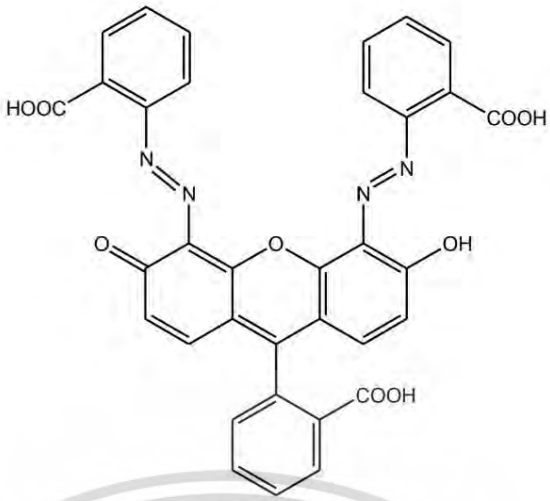

Figure 4.10 The interpreted molecular structure of the as-synthesize NFD.

4.2.3 Study on Characteristics of NFD

The characteristics of the as-prepared NFD were studied in terms of excitation and emission wavelength, selectivity, effect of pH, stoichiometry, fluorescence response toward Cr (III), and applicability for the determination of Cr (III) in water sample. Note that each study was carried out in liquid phase (not on the BNC platform). The results are described as the following sub-sections.

4.2.3.1 Excitation and Emission Wavelengths

Excitation of NFD was carried out by monitoring the absorption spectrum of 10 μM NFD solution by UV-Visible spectrophotometer in the range 200-800 nm. The maximum absorption was considered as the excitation wavelength and was employed for investigating the appropriate emission wavelength. The absorption and emission spectrum are obtained as illustrated in Figure 4.11.

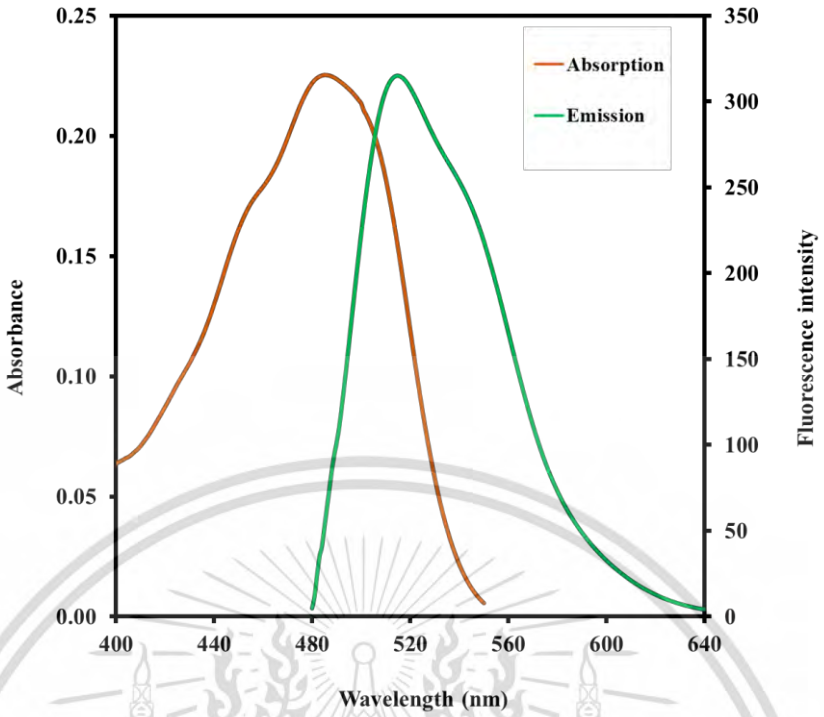

Figure 4.11 The absorption and emission spectra of NFD.

Figure 4.11, we observed that the maximum absorption of NFD is located at 485 nm. By applying this wavelength as the excitation wavelength for fluorometric detection, the highest emission wavelength of 520 nm is obtained. We then assigned the excitation and emission wavelengths of 485 nm and 520 nm, respectively, for all fluorometric measurements.

4.2.3.2 Selectivity study

A selectivity study was carried out through mixing the metal ion solutions with the NFD. The results are demonstrated in Figure 4.12.

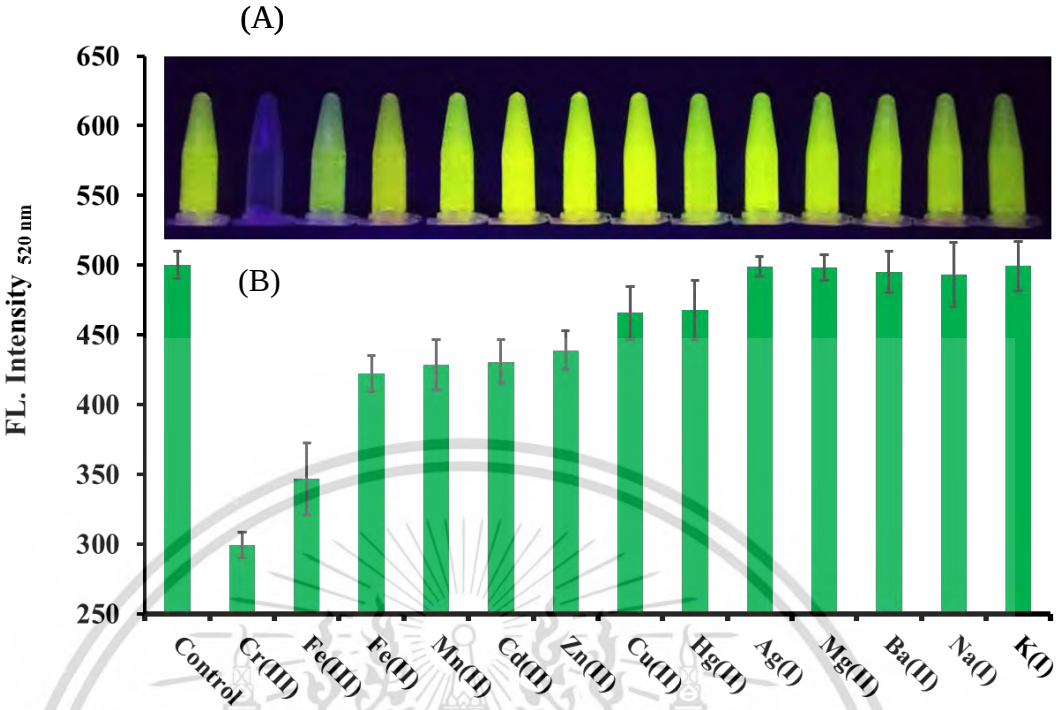

Figure 4.12 (A) An Optical image of the NFD (10 μM) underneath the UV irradiation in the presence of many investigated cations (100 μM) and (B) the related fluorescence intensity.

The fluorescence intensity of NFD is obviously quenched by Cr (III). However, we found that Fe (III) can slightly reduce the intensity, whereas the other ions do not affect the quenching reaction. The quenching effect by Cr (III) and Fe (III) can be because coordinated covalent bond between these two metal ions and the NFD ligand is occurred. These ions are kinds of transition metal ions, where their d-orbitals is much plenty for absolutely bounded with the NFD ligand. In contrast to the metal ions existed in 1A and 2A group such as Na (I), K (I), Mg (II) and Ba (II), their d-orbital are occupied, the NFD ligand cannot being bounded with these metal ions.

However, the complex formation also depends on the valent charge of ion. The chelation prefers to occur when the ligand is exposed to tri-valent ion. This may be due to electrostatic force that can strongly induce the interaction between the electron of NFD ligand and the ion. Note that, in this experiment, Cr (III) is the most selective ion which can be bound with the NFD and successfully quenched the

fluorescence intensity of the dye. Therefore, it is very interesting to apply this phenomenon for the quantitative analysis of Cr (III).

4.2.3.3 Effect of pH

The fluorescence intensity of the NFD in the absence and presence of Cr (III) are individually studied in different pH values which varied in the range from pH of 2.00 to 12.00. Results are shown in Figure 4.13.

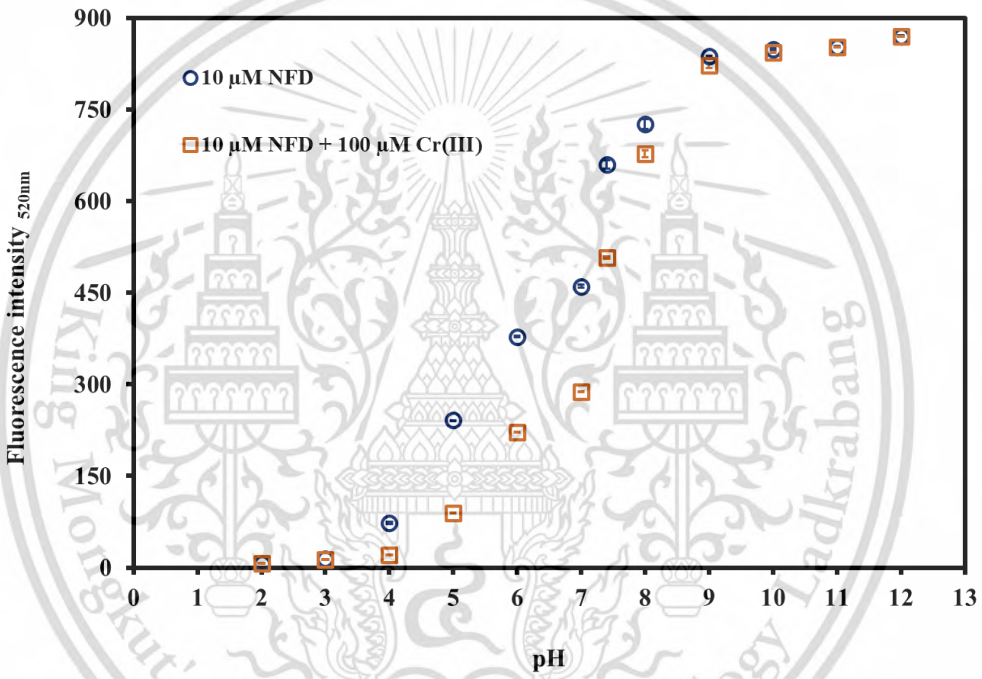

Figure 4.13 The fluorescence intensity of the NFD solution in the absence and presence of Cr (III) in different pH values.

Results in Fig. 4.13 shows that the fluorescence intensity of NFD is very low in acidic solution (pH 2-5). This is because nitrogen atom of the azo group is protonated and there is no lone pair electron for coordinating with Cr (III). At higher pH values (9-13), it is not absolutely appropriate because precipitation of Cr (III) to form $Cr(OH)_3$ was occurred and quenching of the NFD was not observed. The difference of NFD intensity in the absence and presence of Cr (III) is clearly noticed at pH 7.0. Therefore, this pH value is selected as the appropriate value.

4.2.3.4 Stoichiometry

Stoichiometry is studied based on Job's method. The aim of this study is to propose the mechanism of complex formation between Cr (III) and NFD ligand. The result is shown in Figure 4.14.

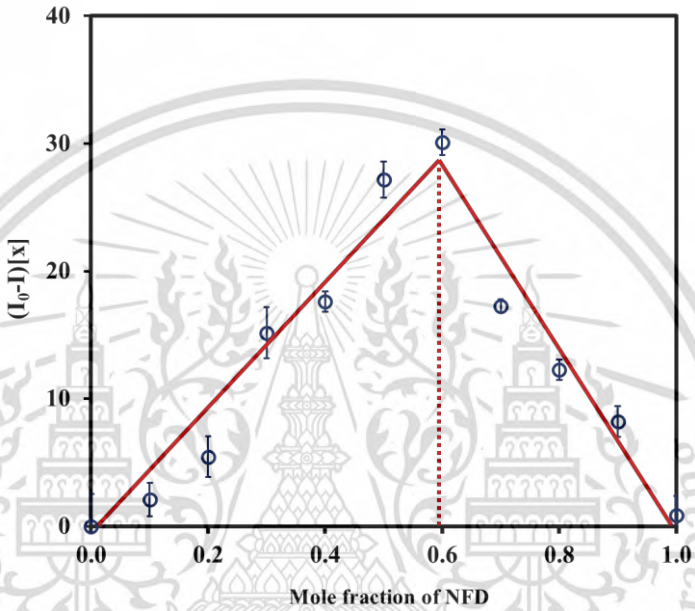

Figure 4.14 Job's plot of the complex formation between Cr (III) and NFD. The y-axis is the difference of the fluorescence intensity of the NFD (520 nm) in the absence (I_0) and presence (I) of the Cr (III), multiplied with the mole fraction of NFD (x) and the x-axis is the mole fraction of NFD.

Result in Figure 4.14 indicates that the maximum value is observed when the mole fraction of the NFD is equivalent to 0.6. This suggests that the stoichiometry of the complex formation between Cr (III) and NFD is 1:2. With this result, we proposed the reaction mechanism as illustrated in Figure 4.15. A single mole of Cr (III) is coordinated with double mole of the NFD via nitrogen atom of azo group (-N=N-) and oxygen atom of hydroxyl group which there are lone pair electron. The complex formation is proposed below:

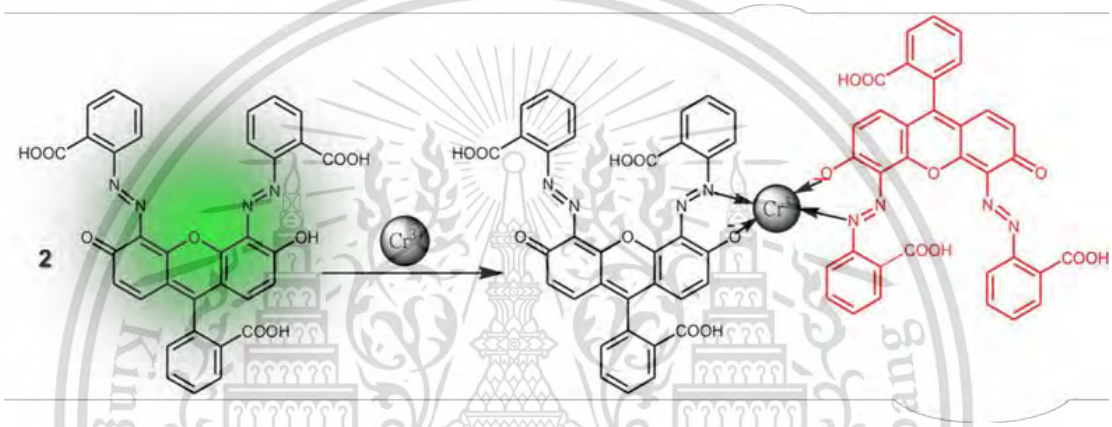

Figure 4.15 Schematic drawing of the proposed mechanism for the complex formation between Cr (III) and the NFD ligand.

4.2.3.5 Fluorescence Response of NFD toward Cr (III)

The fluorescence response of NFD toward Cr (III) was investigated by mixing the standard solution of Cr (III) solution in the concentration range of 0-1000 μM with the NFD solution (10 μM) in the presence of KHP buffer (pH 7.0). The results in terms of the emission spectra are shown in Figure 4.15.

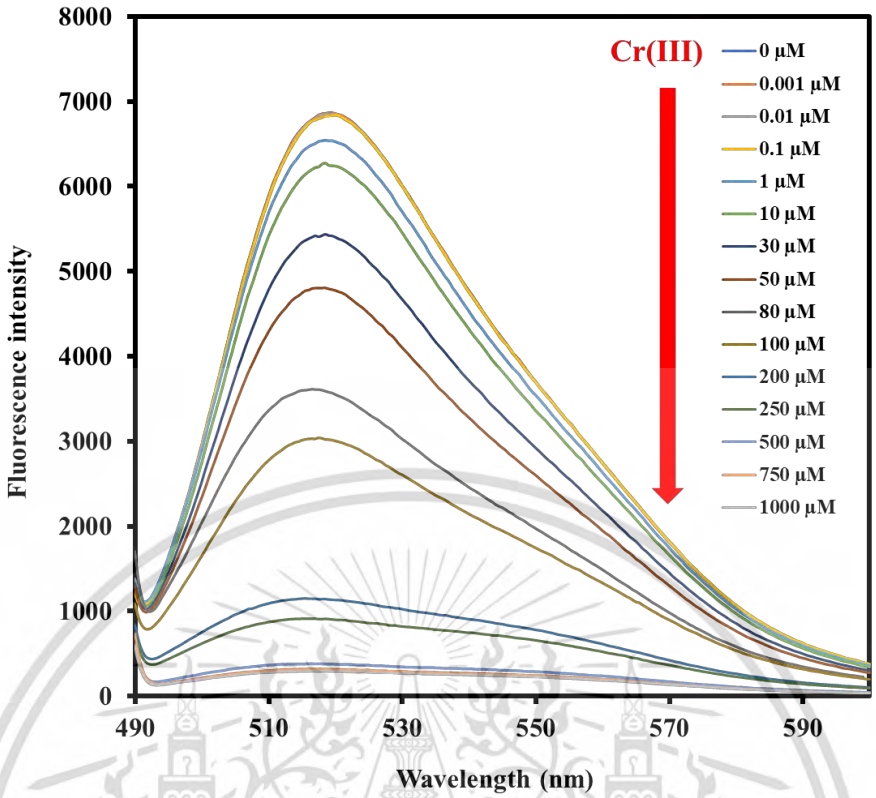

Figure 4.16 Fluorescence emission spectra representing the response of NFD toward various concentrations of standard Cr (III) solutions.

Results in Figure 4.16 show the quenching of NFD in the presence of Cr (III). When the concentration of Cr (III) increases, the fluorescence intensity of NFD decreases. However, when the corresponding intensities are plotted versus the concentration of Cr (III) based on Stern-Volmer's principle, it is found that the linear relationship in the concentration range of 0-100 µM Cr (III) as shown in Figure 4.16.

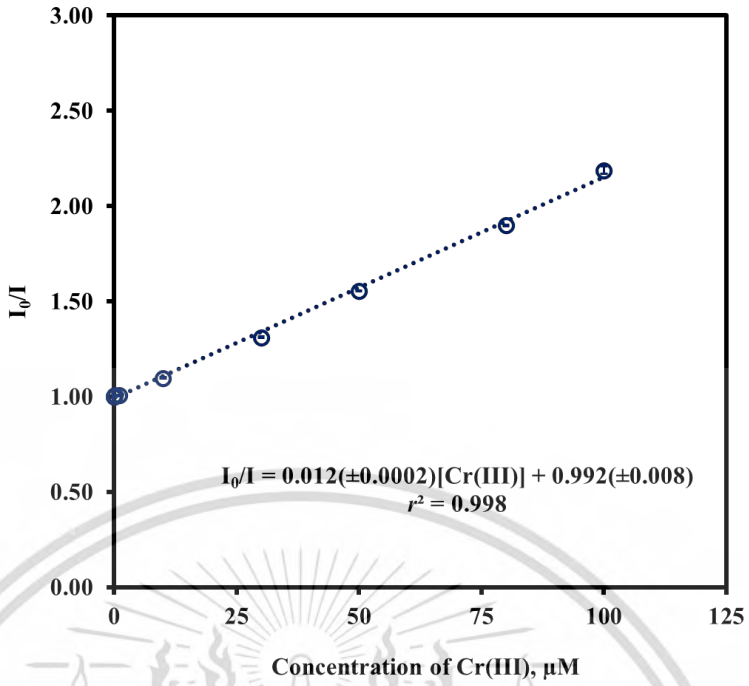

Figure 4.17 The Stern-Volmer's plot of the fluorescence intensity of NFD in the presence of various concentrations of standard Cr (III).

Figure 4.17 represents the linear relationship based on Stern-Volmer's plot in the concentration range of 0-100 µM Cr (III). Good linearity (r^2 = 0.998) indicates that the quenching reaction of NFD by Cr (III) is applicable for the quantitative analysis of Cr (III).

4.2.3.6 Applicability for Determination of Cr (III) in Water Sample

The quenching reaction between the NFD and Cr (III) was applied for the determination of the Cr (III) contents in natural water samples, collected Bangkok and Chi Rai Province. Both water samples with simple and complicated matrices were tested. However, we realized that the natural water the complicated sample matrix can affect accuracy of the developed method. To avoid this problem, the standard addition method is therefore employed. The spiked water samples were prepared to finally obtain the concentration of 10 µM Cr (III). Accuracy test in terms of the analytical recovery was evaluated. Results is summarized in Table 4.4.

Table 4.4 Analytical recovery of the developed method for the determination of Cr (III) in spiked water samples based on its quenching effect of the fluorescence of the NFD.

Sample name	Types of samples	Cr (III) concentration (μM)		Recovery (%)
		Fortified	Observed	
Pra Wet	Canal	10.0	9.71 ± 0.01	97.1
Chao Praya	River	10.0	9.77 ± 0.03	97.7
Mae Khong	River	10.0	9.63 ± 0.02	96.3
Kok	River	10.0	9.98 ± 0.02	99.8
Pha Soet	Hot spring	10.0	9.89 ± 0.01	98.9

The results in Table 4.4 represent the satisfied analytical recoveries (96.3-99.8 %). This indicates that the developed method is not interfered with by the sample matrix.

4.2.4. Preparation of NFD-immobilized BNC

The NFD-immobilized BNC were prepared by soaking the bare BNC in the NFD solution under dark light. The conditions that affect the soaking performance i.e., the concentration of the NFD solution and the soaking time were investigated. The effects of the concentration of NFD were studied from 1 to 20 mM while the soaking time was varied from 1 to 6 hr. The results are shown in Figure 4.18 and Table 4.5.

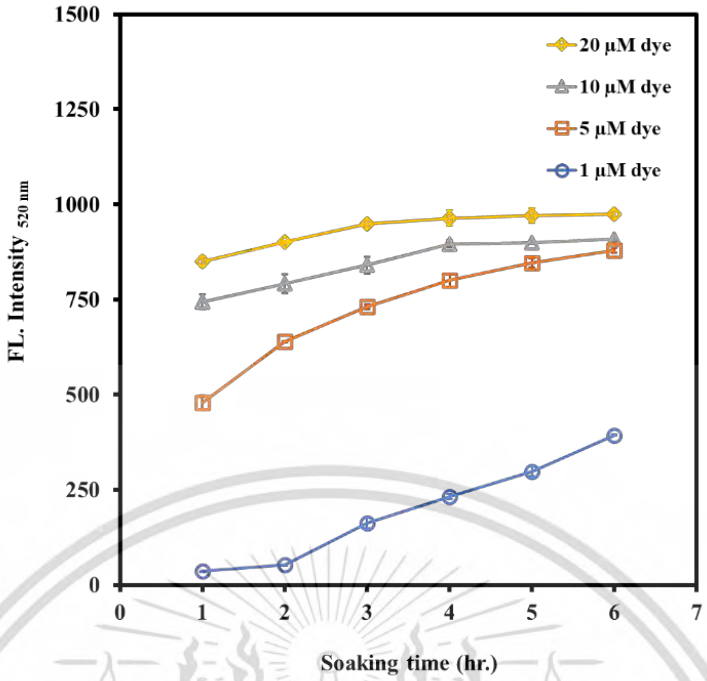

Figure 4.18. The fluorescence intensity of the NFD-immobilized BNC, obtained by the various conditions.

Table 4.5. The optical images of the NFD immobilized BNCs, capturing under various immobilization conditions.

Concentration of NFD (µM)	Soaking time (hr)					
	1	3	6	9	12	24
1	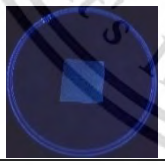				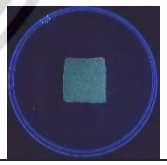	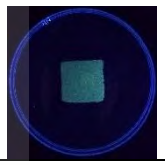
5	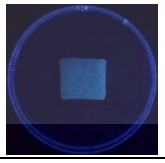	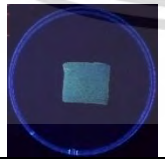	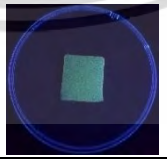	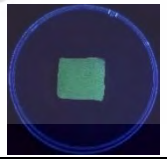	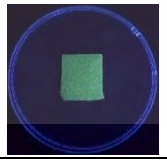	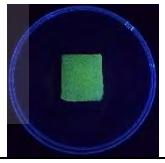
10	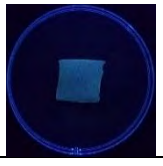	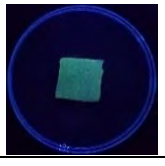	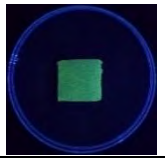	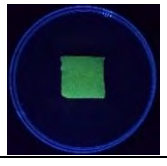	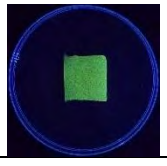	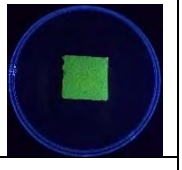
20	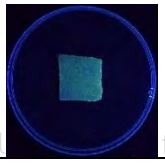	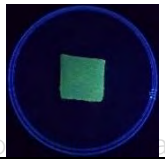	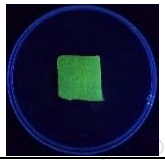	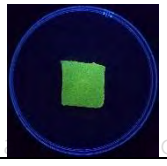	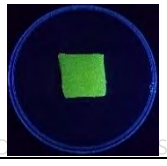	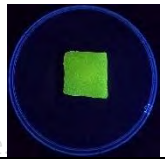

It is found from the result in Figure 4.18 and Table 4.5 that the fluorescence intensity of NFD in BNC is increased when the NFD concentration and soaking time are increased. At concentration as 10 and 20 μM of NFD, the intensity become steady after 9 hrs. soaking, this time is therefore selected as the appropriate time. Regarding in terms of the suitable concentration of NFD, we compromise between the fluorescence intensity and reagent consumption. Therefore, we thus choose 10 μM NFD as the appropriate concentration for immobilization of BNC.

4.2.5 Fluorescence Spectrum of the NFD-immobilized BNC

The fluorescence of the immobilized BNC was investigated using the excitation wavelength of 485 nm. The immobilized BNC was cut to contain a dimension of 16 mm width x 50 mm length and was situated into the BNC holder with subsequent inserted into the sample holder inside the spectrofluorometer. The result is shown in Figure 4.18

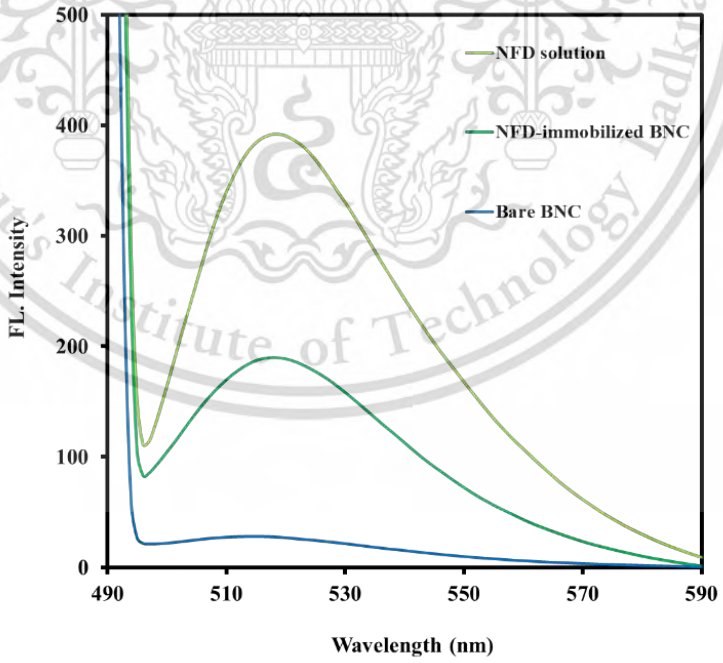

Figure 4.19 Overlaid emission fluorescence spectra of Bare BNC, 10 μM NFD immobilized BNC and 10 μM NFD solution.

The result in Figure 4.19 illustrates that normally, the bare BNC cannot emit the light. However, the immobilized BNC can provide the fluorescence spectrum with the highest emission intensity at 520 nm. This wavelength is the same emission wavelength of the NFD solution. So, this confirms that under the optimal immobilization condition, the NFD can be immobilized into the BNC.

4.2.6 Application to the Cr (III) Determination in Water Samples and Validation

The NFD-immobilized BNC is applied to the quantitative analysis of Cr (III) in natural water sample (river and canal). The determination was started by constructing the calibration curve based on Stern-Volmer's relationship. The standard of Cr (III) in the range of 0-100 µM were individually reacted with the immobilized BNC under optimal conditions, then it was measured the fluorescence intensity at 520 nm. The results are shown in Figure 4.20.

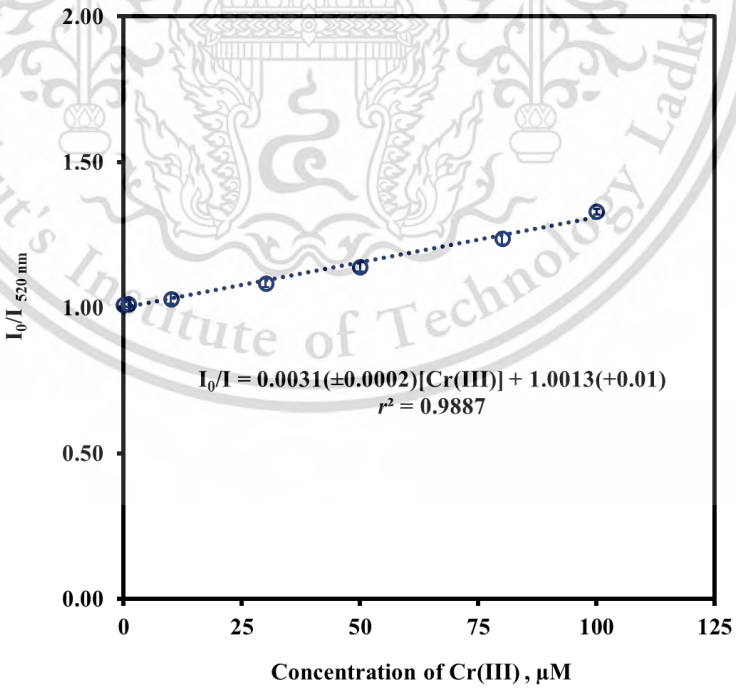

Figure 4.20 The Stern-Volmer's plot of the fluorescence intensity of the NFD-immobilized BNC reacted with standard Cr (III) in the concentration range 0-100 µM.

The results in Figure 4.20 show that the Stern-Volmer's relationship between the fluorescence intensity of the immobilized BNC and concentration of standard Cr (III) is linear the good linearity (r^2 = 0.9887) is achieved. Thus, the calibration equation was therefore determined the amount of Cr (III) in natural water sample and the obtained results were then validated, comparing the results obtained by the ICP-OES method. The results are illustrated in Table 4.6.

Table 4.6 The comparison of the amount of Cr (III) in natural water samples, obtained by the immobilized BNC and by the ICP-OES method.

Natural Water sample*	concentration of Cr (III) (μM, Mean ± SD**)	
	The immobilized BNC	ICP-OES method
Canal	1.97 ± 0.73	1.93 ± 0.01
River	1.85 ± 0.54	1.91 ± 0.03

Note: * Canal and River were collected from Prawet canal and Kok River, respectively.

** The experiments were carried out in three replicate measurements.

The results in Table 4.6 are observed from determination of 2 μM-Cr (III) spiked natural water sample. It shows that the proposed method is applied as the device for quantitative analysis of Cr (III), the results from this method are significantly different with the result obtained from the validation method (ICP-OES) at confident level 95% by Paired *t*-test (n = 2, t_{stat} = 0.20, t_{cri} = 12.71). Moreover, the analytical recovery of two samples is also tested and we observed that the proposed method is accurate, the recovery values are achieved as 98.3 and 92.5 % for canal and river water sample, respectively. These confirm that the NFD-immobilized BNC is capable as the device for determination of Cr (III) in real samples with satisfied results.

Chapter 5
Conclusions and Suggestions

5.1 Conclusions

In this work, there are two kinds of cellulose-based analytical devices that were successfully developed. The first one is made of the filter paper device and the second one is constructed from the bacterial nanocellulose. Details of both the devices can be summarized as the following issues:

5.1.1 The paper-based analytical device (PAD) for the determination of total iron (Fe) ions in water samples:

5.1.1.1 The PAD is designed as the double-layered platform. The top and bottom layers are used for filtration and detection of Fe, respectively.

5.1.1.2 Detection reaction is based on the colorimetric measurement of the stable, red-colored complex of Fe (II) and bathophenanthroline.

5.1.1.3 The analytical performance of the developed device offers the working range in 0.0-0.5 mg L^{-1} with good linearity, high selectivity, high accuracy (Recovery = 92.6-102 %) and precision (RSD = 5.81 %).

5.1.1.4 The PAD is successfully developed for the quantitative analysis of total iron (Fe) contents in water samples including drinking, tap, and canal water samples.

5.1.1.5 The results observed by the developed device are not significantly different with the results attained by the spectrometric validation method at confidence level 95% using Pair *t*-test. These confirm that the device is applicable for quantitative analysis of Fe in real water sample.

5.1.2 The bacterial nanocellulose (BNC)-based analytical device for the determination of Cr (III).

5.1.2.1 The device was fabricated by immobilizing the new fluorescein derivative (NFD) onto the transparent BNC. The as-prepared BNC was exploited as a 2D microcuvette instead of a conventional fluorescence quart cell.

5.1.2.2 Detection principle is based on the quenching of the fluorescence of the NFD-immobilized BNC platform by Cr (III).

5.1.2.3 The fluorescence response of the NFD toward Cr (III) was examined in the solution phase and it was found that the NFD is highly selective to Cr (III) than the other investigated cations. Additionally, good linear response was obtained in the concentration range of 1-100 μM Cr (III) where the value of r^2 of 0.998 was achieved.

5.1.2.4 The NFD can be applied to determination of Cr (III) in water sample by standard addition method. the accurate result with the good recovery 96.3-99.8 %. Note that this experiment was carried out in the solution phase.

5.1.2.5 Under optimal condition, the NFD-immobilized bacteria nanocellulose (NFD/BNC) was successfully prepared. When the as-immobilized BNC platform was applied to the detection of standard Cr (III), it was observed that the calibration curve in the concentration range of 1-100 μM Cr (III) with good linearity (r^2 = 0.9887) was accomplished. This confirm that the NFD/BNC is possible to apply for quantitative analysis of Cr (III).

5.1.2.6 The NFD/BNC is successfully developed for the quantitative analysis of Cr (III) contents in natural water samples including canal and river water samples.

5.1.2.7 The results observed by the developed device are not significantly different with the results attained by the ICP-OES validation method at confidence level 95% using Pair *t*-test. These confirm that the device is applicable for quantitative analysis of Cr (III) in real water sample.

5.2 Suggestion

The double-layered platform for determination of Fe in this work is a new idea for monitoring the metal ion in natural water. By this concept, the immobilized specific reagent in the bottom layer can be change to the other, for determination of many ions. However, the top layer was necessary for applying as the filtration platform to eliminate the suspended particles in real samples.

The NFD-BNC is successfully prepared. Nevertheless, its analytical performance such as the detection limit is not satisfied. Therefore, the optimal condition of the detection must be further studied to develop the NFD-BNC for quantitative analysis of Cr (III) in real sample with reliable results. Moreover, the NFD-BNC may be developed for determination of Cr (VI) by reducing Cr(VI) to Cr (III) using the strong reducing agent.

References

[1] Chaikhan, P. Udnan, Y. Sananmuang, R. Ampiah-Bonney, R. J. and Chuachuad Chaiyasith, W. 2020. "A Low-Cost Microfluidic Paper-Based Analytical Device (μpad) with Column Chromatography Preconcentration for the Determination of Paraquat in Vegetable Samples." *Microchemical Journal.* 159 : 105355.

[2] Mathaweesansurn, A. Thongrod, S. Khongkaew, P. Matayatsuk Phechkrajang, C. Wilairat, P. and Choengchan, N. 2019. "Simple and Fast Fabrication of Microfluidic Paper-Based Analytical Device by Contact Stamping for Multiple-Point Standard Addition Assay: Application to Direct Analysis of Urinary Creatinine." *Talanta.* 210 : 102675.

[3] Aparecido Oliani Pedro da Silva, V. Cristina de Freitas, R. Roberto de Oliveira, P. Cardoso Moreira, R. Humberto Marcolino-Júnior, L. Fernando Bergamini, M. Coltro, W. K. T. and Campos Janegitz, B. 2020. "Microfluidic Paper-Based Device Integrated with Smartphone for Point-of-Use Colorimetric Monitoring of Water Quality Index." *Measurement.* 164 : 108085.

[4] Lert-itthiporn, A. Srikritsadawong, P. and Choengchan, N. 2021. " Foldable Paper-Based Analytical Device for Membraneless Gas-Separation and Determination of Iodate Based on Fluorescence Quenching of Gold Nanoclusters." *Talanta.* 221 : 121574.

[5] Yang, Y. Chen, X. Wang, Y. Wu, M. Ma, Y. and Yang, X. 2020. "A Novel Fluorescent Test Papers Based on Carbon Dots for Selective and Sensitive Detection of Cr (VI)." *Frontiers in Chemistry.* 8 : 595628.

[6] Lu, K.-H. Lin, J.-H. Lin , C.-Y. Chen, C.-F. and Yeh, Y.-C. 2019. "A Fluorometric Paper Test For Chromium(VI) Based on the Use of N-Doped Carbon Dots." *Microchimica Acta.* 186 : 227.

[7] Didier Pedrosa de Amorim, J. Carvalho de Souza, K. Rodrigues Duarte, C. Da Silva Duarte, I. De Assis Sales Ribeiro, F. Santos Silva, G. Maria Albuquerque de Farias, P. Stingl, A. Fernanda Santana Costa, A. Maria Vinhas, G. and Asfora Sarubbo, L. 2020. "Plant and Bacterial Nanocellulose: Production, Properties and Applications in Medicine, Food, Cosmetics, Electronics and Engineering. A Review." *Environmental Chemistry Letters.* 18 : 851-869.

[8] Torres, F.G. Arroyo, J.J. and Troncoso, O.P. 2019. "Bacterial Cellulose Nanocomposites: An All-Nano Type of Material." *Materials Science & Engineering C.* 98 : 1277-1293.

[9] Sharma, C. and Bhardwaj, N. K. 2019. "Bacterial Nanocellulose: Present Status, Biomedical Applications and Future Perspectives." *Materials Science & Engineering C.* 104 : 109963.

[10] Zor, E. 2018. "Silver Nanoparticles-Embedded Nanopaper as a Colorimetric Chiral Sensing Platform." *Talanta.* 184 : 149–155.

[11] Fu, J. Zhu, J. Tian, Y. He, K. Yu, H. Chen, L. Fang, D. Jia, D. Xie, J. Liu, H. Wang, J. Tang, F. Tao, J. and Liu, J. 2020. "Green and Transparent Cellulose Nanofiber Substrate-Supported Luminescent Gold Nanoparticles: A Stable and Sensitive Solid-State Sensing Membrane for Hg(II) Detection." *Sensor and Actuators B: Chemical.* 319 : 128295.

[12] Lert-itthiporn, A. Phunpruch, S. Prommajun, M. Srikritsadawong, P. and Choengchan, N. 2020. " Gold Nanoparticles-Bacterial Cellulose Nanopaper for Colorimertic Determination of Hydrogen Peroxide" *Chiang Mai Journal of Science.* 47 : 175-185.

[13] Meeravali, N. N., Madhavi, K. and Sahayam, A. C. 2021. "Novel Ionic Reverse Mixed Micelle Supramolecules in Dispersive Liquid-Liquid Microextraction for The Successive/Individual Sensitive Speciation Analysis of Iron In Natural Water By UV–Vis Spectrophotometry." *Microchemical Journal*. 164 : 105986.

[14] Andreani, A. S., Kunarti, E. S., Hashimoto, T., Hayashita, T. and Santosa, S. J. 2021. "Fast and Selective Colorimetric Detection of Fe^{3+} Based on Gold Nanoparticles Capped with Ortho-Hydroxybenzoic Acid." *Journal of Environmental Chemical Engineering*. 9(5) : 105962.

[15] Department of Health, 2020. Declaration of quality criteria of drinkable tap water. [online] Available at: https://www.laws.anamai.moph.go.th/th/practices/201133.

[16] Industrial Estate Authority of Thailand, 2018. Declaration of general standard criteria for draining pretreated wastewater. [online] Available at: https://www.env.ieat.go.th/th.

[17] Yaman, M. and Kaya, G. 2005. "Speciation of Iron (II) and (III) by Using Solvent Extraction and Flame Atomic Absorption Spectrometry." *Analytica Chimica* Acta. 540 : 77-81.

[18] Proch, J. and Niedzielski, P. 2021. “Iron Species Determination by High Performance Liquid Chromatography with Plasma Based Optical Emission Detectors: HPLC–MIP OES and HPLC–ICP OES.” *Talanta*. 231 : 122403.

[19] Okabe, S., Oda, K., Muto, M., Sahoo, Y. V. and Tanaka, M. 2021. “Speciation and Determination of Iron in Aqueous Solution and River Water by High-Resolution Electrospray Ionization Mass Spectrometry.” *Journal of Molecular Liquids*. 329 : 115532.

[20] Ugo, P., Moretto, L.M., De Boni, A., Scopece, P. and Mazzocchin, G.A. 2002. “Iron (II) and Iron (III) Determination by Potentiometry and Ion-Exchange Voltammetry at Ionomer-Coated Electrodes.” *Analytica Chimica Acta*. 474(1-2) : 147-160.

[21] Dieker, J. W. and Van Der Linden, W. E. 1980. “Determination of Iron (II) and Iron (III) by Flow Injection and Amperometric Detection with a Glassy Carbon Electrode.” *Analytica Chimica Acta*. 114 : 267-274.

[22] Gong, X., Zhang, H., Jiang, N., Wang, L. and Wang, G. 2019. “Oxadiazole-Based ‘on-off’ Fluorescence Chemosensor for Rapid Recognition and Detection of Fe^{2+} And Fe^{3+} in Aqueous Solution and in Living Cells.” *Microchemical Journal*. 145 : 435-443.

[23] Iqbal, A., Tian, Y., Wang, X., Gong, D., Guo, Y., Iqbal, K., Wang, Z., Liu, W. and Qin, W. 2016. “Carbon Dots Prepared by Solid State Method via Citric Acid and 1,10-Phenanthroline for Selective and Sensing Detection of Fe^{2+} And Fe^{3+}.” *Sensors and Actuators B: Chemical*. 237 : 408-415.

[24] Lv, P., Xu, Y., Liu, Z., Li, G. and Ye, B. 2020. “Carbon Dots Doped Lanthanide Coordination Polymers as Dual-Function Fluorescent Probe for Ratio Sensing Fe^{2+}/Fe^{3+} and Ascorbic Acid.” *Microchemical Journal*. 152 : 104255.

[25] Senanayake, D. A. K., Perera, P. P. P., De Costa, M. D. P. and Senthilnithy, R. 2021. “Bathophenanthroline as Turn-off Fluorescence Sensors for Selective and Sensitive Detection of Fe (II).” *Research square*.

[26] Perry, R. D. and San Clemente, C. L. 1977. “Determination of Iron with Bathophenanthroline Following an Improved Procedure for Reduction of Iron (III) Ions.” *Analyst*. 102 : 114-119.

[27] Ferreira, F. T. S. M., Catalão, K. A., Mesquita, R. B. R. and Rangel, A. O. S. S. 2021. “New Microfluidic Paper-Based Analytical Device for Iron Determination in Urine Samples.” *Analytical and Bioanalytical Chemistry*. 413 : 7463–7472.

[28] กรมอนามัย กระทรวงสาธารณสุข. 2015. “มลพิษทางน้ำและผลกระทบต่อสุขภาพ.” เอกสารประกอบการดำเนินงานตอบโต้ภาวะฉุกเฉินด้านอนามัยสิ่งแวดล้อม. พิมพ์ครั้งที่ 1. นนทบุรี: โรงพิมพ์ชุมนุมสหกรณ์การเกษตรแห่งประเทศไทย จำกัด. 17-18.

[29] ชนัตถ์ โชคเจริญรัตน์. 2017. “การตรวจวิเคราะห์หาปริมาณโครเมี่ยมชนิดเฮกซะวาเลนซ์ในลำน้ำแม่กลองด้วยวิธีสเปคโทรโฟโตเมทรี.” นเรศวรวิจัยครั้งที่ 13: วิจัยและนวัตกรรม ขับเคลื่อนเศรษฐกิจและสังคม. 131-137.

[30] กรมควบคุมมลพิษ กระทรวงทรัพยากรธรรมชาติและสิ่งแวดล้อม. 2016. มาตรฐานคุณภาพน้ำ. แหล่งที่มา: http://pcd.go.th/info_serv/reg_std_water04.html (16 กุมภาพันธ์ 2561)

[31] Kiran, K. Suresh Kumar, K. Prasad, B. Suvardhan, K. Ramesh Babu, L. and Janardhanam, K. 2008. “Speciation Determination of Chromium(III) and (VI) Using Preconcentration Cloud Point Extraction with Flame Atomic Absorption Spectrometry (FAAS).” *Journal of Hazardous Materials.* 150 : 582-586.

[32] Matos, G. D. Dos Reis, E. B. Costa, A. C. S. and Ferreira, S. L.C. 2009. “Speciation of Chromium in River Water Samples Contaminated with Leather Effluents by Flame Atomic Absorption Spectrometry After Separation/Preconcentration by Cloud Point Extraction.” *Microchemical Journal.* 92 : 135-139.

[33] Pantsar-Kallio, M. and Manninen, P. K. G. 1996. “Speciation of Chromium in Aquatic Samples by Coupled Column Ion Chromatography-Inductively Coupled Plasma-Mass Spectrometry.” *Analytica Chimica Acta.* 318 : 335-343.

[34] Chen, B.-H. Jiang, S.-J. and Sahayam, A.C. 2020. “Determination of Cr(VI) in Rice Using Ion Chromatography Inductively Coupled Plasma Mass Spectrometry.” *Food Chemistry.* 324 : 126698.

[35] Wan, Y. Guo, Q. Wang, X. and Xia, A. 2010. “Photophysical Properties of Rhodamine Isomer: A Two-Photon Excited Fluorescent Sensor for Trivalent Chromium Cation (Cr^{3+}).” *Analytica Chimica Acta.* 665(2) : 215-220.

[36] Zhou, Y. Zhang, J. Zhang, L. Zhang, Q. and Ma, T. Niu, J. 2013. “A Rhodaminebased Fluorescent Enhancement Chemosensor for the Detection of Cr^{3+} in Aqueous Media.” *Dyes and Pigment.* 97(1) : 148-154.

[37] Kumar Gupta, V. Mergu, N. and Kumar Singh, A. 2015. “Rhodamine-Derived Highly Sensitive and Selective Colorimetric and off-on Optical Chemosensors for Cr^{3+}.” *Sensors and Actuators B: Chemical.* 220 : 420-432.

[38] Mao, J. He, Qun and Liu, W. 2010. “An“off-on” Fluorescence Probe for Chromium(III) Ion Determination in Aqueous Solution.” *Analytical and Bioanalytical Chemistry.* 396(3) : 1197-1203.

[39] Wang, D. Shiraishi, Y. and Hirai, T. 2010. “A Distyryl BODIPY Derivative as a Fluorescent Probe for Selective Detection of Chromium(III).” *Tetrahedron Letters.* 51(18) : 2545-2549.

[40] Li, Z. Zhao, W. Zhang, Y. Zhang, L. Yu, M. Liu, J. and Zhang, H. 2011. “An ‘off-on’ Fluorescent Chemosensor of Selevtivity to Cr^{3+} and Its Application to MCF-7 Cells.” *Tetrahedron.* 67(37) : 7096-7100.

[41] Guha, S. Lohar, S. Banerjee, A. Sahana, A. Hauli, I. Mukherjee, S. K. Matalobos, J. S. and Das, D. 2012. “Thiophene Anchored Coumarin Derivative as a Turn-On Fluorescent Probe For Cr^{3+} : Cell Imaging and Speciation Studies.” *Talanta.* 91 : 18-25.

[42] Zhang, J. Zhang, L. Wei, Y. Chao, J. Wang, S. Shuang, S. Cai, Z. and Dong, C. 2013. “A Selective Carbazole-Based Fluorescent Probe for Chromium(III).” *Analytical Methods.* 5 : 5549.

[43] Wu, Y.-S. Li, C.-Y. Li, Y.-F. Tang, J.-L. and Liu, D. 2014. “A Ratiometric Fluorescent Chemosensor for Cr^{3+} Based on Monomer-Excimer Conversion of a Pyrene Compound.” *Sensors and Actuators B: Chemical*. 203 : 712-718.

[44] Zhu, A. Pan, J. Liu, Y. Chen, F. Ban, X. Qiu, S. Luo, Y. Zhu, Q. Yu, J. and Liu, W. 2020. “A Novel Dibenzimidazole-Based Fluorescent Organic Molecule as a Turn off Fluorescent Probe for Cr^{3+} Ion with High Sensitivity and Quick Response.” *Journal of Molecular Structure.* 1206 : 127696.

[45] Seenan, S. Manickam, S. and Iyer, S. K. 2021. “A New Furan Based Fluorescent Chemosensor for the Recognition of Cr^{3+} Ion and Its Application in Real Sample Analysis.” *Journal of Photochemistry and Photobiology A: Chemistry.* 418 : 113441.

[46] ขวัญชนก จันทลักขณา, ภาณุมาศ ทองอยู่. 2557. “การสังเคราะห์และพัฒนาสีย้อมฟลูออเรสเซนต์ชนิดใหม่เพื่อใช้เป็นเซ็นเซอร์ตรวจหาไอออนโลหะ” วิทยานิพนธ์วิทยาศาสตรมหาบัณฑิต สาขาวิชาเคมี ภาควิชาเคมี คณะวิทยาศาสตร์และเทคโนโลยี, มหาวิทยาลัยธรรมศาสตร์.

[47] Mentele, M. M. Cunningham, J. Koehler, K. Volckens, J. and Henry, C. S. 2012. “Microfluidic Paper-Based Analytical Device for Particulate Metals.” *Analytical Chemistry*. 84 : 4474-4480.

[48] Ogawa, K. and Kaneta, T. 2016. “Determination of Iron Ion in the Water of a Natural Hot Spring Using Microfluidic Paper-Based Analytical Devices.” *Analytical Sciences*. 32(1) : 31-34.

[49] Elavarasi, M. Rajeshwari, A. Chandrasekaran, N. and Mukherjee, A. 2013. “Simple Colorimetric Detection of Cr (III) in Aqueous Solutions by as Synthesized Citrate Capped Gold Nanoparticles and Development of a Paper Based Assay.” *Analytical Methods*. 5 : 6211-6218.

[50] Mettakoonpitak, J. Khongsoun, K. Wongwan, N. Kaewbutdee, S. Siripinyanond, A. Kuharuk, A. and Henry, C. S. 2021. “Simple Biodegradable Plastic Screen-Printing for Microfluidic Paper-Based Analytical Devices.” *Sensors and Actuators: B. Chemical.* 331 : 129463.

[51] Asano, H. and Shiraishi, Y. 2018. “Microfluidic Paper-Based Analytical Device for the Determination of Hexavalent Chromium by Photolithographic Fabrication Using a Photomask Printed with 3D Printer.” *Analytical science.* 34(1) : 71-74.

[52] Muhammed, A. Hussen, A. Redi, M. and Kaneta, T. 2021. “Remote Investigation of Total Chromium Determination in Environmental Sample of the Kombolcha Industrial Zone, Ethiopia, Using Microfluidic Paper-Based Analytical Devices.” *Analytical science.* 37(4) : 585- 592.

[53] Muhammed, A. Hussen, A. and Kaneta T. 2021. “Speciation of Chromium in Water Samples Using Microfluidic Paper-Based Analytical Devices with Online Oxidation of Trivalent Chromium.” *Analytical and Bioanalytical Chemistry.* 413 : 3339–3347.

[54] Pourreza, N. Golmohammadi, H. Naghdi, T. and Yousefi H. 2015. “Green In-Situ Synthesized Silver Nanoparticles Embedded in Bacterial Cellulose Nanopaper as a Bionanocomposite Plasmonic Sensor.” *Biosensors and Bioelectronics.* 74 : 353-359.

[55] Zor, E. Alpaydin, S. Arici, A. Saglam, M. E. and Bingol, H. 2018. “Photoluminescent Nanopaper-Based Microcuvette for Iodide Detection in Seawater.” *Sensor and Actuators B: Chemical.* 254 : 1216-1224.

[56] Faham, S. Golmohammadi, H. Ghavami, R. and Khayatian, G. 2019. “A Nanocellulose-Based Colorimetric Assay Kit for Smartphone Sensing of Iron-Chelating Deferoxamine Drug in Biofluid.” *Analytica Chimica Acta.* 1087 : 104-112.

[57] Naghdi, T. Golmohammadi, H. Vosough, M. Atashi, M. Saeedi, I. and Maghsoudi, M. T. 2019. “Lab-on-Nanopaper: An Optical Sensing Bioplatform Based on Curcumin

Embedded in Bacterial Cellulose as an Albumin Assay Kit.*" Analytica Chimica Acta.* 1070 : 104-111.

[58] Faham, S. Ghavami, R. Golmohammadi, H. and Khayatian, G. 2019. "Spectrophotometric and Visual Determination of Zoledronic Acid by Using a Bacterial Cell-Derived Nanopaper Doped with Curcumin." *Microchimica Acta.* 186 : 719.

[59] Lert-itthiporn, A. Phunpruch, S. Prommajun, M. Srikritsadawong, P. and Choengchan, N. 2 0 2 0. " Gold Nanoparticles-Bacterial Cellulose Nanopaper for Colorimertic Determination of Hydrogen Peroxide" *Chiang Mai Journal of Science.* 47 : 175-185.

[60] Sheikhzadeh, E. Naji-Tabasi, S. Verdian, A. and Kolahi-Ahari, S. 2021. "Equipment-Free and Visual Detection of Pb^{2+} Ion Based on Curcumin-Modifed Bacterial Cellulose Nanofber." *Journal of the Iranian Chemical Society.* 19 : 283–290.

[61] Noviana, E. Ozer, T. Carrell, C. S. Link J. S. McMahon, C. Jang, I. and Henry, C. S. "Microfluidic Paper-Based Analytical Devices: From Design to Applications." *Chemical reviews.* 121(19) : 11835–11885.

[62] Joseph, B. Sagarika, V. K. Sabu, C. Kalarikkal, N. and Thomas, S. 2020. "Cellulose Nanocomposites: Fabrication and Biomedical Applications." *Journal of Bioresources and Bioproducts.* 5 : 223-227.

[63] Abdul Khalil, H.P.S. Davoudpour, Y. Nazrul Islama, Md. Mustapha, A. Sudesh, K. Dungani, R. and Jawaid, M. 2014. "Production and Modification of Nanofibrillated Cellulose Using Various Mechanical Processes: A Review." *Carbohydrate Polymers.* 99 : 649-655.

[64] De Amorim, J. D. P. De Souza, K. C. Duarte, C. R. Da Silva Duarte, I. De Assis Sales Ribeiro, F. Silva, G. S. De Farias, P. M. A. Stingl, A. Santana Costa, A. F. Vinhas, G. M. and Sarubbo, L. A. 2020. "Plant and Bacterial Nanocellulose: Production, Properties and Applications in Medicine, Food, Cosmetics, Electronics and Engineering. A Review." *Environmental Chemistry Letters.* 18 : 851-869.

[65] Ossila enabling science, The Jablonski Diagram. [online] Available at: https://www.ossila.com/pages/jablonski-diagrams.

[66] แม้น อมรสิทธิ์. 2552. **หลักการและเทคนิควิเคราะห์เชิงเครื่องมือ.** กรุงเทพฯ : บริษัท ชวนพิมพ์ จำกัด.

[67] Johansson, M. K. 2006. “Choosing Reporter-Quencher Pairs for Efficient Quenching Through Formation of Intramolecular Dimers.” *Fluorescent Energy Transfer Nucleic Acid Probes*. 335 : 17–30.

[68] Principles of Fluorescence Spectroscopy, Mechanisms and Dynamics of Fluorescence Quenching. [online] Available at: https://link.springer.com/chapter/10.1007/978-0-387-46312-4_9.

[69] Physikalisch-chemisches Praktikum I, 2016. Fluorescence Quenching. [online] Available at: https://www.chem.uzh.ch/dam/jcr:571775eb-8b0e-4930-8aa4-ad0da5c11aec/FluorescenceQuenching_HS16.pdf.

Appendix/Appendices

Appendix A

The raw data result of NFD from spectroscopy techniques including FTIR, MS and NMR are illustrated as the following Figure

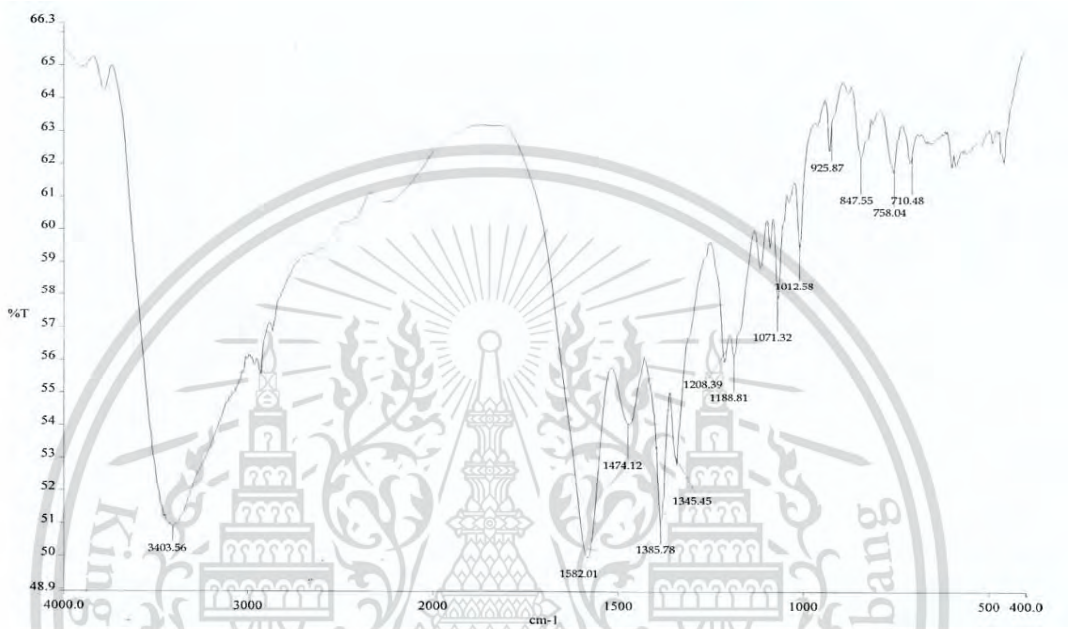

Figure S1. FTIR Spectrum of NFD.

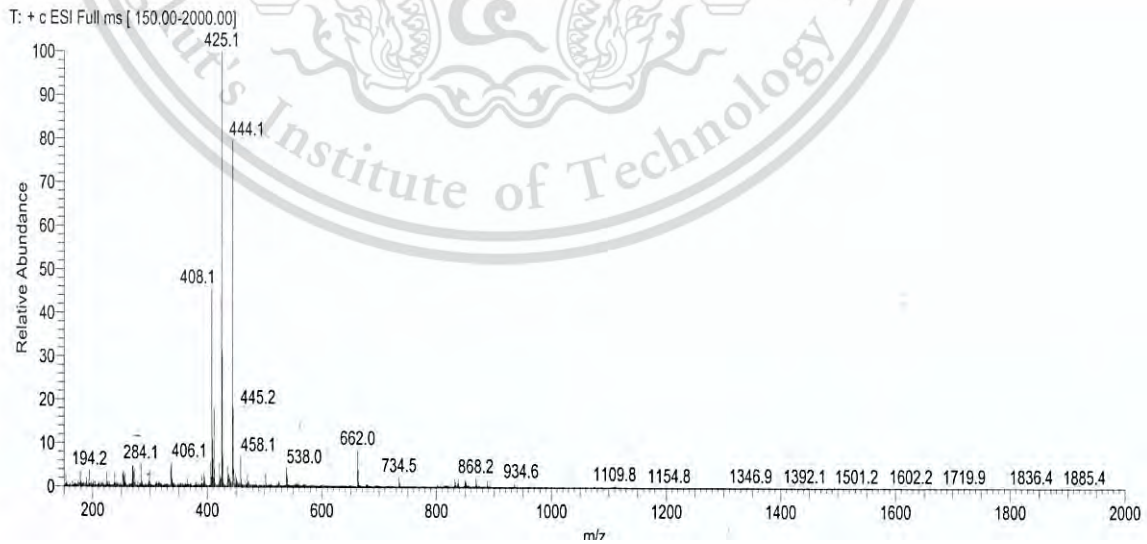

Figure S2. MS Spectrum of NFD.

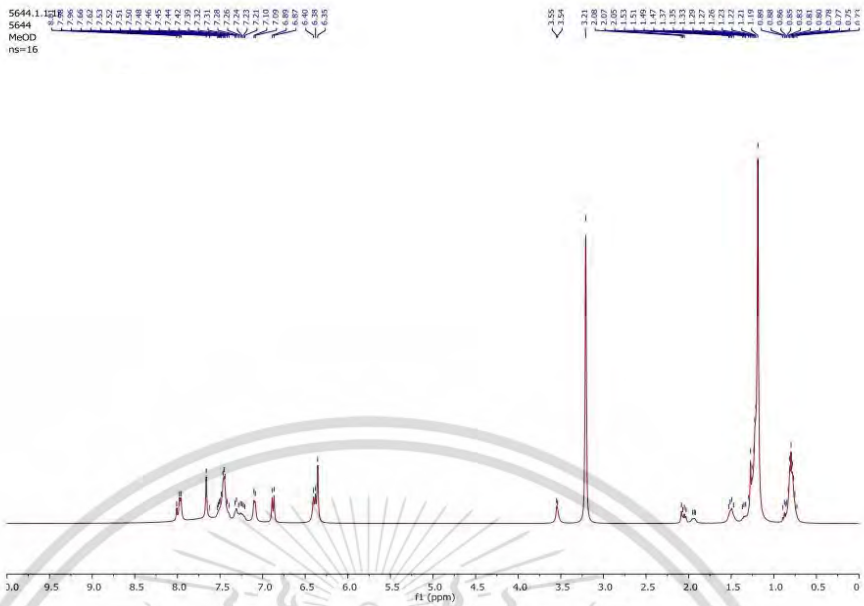

Figure S3. ^{1}H-NMR Spectrum of NFD.

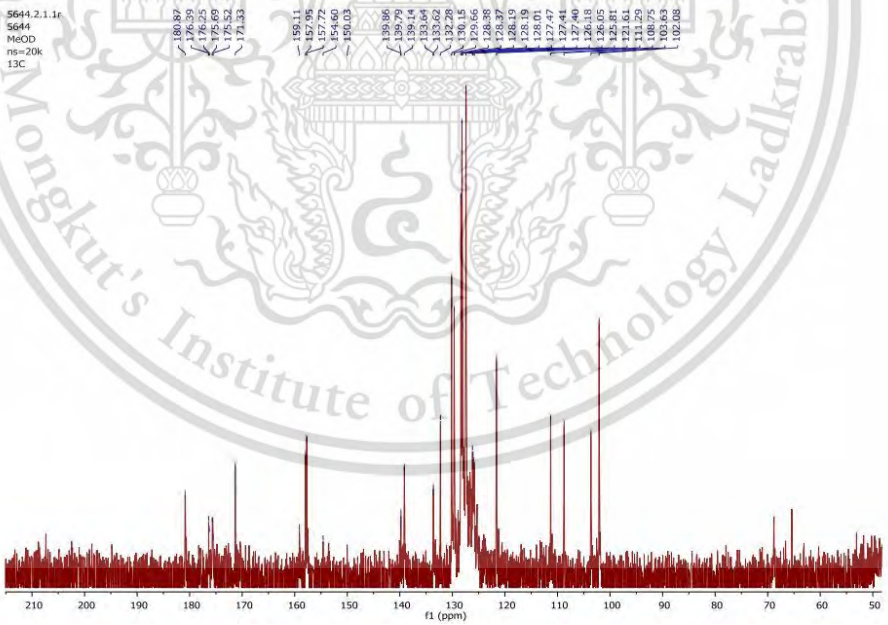

Figure S4 ^{13}C-NMR Spectrum of NFD.

The NMR values from both ^{1}H-NMR and ^{13}C-NMR are clearly summarized in Table S1.

Table S1. ^{1}H-NMR and ^{13}C-NMR value of NFD

Position	NFD		Position	NFD	
	^{1}H-NMR	^{13}C-NMR		^{1}H-NMR	^{13}C-NMR
1	-	126.66	18	7.52-7.24 (m, 4H)	128.38
2	7.09 (d, 1H)	150.03	19	-	133.64
3	6.88 (d, 1H)	111.29	20	-	175.52
4	-	180.87	21	-	157.95
5	-	102.08	22	7.71-7.55 (m, 8H)	125.81
6	-	171.33	23	7.71-7.55 (m, 8H)	139.14
7	-	157.72	24	7.71-7.55 (m, 8H)	132.28
8	-	127.40	25	7.71-7.55 (m, 8H)	130.15
9	-	154.60	26	-	121.61
10	6.39 (d, 1H)	108.75	27	-	176.39
11	7.97 (d, 1H)	128.01	28	-	128.19
12	-	103.63	29	7.71-7.55 (m, 8H)	127.41
13	-	128.37	30	7.71-7.55 (m, 8H)	133.62
14	-	137.79	31	7.71-7.55 (m, 8H)	127.47
15	7.52-7.24 (m, 4H)	125.05	32	7.71-7.55 (m, 8H)	129.66
16	7.52-7.24 (m, 4H)	132.62	33	-	125.29
17	7.52-7.24 (m, 4H)	126.18	34	-	175.69

In Table S1., each value are related to the specified position of NFD structure as shown in Figure S5

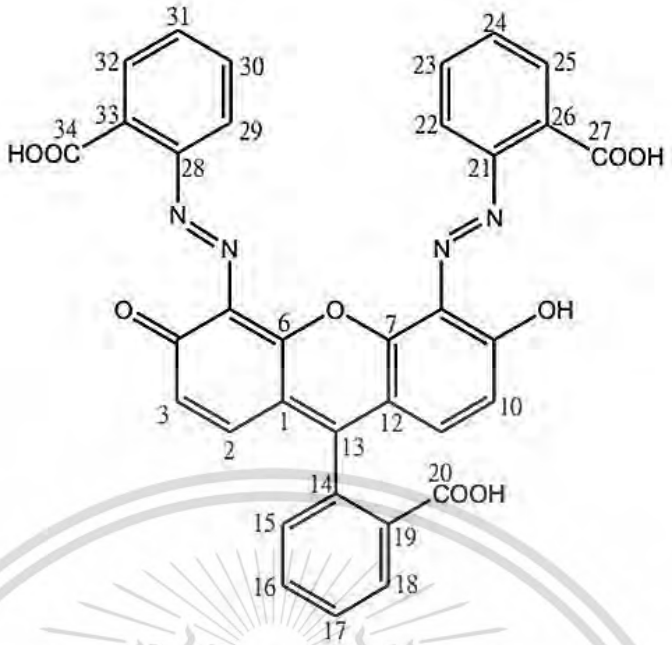

Figure S5. The NFD structure specified the related position with NMR values.

Author Biography

Name Mr. Pongpichet Srikritsadawong **(P. Srikritsadawong)**

Date of Birth 18 July 1997

Address Department of Chemistry, Applied Analytical Chemistry Research Unit and, School of Science, King Mongkut's Institute of Technology Ladkrabang (KMITL), Chalongkrung Road, Ladkrabang, Bangkok 10520, Thailand

Education 2019 Bachelor of Science in Industrial chemistry GPA 3.07 KMITL
2022 Master of Science in Industrial chemistry GPA 4.00 KMITL

Scholarship **2020-2022** Research Assistant/Teaching Assistant (RA/TA) Scholarship, School of Science, KMITL

Research/Academic experiences:

Feb. 2020 Poster Presentation, 2020 PACCON, Bangkok, Thailand
Jan. 2023 Oral Presentation, 2023 PACCON, Chiang Rai, Thailand

List of International Publications:

1. "Foldable paper-based analytical device for membraneless gas-separation and determination of iodate based on fluorescence quenching of gold nanoclusters." A. Lert-itthiporn, **P. Srikritsadawong**, N. Choengchan. (2021). *Talanta*. 221 : 121574.
2. "Preparation of Gold Nanoparticles-Bacterial Cellulose Nanopaper and Its Application as 2D-Microcuvette for Spectrophotometric Determination of

Hydrogen Peroxide." A. Lert-itthiporn, S. Phunpruch, M. Prommajun, **P. Srikritsadawong**, N.Choengchan. (2021). *Chiang Mai J. Sci.* 48(1) : 185-195.

3. "A Double-layered Paper-based Analytical Device for Determination of Iron in Water Samples based on Standard Addition Method." **P. Srikritsadawong**, P. Sookpotarom, S. Thongchan, N. Choengchan. (2023). *Current Applied Science and Technology*. In press.

List of International Proceedings:

1. "Synthesis of Gold Nanoparticles-Embedded Bacterial Cellulose Nanopaper for Colorimetric Detection of Hydrogen Peroxide." **P. Srikritsadawong**, M. Prommajun, A. Lert-itthiporn, S. Phunpruch and N. Choengchan. Proceeding of Pure and Applied Chemistry International Conference (PACCON 2020). Bangkok, Thailand. 13-14 February 2020; AC102-AC107.
2. "A paper-based analytical device for determination of iodate based on redox reaction of tri-iodide and gold nanoclusters." A. Lert-itthiporn, N. Luekijna, T. Kamenmai, T. Seenamngoen, **P. Srikritsadawong** and N. Choengchan. Proceeding of Pure and Applied Chemistry International Conference (PACCON 2019). Bangkok, Thailand. 7-8 February 2019; 51-55.

Certificates:

2019 **Primary Safety Management and Fire Management**

offered by the Department of Chemistry, Faculty of Science, KMITL

2019 **Introduction to Uncertainty Measurement and Laboratory Glassware Calibration**

offered by The Department of Science Service, Ministry of Higher Education, Science, Research, and Innovation

2019 **Introduction to ISO 9001 and ISO/IEC 17025 Course**

offered by Management System Certification Institute (Thailand) incorporated with Department of Chemistry, Faculty of Science, KMITL